Thesis for the degree
Doctor of Philosophy

Submitted to the Scientific Council of the
Weizmann Institute of Science
Rehovot, Israel

עבודת גמר (תזה) לתואר
דוקטור לפילוסופיה

מוגשת למועצה המדעית של
מכון ויצמן למדע
רחובות, ישראל

By
Janni Yuval

מאת
יאני יובל

הרגישות של מערבלים ברוקליניים למבנה המרחבי של הברוקליניות: אימפליקציות לסופות ושינויי אקלים

Sensitivity of atmospheric turbulence to the spatial structure of baroclinicity: implications for storm tracks and climate change

Advisor:
Yohai Kaspi

מנחה:
יוחאי כספי

May 2017

אייר התשע״ז

Acknowledgements

My deep gratitude goes first to my advisor, Yohai Kaspi, who guided me through my graduate education. I should thank him mostly for his optimistic view regarding my results, and even when I thought things were hopeless, he encouraged me to continue. His patience, motivation, enthusiasm, and knowledge helped me accomplishing my Ph.D degree.

Besides my advisor, I would like to thank Prof. Eli Tziperman, who was willing to assist me in any scientific or personal issue I had during my Ph.D. I feel lucky that I have had to opportunity to learn from Eli. His immense knowledge was an invaluable asset for me.

I would like also to thank Prof. Nili Harnik that was a part of my research committee, found the time to assist when I needed, consulted me during my research, and contributed to my scientific education with her sharp comments.

Furthermore, a huge gratitude should go to Rei Chemke, who as a good friend, supported me during my Ph.D even when I was unbearable. I would also like to acknowledge my colleagues here at Weizmann, Talia Tamarin, Hilla Afargan, Morgan O'Neill, Eli Galanti and Marzia Parisi, who were always there to help me with different issues.

I hereby declare that this thesis summarizes my own independent research.

Contents

List of Abbreviations

Acronym	Definition
AR	Assesment report
CMIP5	Coupled model intercomparison project (phase 5)
CO_2	Carbon dioxide
EAPE	Eddy available potential energy
ECMWF	European centre for Medium-Range Weather Forecasts
EHF	Eddy heat flux
EKE	Eddy kinetic energy
EMF	Eddy momentum flux
EMFC	Eddy momentum flux convergence
EP flux	Eliassen–Palm flux
GCM	General circulation model
HS	Held and Suarez (1994)
IPCC	Intergovermental panel for climate change
MAPE	Mean available potential energy
MKE	Mean kinetic energy
NCEP	National centers for environmental prediction
NH	Northern hemisphere
PE	Primitive equation
PV	Potential vorticity
QG	Quasi-geostrophic
QL	Quasi-linear
RCP	Representative concentration pathways
SH	Southern hemisphere
WMO	World meteorological organization

Abstract

The main goal of my Ph.D was to better understand the response of baroclinic eddies to changes in the mean flow of the atmosphere. The problem of how eddies interact with the mean flow is almost as old as the field of geophysical fluid dynamics. Interestingly, the results derived more than 65 years ago by Charney (1947) and Eady (1949) still serve as the main measure of baroclinicity in current research. Along the years, other scaling relations, closure schemes and semi-empirical relations that relate the mean and eddy fields have been suggested. These relations have improved our understanding, but in order to derive these relations many assumptions are needed, and these relations ignore many physical aspects of the circulation. The goal of this work was to study the sensitivity of eddies to changes in the vertical and meridional temperature structure.

Using an idealized general circulation model enabled us to investigate a variety of circulation regimes, and deduce qualitative results that can serve as general guidelines for the sensitivity of eddies to changes in the vertical and meridional structure of the zonal mean circulation. In order to produce meaningful results, we needed to use methods that enabled us to control the mean temperature profiles in simulations, which in turn enabled us to change the temperature profile systematically.

It was found that when the meridional temperature gradient or the vertical temperature gradient are modified at different vertical levels, the eddy activity is affected mostly from changes in the mid/upper temperature gradient. We suggested that the reason for the large sensitivity of eddies to changes in the upper tropospheric levels is the vertical structure of baroclinicity, which is maximal in the upper tropospheric levels. To support this hypothesis, it was demonstrated in a simple 1D Eady-like model that the growth rate is sensitive to wind shear changes were it is large. Furthermore, the relation between the mean available potential energy (MAPE) and eddy quantities was studied for cases where the vertical structure of the lapse rate and meridional temperature gradient are modified. It was found that there is no universal linear relation between the mean available potential energy and eddy quantities.

Later we investigated eddy response to changes in the meridional temperature gradient at different latitudes. It was found that the eddy fields are most sensitive to changes in the temperature gradient in the vicinity the eddy-driven jet, and less sensitive to gradient changes near the subtropical jet. In order to study the relevance of this conclusion to Earth's atmosphere, realistic (zonally symmetric) Pacific temperature distributions for different months were simulated. A MWM in the EKE was reproduced, and it was shown that the poleward shift of the jet in transition seasons relative to midwinter contributes to the presence of the MWM.

Finally, we investigated the effects of realistic global warming-like temperature changes on the circulation. We found that the background reference state as well as the specific shape temperature changes could lead to a different circulation response. Using a 3D reproduction of a realistic temperature field we found that polar surface warming leads to an equatorward shift in the jet stream, but it has a different effect on the Atlantic and Pacific storm tracks. Furthermore, we show that the increase in the upper tropospheric temperature causes a poleward jet shift.

תקציר

המטרה העיקרית של עבודת הדוקטורט שלי היתה לשפר את ההבנה כיצד ערבלים ברוקליניים מושפעים משינויים בזרימה האטמוספירית הממוצעת. השאלה כיצד ערבולים עושים אינטראקציה עם הזרימה הממוצעת היא בעיה הקיימת עוד מראשית המחקר בנושא של דינאמיקת נוזלים. בעייה זו היא בעייה בסיסית ולא פתורה, ואף זה מעט מפתיע כי הערכות לברוקליניות שהתגלו מלפני למעל ה מ 65 שנים ע״י צ׳ארני (1947) ואידי (1949) עדיין משמשות כמידות לברוקליניות באטמוספירה במחקר עכשווי. במרוצת השנים קשרים תיאורטיים וקשרים אמפיריים למחצה הקושרים בין משתנים אטמוספריים לבין אי יציבות אטמוספירית התגלו. למרות שקשרים אלו שיפרו את ההבנה של הדינאמיקה האטמוספירית, במקרים רבים קשרים אלה לא יכולים לשמש אותנו, מכיוון שהנחות ופישוטים רבים בוצעו על מנת לגזור אותם. המטרה של עבודת דוקטורט זו היתה ללמוד את הרגישות של מערבליים אטמוספריים לשינויים במבנה של הטמפרטורה באטמוספירה.

הכלי העיקרי ששימש אותנו היה מודל סירקולציה גלובאלי אידיאלי שאיפשר לנו לחקור מגוון רחב של משטרי זרימה, ולהסיק מסקנות איכותיות שיכולות לשמש כקווים מנחים כלליים בנוגע לרגישות של מערבלים לשינויים במבנה הורטיקאלי והמרידיונאלי של הזרימה הממוצעת. על מנת לדמות שינויים בזרימה הממוצעת של האטמוספירה בצורה סיסטמטית, השתמשנו במודל המאפשר לנו לשלוט בטמפרטורה הממוצעת של הסימולציה.

מצאנו שמערבלים רגישים יותר לשינויים בגראדינט הטמפרטורה המרידיונאלי כאשר הוא משתנה בשכבות העליונות של בהשוואה לשינויים בשכבות התחתונות. ההיפותיזה שהצענו על מנת להסביר את התוצאה היא שמערבלים רגישים לשינויים בזרימה הממוצעת באיזורים בהם הברוקליניות גדולה, ומכיוון שבשכבות העליונות באטמוספירה הברוקליניות גדולה יותר, המערבלים רגישים לשינויים בזרימה הממוצעת באיזורים אלה. על מנת לבסס את ההיפותיזה, הראינו במודל חד מימדי שקצב הגדילה הלינארי של הפרעות רגיש יותר לשינויים בזרימה הממוצעת בגבהים בהם הברוקליניות גדולה יותר. בנוסף הראינו כי ההיפותיזה קונסיסטנטית עם הרעיון שעוצמת המערבלים קשורה בצורה לינארית לאנרגיה הפוטנטציאלית הזמינה. תוצאות אלה מצביעות ששינויי טמפרטורה עתידיים, כתוצאה מהתחממות גלובאלית, עשויים להגביר את עוצמת המערבלים.

לאחר מכן חקרנו את התגובה של מערבלים לשינויים בגראדינט הטמפרטורה בקווי רוחב שונים. מצאנו שמערבלים רגישים לשינויים בגראדינט בקווי רוחב הקרובים לזרם הסילון הקוטבי ופחות רגישים לשינויים בקווי רוחב הקרובים לזרם הסילון הסאבטרופי. על מנת לחקור את הרלוונטיות של מסקנה זו לאטמוספירה של כדור הארץ, הראינו שכאשר הטמפרטורה הממוצעת של האטמוספירה מעל האוקיאנוס השקט מדומה במודל סירקולציה גלובאלית, ניתן לשחזר את המינימום במערבלים בחורף בצורה דומה הקוראת באטמוספירה של כדור הארץ. כמו כן, הראינו שתופעה זו מושפעת משינויים בקו הרוחב בו ממוקם גראדינט הטמפרטורה.

בחלקה האחרון של התיזה חקרנו כיצד שינויי טמפרטורה עתידיים, הצפויים לקרות כתוצאה מהתחממות גלובאלית, עשויים להשפיע על הסירקולציה האטמוספירית. מצאנו ששינויים שונים במערבלים מתרחשים כאשר מצב הבסיס בסימולציה שונה. לכן יצרנו מצב בסיס המדמה את הזרימה התלת מימדית באטמוספירה של כדור הארץ ומצאנו כי התחממות בקוטב הצפוני בגבהים נמוכים מובילה להתקרבות של זרם הסילון לכיוון קו המשווה. בנוסף מצאנו שהתחממות זו גורמת למערבלים להגיב בצורה שונה מעל האוקיאנוס האטלנטי ומעל האוקיאנוס השקט. בנוסף הראינו כי ההתחממות הצפוייה בחלק העליון של האטמוספירה בקווי רוחב נמוכים, גורמת להזזת זרם הסילון לכיוון הקוטב.

Chapter 1

Introduction

1.1 Introduction

1.1.1 The vertical structure of baroclinicity

Relating eddy fields to the mean state has been a fundamental problem in geophysical fluid dynamics. Basic theory of linear baroclinic instability dates back to the work of Charney (1947) and Eady (1949). Eady (1949) expressed the linear growth rate of baroclinic instabilities as

$$\lambda \propto \frac{g}{NT}\left|\frac{\partial T}{\partial y}\right|, \tag{1.1}$$

where λ is the (Eady) growth rate, N is the Brunt-Väisälä frequency, g is the acceleration due to gravity, T is the temperature and y is the meridional direction. Although originating from linear theory, the Eady growth rate has been used extensively even in recent studies as a measure of baroclinicity (e.g., Ioannou and Lindzen, 1986; Hoskins and Valdes, 1990; Lorenz and Hartmann, 2001; Li and Battisti, 2008; Merlis and Schneider, 2009; Thompson and Barnes, 2014).

Despite the fact that the Eady growth rate provides a useful measure for baroclinicity, one should recognize its limitations. For example, considering the linear theory, Eq. 1.1 is valid in the case that the meridional temperature gradient divided by the temperature is constant with height, but in cases that it varies with height (non-uniform wind shear) Eq. 1.1 might be misrepresenting, and a theoretical prediction is missing.

Furthermore, the dependence of eddy fluxes on the mean meridional and vertical temperature gradients has been addressed by various eddy flux closure schemes, such as those of Green (1970) and Held (1978). Most closure schemes rely on qualitative arguments that neglect some of the physical details, and therefore their use is limited in cases where these details play an important role. For example, in order to derive such closure schemes it was necessary to simplify the problem and assume that the vertical mean meridional and vertical temperature gradients are the relevant quantities, and not their vertical structure. Therefore, these closures do not predict the dependence of eddy fluxes on the vertical structure of the temperature gradients.

Later, Schneider and Walker (2008) and O'Gorman and Schneider (2008) showed that for a wide range of parameters, idealized GCM simulations follow semi-empirical scaling laws relating linearly the EKE to the MAPE derived by Lorenz (1955). Furthermore, Schneider and Walker (2008) obtained semi-empirical scaling between vertically averaged eddy momentum flux convergence (EMFC) and surface eddy heat flux (EHF) to MAPE. Schneider and Walker (2008) used a macroturbulence closure that linearly relates eddy available potential energy (EAPE) to MAPE, and showed that this closure is consistent with a linear relation between EKE and eddy fluxes to MAPE. Later, O'Gorman (2010a) showed that the linear scaling between EKE and MAPE approximately holds for reanalysis data as well as in global warming simulations. O'Gorman (2010a) used the MAPE changes in global warming simulations to explain the variability in the EKE between different models. The fact that MAPE and EKE scale linearly also on Earth (O'Gorman, 2010a), where there are zonal asymmetries and time dependent diabatic heating, implies that the scaling is robust and is not limited to idealized models.

Held and O'Brien (1992) were the first to study the effect of the vertical structure of the mean shear on eddy fluxes. They used a 3-layer QG model (including a beta effect), which is the simplest model possible to address this question since the wind shear in the two-layer model is constant. They concluded that for equal values of mean vertical shear, the eddy fluxes are greater when the shear is concentrated at the lower levels ($U_{zz} < 0$). Furthermore, they found that the eddy fluxes are more sensitive to the lower level shear than to the upper level shear, although the eddies were deeper in the case that the shear was concentrated in the upper layer. Pavan (1996), using a multi-layer QG model, supported the results of Held and O'Brien (1992), and concluded that eddy activity (eddy fluxes, eddy kinetic energy) is more sensitive to the lower-level than to upper-level baroclinicity. Pavan (1996) interpreted this result as a consequence of the importance of shallow eddies in the dynamics. Later, Kodama and Iwasaki (2009) showed in aquaplanet experiments that wave activity is affected mainly by the lower-tropospheric temperature gradient. In a different study Iwasaki and Kodama (2011) showed that wave activity is also affected by an increased lower-stratospheric and upper-tropospheric temperature gradient, but the relative importance of upper and lower levels was not clear.

The effect of the vertical structure of baroclinicity on eddy activity has potentially important implication to atmospheric circulation during global warming. Global warming modeling experiments show a robust trend, where the equator to pole temperature difference in the lower levels of the atmosphere will decrease, while in the upper levels the tendency is opposite (Manabe and Wetherald, 1975; Meehl et al., 2007). Consequently, the resulting baroclinicity tends to weaken in the lower troposphere but strengthen in the upper troposphere (this is mostly true in NH winter - see Fig. 5 in Wu et al., 2010). Fig. 1.1, which is taken from Vallis et al., 2014, shows the zonal and ensemble mean of the temperature tendency from year 1 to year 70 for the representative concentration pathways 8.5 (RCP8.5) scenario for models that participate in the fifth assessment report (AR5) of the Intergovernmental Panel on Climate Change (IPCC), and demonstrates the opposite trends in the temperature gradient.

The projections of temperature changes in an increased CO_2 scenario stem from robust

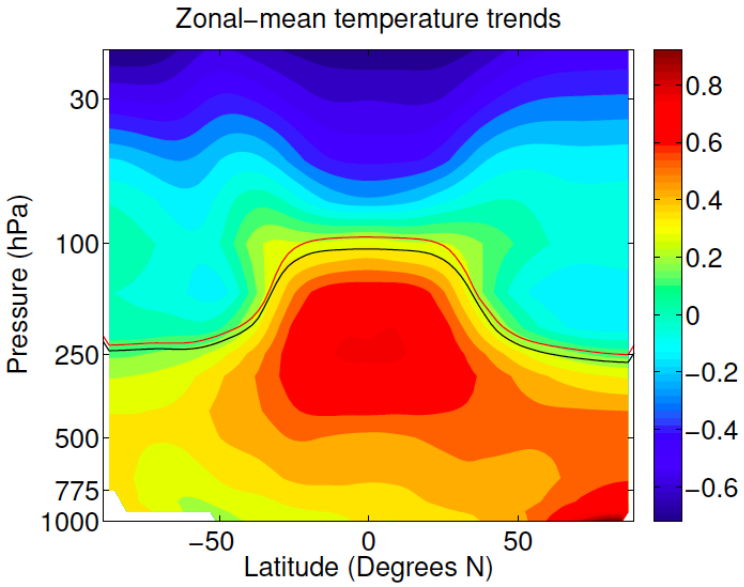

Figure 1.1: The ensemble-mean zonal mean temperature trend (degrees per decade) from IPCC RCP8.5. The thin black and red lines mark the ensemble average tropopause position, using the WMO definision, at year 1 and year 70.

thermodynamic effects and any feedbacks are unlikely to conceal them. The tropical warming aloft can be attributed to the decrease in the saturated lapse rate with increased water content following warming (Manabe and Wetherald, 1980; Vallis et al., 2014). An increase in surface temperature of 1K causes a decrease of approximately 0.1K km^{-1} in the saturated lapse rate (Vallis et al., 2014). Therefore, every degree of surface warming will cause a two-degree warming at a height of 10km. This argument is valid for convective regions where the moist adiabatic lapse rate controls the temperature aloft, such as parts of the tropics. Since the mean circulation in the Hadley cell flattens efficiently and horizontal temperature gradients at low latitudes (e.g., Sobel et al., 2001), the enhanced warming in the upper troposphere extends across the tropics. The large warming in the Arctic happens mostly in winter when the ice-albedo feedback is weak, and different studies showed in models that even without the ice-albedo effect, the polar amplification is present (e.g., Schneider et al., 1997; Alexeev, 2003; Lu and Cai, 2010). Cai (2005, 2006) suggested that polar amplification is caused by increased heat transport. Different studies by Hansen et al. (1984) and Britanja et al. (2011) showed that the winter arctic warming near the surface is a result of large atmospheric static stability concentrated at low levels. Large static stability causes the polar atmosphere to emit a larger fraction of the longwave radiation downward (Britanja et al., 2011), which warms the surface.

These changes might lead to changes in the extratropical atmospheric circulation, such as a shift of the jet and storm tracks and changes in their intensity (e.g., Held, 1993; Stephenson and Held, 1993; Hall et al., 1994; Bengtsson and Hodges, 2006; Yin, 2005; O'Gorman and Schneider, 2008; Wu et al., 2010; O'Gorman, 2010b). Changes in the location and amplitude of the storm track in response to global warming have significant impact on the poleward transport of heat, momentum, moisture and on the hydrological cycle (Wu et al., 2010; O'Gorman, 2015).

Despite the fact that models predict similar sign in temperature trends in most regions, in

the arctic surface region there is a very large temperature variations between models. Fig. 1.2 shows the zonal mean surface temperature trends between year 1 to year 70 for the RCP8.5 scenario for different models (grey) and their average (black,taken from Vallis et al., 2014). The surface polar amplification in the NH occurs in nearly all models, but the standard deviation is largest at the high latitudes of the NH where the response of sea ice varies between models. These temperature trends differences between models might lead to a significant trend differences in the circulation (Barnes and Screen, 2015).

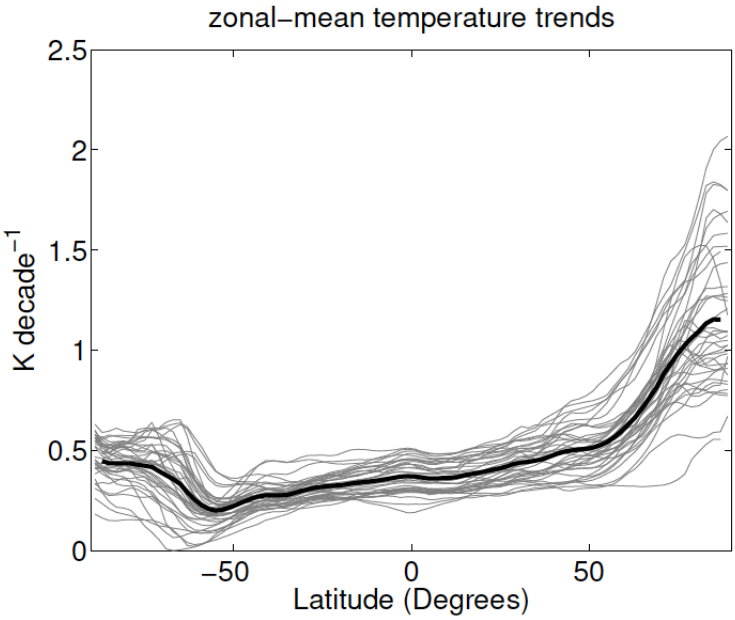

Figure 1.2: The zonal mean surface temperture trend from year 1 to year 70 in the IPCC RCP8.5 scenario. The grey lines are for the infividual models and the thicker black line is the ensemble mean.

Lunkeit et al. (1998) used an idealized model with realistic temperature profiles to investigate the effects of global warming on atmospheric circulation, and concluded that the lower level baroclinicity will affect eddy activity more than upper level baroclinicity. On the other hand, using a comprehensive climate model (the GFDL CM2.1), Wu et al. (2010) investigated the effects of global warming on atmospheric circulation and concluded that the change in eddy kinetic energy (EKE) correlates better with the change in upper baroclinicity than the change in lower baroclinicity.

1.1.2 The meridional structure of the jet

Another possible weakness of linear measures such as the Eady growth rate, supercriticality (Held and Larichev, 1996) or closure schemes is that the predictions of these relations do not involve any information about the jet type. The current scientific understanding is that two types of jets exist in the atmosphere, a subtropical jet (STJ) and an eddy-driven jet (EDJ) also referred to in the literature as the sub-polar jet. Two different mechanisms are responsible for the existence of these jets. The STJ is primarily driven by advection of planetary angular momentum by the thermally direct Hadley circulation (Held and Hou, 1980), and eddies

usually act to weaken this jet. On the other hand, the EDJ is driven by eddy momentum flux convergence (EMFC), which accelerates the zonal mean westerly wind (Held, 1975; Rhines, 1975; Panetta, 1993).

Since these jets are a result of different processes, the location of these jets is different. The STJ is located at the edge of the Hadley cell, while the EDJ is located inside the Ferrel cell, where the EMFC is maximal. In practice, there are different regimes for the atmospheric jets and not always both jets are present or can be clearly distinguished. For example, in the summer hemisphere when the Hadley cell is very weak, the STJ typically does not exist and there is a relatively weak EDJ. In transition seasons and winter, when the Hadley cell is present, there are two possible regimes; (a) two well separated jets as in the Northern Atlantic in January where EMFC is found only in the vicinity of the EDJ (Fig. 1.3a and also in Eichelberger and Hartmann, 2007); (b) a single merged (mixed) jet as in the Northern Pacific in January, which is driven both from thermally direct Hadley cell in its more equatorward regions and by EMFC in its poleward flank (Fig. 1.3b). In addition, the STJ and the EDJ are also distinguished by their vertical structure. The STJ is more baroclinic and has very weak surface winds below its maximum, while the EDJ is more barotropic and surface westerlies are located below its maximum to balance the upper tropospheric EMFC (Vallis, 2006).

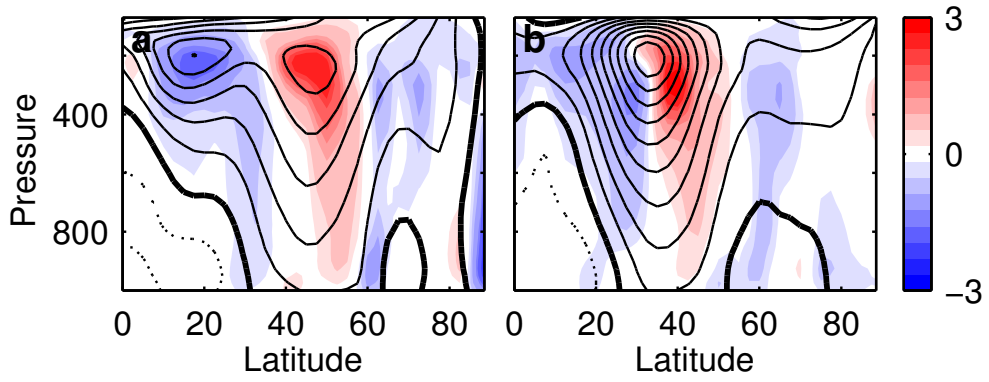

Figure 1.3: Zonal wind in January averaged for the years 1979-2015 (contours) and EMFC$\times 10^5$ (color) for the zonally averaged northern Atlantic (longitudes $0°\text{W}-60°\text{W}$, panel a) and for the zonally averaged northern Pacific (longitudes $150°\text{E}-120°\text{W}$, panel b) calculated from the ECMWF reanalysis data. Eddies are calculated using a Butterworth bandpass filter with a cutoff period of $3-10$ days on 6 hourly data. The zonal wind contour intervals are 5 m s^{-1} where the bold contour is the zero wind line and the dotted lines are for negative values.

A number of previous studies investigated the relationship between the jet characteristics and eddies. Lee and Kim (2003) used linear stability analysis to show that when a weak STJ is present, and the Eady growth rate (Eady, 1949) is maximal poleward of the jet peak, the growth of eddies will occur $20°-30°$ poleward of the STJ and a second jet (an EDJ) will emerge. On the other hand, when the STJ is strong, and baroclinicity peaks close to its core, eddies will grow in its vicinity and only a single (merged) jet will be present. Consistent with this result, Son and Lee (2005) showed in an idealized GCM with a Newtonian relaxation scheme, that a double jet state is favored when the STJ is weak and the baroclinic zone is wide. In a different study Nakamura and Sampe (2002) used reanalysis data, to show that when the STJ is strong

above the Pacific, it can trap eddy activity within its core, away from the strong SST gradients in the Pacific ocean, and concluded that this trapping effect can suppress eddy activity in the baroclinic zone. In a later study, Nakamura and Shimpo (2003) showed that in the south Pacific winter, where the strong STJ traps eddy activity, the storm tracks are suppressed at the lower levels, but not at the upper levels.

Brayshaw et al. (2008) investigated the sensitivity of eddies to changes in SST gradient at different latitudes. They showed in an aquaplanet GCM that in the presence of a merged jet, eddies are most sensitive to changes in the SST gradient in the vicinity of the jet where baroclinicity is large, less sensitive when the SST gradient is modified in low latitudes (inside the Hadley cell) and least sensitive when the gradient was modified at high latitudes (significantly poleward of the jet maximum). In another study Sampe et al. (2010) found that when a strong SST gradient (frontal SST gradient) exists in the vicinity of the jet, eddies are much stronger than the case the gradient is flattened across wider latitudinal range (but with a similar mean SST gradient). They concluded that a polar front SST below the jet has a large effect on the storm tracks. These results are consistent with the idea that that eddies are most sensitive to baroclinicity changes where it is already large and not to the mean baroclinicity (Yuval and Kaspi, 2016, 2017).

Lachmy and Harnik (2014) showed in a two-layer quasigeostrophic (QG) model that the transition between a merged jet and STJ is accompanied by a significant change in the waves' spectrum. They found that while a merged jet is dominated by wavenumbers $4-6$, a STJ is dominated by longer waves (wavenumbers $1-3$) with a weaker amplitude. Furthermore, Lachmy and Harnik (2014) suggested that in the STJ regime eddies are weak despite the strong STJ shear, since the potential vorticity gradient does not change sign in the jet's vicinity, and therefore the Charney and Stern (1962) criterion is not satisfied.

Despite the different mechanisms leading to two different types of jets, baroclinicity measures used in the literature, do not treat different jets in a different manner and only the mean jet characteristics are taken into account when calculating these measures.

1.1.3 The Pacific midwinter minimum

Linear theories of baroclinic instability (Charney, 1947; Eady, 1949) contributed significantly to the understanding of synoptic-scale storms in the midlatitudes. These linear theories, provided a scaling which relates between the mean climate state and climatological eddy magnitudes. Despite the success of linear theory to explain many phenomena in midlatitudes (e.g., Ioannou and Lindzen, 1986; Nakamura and Shimpo, 2003; Li and Battisti, 2008; Thompson and Barnes, 2014), the midwinter minimum (MWM) of the Pacific storm tracks in the NH remains a remarkable example of the limitations of the linear theory to give a correct prediction to the relation between the mean state and eddies.

Nakamura (1992) was the first to show that the intensity of baroclinic wave activity exhibits a MWM above the northern Pacific. This observation is inconsistent with linear instability theories since baroclinicity measures are on average largest in January, but the eddy kinetic energy

(EKE) is at a local minimum during midwinter. Nakamura (1992) showed that the intensity of EKE is positively correlated to jet strength below 45 m s^{-1} and negatively correlated at higher jets velocities, both on annual and interannual time scales (see also Zhang and Held, 1999; Chang, 2001). Nakamura (1992) suggested a few possible explanations that might contribute to the MWM, such as wave trapping, interactions between planetary waves and baroclinic waves, strong advection that advects eddies fast in regions of large baroclinicity and the high specific humidity during spring and autumn which acts to increase the effective baroclinicity.

Since the pioneering work of Nakamura (1992) many studies tried to explain the physical mechanisms for the MWM. Harnik and Chang (2004) used a channel model, and in a linear model on a sphere, to show that linear theory can be consistent with the MWM when considering the meridional structure of the jet. They concluded that strong advection alone can't explain the slower growth rate in winter, but when considering the narrowing of the jet that occurs in winter, the growth rate reduces. Deng and Mak (2005) suggested that the increased local baroclinicity in midwinter could act like a generalized barotropic governor mechanism (James, 1987), and lead to a decrease in the EKE. Penny et al. (2010, 2011, 2013) suggested that a reduction of seeding associated with topographic effects of baroclinic waves propagating from Asia to the Pacific in the midwinter might be the explanation to the midwinter minimum, and Lee et al. (2013) showed that the presence of the Tibetan plateau tends to suppress storm track activity in the Pacific midwinter.

Chapter 2

Methods

2.1 Idealized global circulation model

The main tool used in this thesis was an idealized GCM based on the Flexible Modeling System of the US National Oceanic and Atmospheric Administration (NOAA) Geophysical Fluid Dynamics Laboratory (GFDL). This is a 3D spherical coordinate spherical coordinate primitive equation (PE) model of an ideal-gas atmosphere. The dynamical core of the idealized GCM is a hydrostatic spectral transform in vorticity-divergence form (Bourke, 1974), with semi-implicit time differencing and a vertical σ coordinate. The spectral truncation is triangular, and the horizontal resolution we use is T42, corresponding to grid resolution of about $2.8^\circ \times 2.8^\circ$. The vertical discretization is based on a centered difference scheme, with 60 unequally spaced σ levels (except in chapter 8 where we used 30 vertical levels). The dynamical core of the idealized GCM is identical to the spectral dynamical core described by Held and Suarez (1994) and more details can be found there. We worked with a dry version of the model, which is driven by a Newtonian cooling scheme, and in nearly all of the simulations in this work, linear damping of near surface winds represents turbulent dissipation in the planetary boundary layer (see Held and Suarez, 1994). The model is run without a coupled ocean or orography, and unless stated differently at perpetual equinox. When a dry convection scheme is used it is mentioned in the text, and an explanation for the dry convection scheme appears in section 2.2. In Appendix B we describe the standard Held-Suarez (HS) parametrization for the diabatic heating that is used in some of the chapters as a reference temperature.

2.2 Diabatic forcing in the Newtonian relaxation scheme

The thermodynamic equation used in the idealized GCM, which is driven by a Newtonian cooling scheme is

$$\frac{DT}{Dt} = \frac{1}{\rho}\frac{Dp}{Dt} + \frac{T_{\text{relax}} - T}{\tau}, \tag{2.1}$$

where $\frac{D}{Dt}$ is the material derivative that includes the nonlinear advection terms, T is the temperature, ρ is the density, p is the pressure, T_{relax} is the relaxation temperature and τ is the

relaxation time which can be space-dependent. In general, the relaxation temperature can be space and time-dependent. In this Ph.D work we use a time independent relaxation temperature (except in chapter 8 where it is mentioned explicitly), and in most sections, and unless stated differently, it depends on latitude and pressure only. The second term on the right hand side is the diabatic heating as a result of Newtonian cooling.[1]

When using a Newtonian relaxation scheme, a common method to change the temperature field in a certain region is modifying the relaxation temperature field at the desired region. This method does not give a full control on the mean temperature profile that will be reproduced in the simulation for two main reasons. First, when the relaxation temperature is modified in one region, the temperature field is changed in many other regions, mainly as a result of advection. Generally, a linear relationship between the relaxation temperature T_{relax} and the time mean temperature field $\hat{T}$ can't be expected because the contribution of the nonlinear advection terms is large. Second, the relaxation time τ is usually a function of height and latitude (see Appendix B). Changing the relaxation temperature at different levels will cause different diabatic forcing and will cause very different temperature amplitude changes.

This is demonstrated in Fig. 2.1(a-c) that shows the temperature changes as a result of modifications in the relaxation temperature at different levels that are plotted in Fig. 2.1(d-f). The temperature response at lower levels (Fig. 2.1c) is significantly larger than the temperature response to changes in the relaxation temperature at higher levels (Fig. 2.1a), and the induced temperatures changes at different levels are very different in magnitude. The EKE is plotted in Fig. 2.1(g-i). Although the temperature gradient modifications at the lower levels are significantly larger than at the upper levels, the modification in the EKE is of the same order of magnitude. The reference simulation used in Fig. 2.1 is a simulation with the Held and Suarez (1994) parameters that includes a dry convection scheme with $\gamma = 0.7$, where $\Gamma_{\text{dry}} = g/c_p$ is the dry adiabatic lapse rate. The dry convection scheme relaxes the temperature lapse rate to the value of 0.7 Γ_{dry} on a short time scale of 4 hours when the lapse rate exceeds this value.

In the context of this Ph.D work, where we study the changes in eddy fields as a result of changes in the vertical and meridional structure of baroclinicity we find the method above unsatisfactory since similar amplitude changes in the relaxation temperature lead to a very different mean temperature response. In order to investigate the effect of the temperature structure of eddies it was beneficial to use methods that allow controlling the mean temperature distribution (or inducing similar diabatic heating), and these methods are described in sections 2.3.1, 2.3.2, 2.3.3.

What distinguishes our simulations in most sections from what is used in Held and Suarez (1994) is the relaxation temperatures and relaxation times we use, which are different. The diabatic heating schemes we use allows obtaining any desired temperature profile (see section 2.3 for details), which is beneficial for studying the effect of the mean temperature structure on baroclinic eddies.

[1] The thermodynamic equation for the potential temperature can be expressed as $\frac{D\theta}{Dt} = Q$, where Q is the diabatic heating and $\theta = T(\frac{p_{\text{ref}}}{p})^{\kappa}$ is the potential temperature. This means that the second term on the RHS of equation 2.1 is proportional to $\frac{T_{\text{relax}}-T}{\tau} \propto Q(\frac{p}{p_{\text{ref}}})^{\kappa}$.

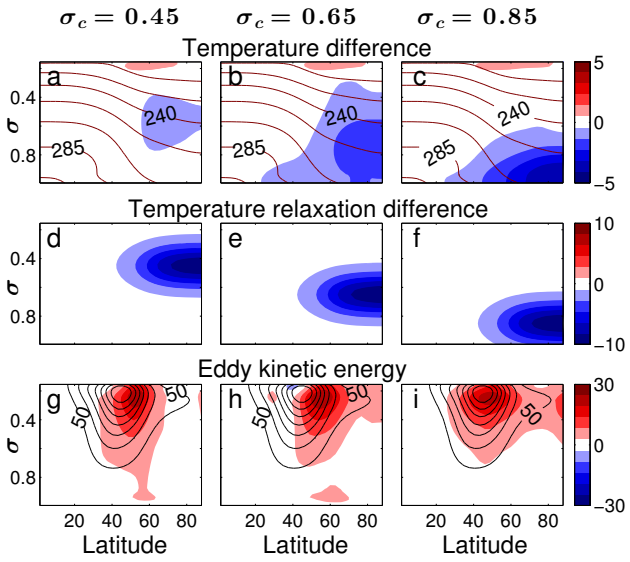

Figure 2.1: Contours show the Held-Suarez like reference fields while colors show the deviation from the reference. (a-c) Change in the temperature field as a response to changes in relaxation temperarure (d-f) in different levels, and the EKE (g-i). The reference simulation used here is a simulation with the Held and Suarez (1994) parameters but includes a dry convection scheme with $\gamma = 0.7$. Contours intervals are 15 K for the temperature and 50 m^2 s^{-2} for the EKE.

2.3 Diabatic heating methods

During my Ph.D I used three diabatic heating schemes to study the effect of the vertical and meridional structure of baroclinicity on eddy activity:

(a) **Iterative method:** Controlling the mean temperature distribution by finding a relaxation temperature that reproduces a target temperature field (model setup is discussed in section 2.3.1).

(b) **Fast zonal relaxation:** Controlling the mean temperature distribution by relaxing the zonal mean temperature back to its target value on a very short time scale (discussed in section 2.3.2).

(c) **Uniform relaxation time:** Changing the diabatic forcing with similar amplitude (model setup is discussed in section 2.3.3). This is achieved by conducting experiments where the relaxation time τ is taken to be uniform in space.

In general, all three approaches are useful. As demonstrated in this thesis, both the iterative and the fast zonal relaxation methods can reproduce any zonally symmetric temperature field with a good accuracy, and allow changing the temperature field in a systematic manner and study the response of eddies. These two approaches give similar results when similar zonally symmetric temperature distributions are simulated (see appendix A).

The main advantage of the iterative method over the fast zonal relaxation method is that it can also reproduce a zonally asymmetric 3D temperature structure, which we use in chapter 8 to simulate a realistic 3D temperature distribution. The advantage of the fast zonal relaxation method over the iterative method that it is computationally much more efficient (see sections 2.3.1 and 2.3.2 for the differences). The uniform relaxation time method allows changing the

diabatic forcing with similar magnitude in different regions.

2.3.1 Controling the temperature profile - iterative method

In this section a method that permits simulations with a predetermined temperature field is presented. This method allows running simulations with different temperature fields, such that we change the temperature field in a chosen section of the atmosphere, while keeping the average temperature field at other sections approximately constant. This enables investigating the response of eddy activity to modifications in the vertical structure of the meridional temperature gradient field in section 3.

In order to simulate a desired temperature profile (T_{target}), it is necessary to find the relaxation temperature (T_{relax}, see Eq. 2.1) that will produce the prescribed profile. The method we use is described below and is similar to the method used by Lunkeit et al. (1998).

1. The desired target temperature (T_{target}) is chosen. The target temperature is the time and zonal mean temperature we wish the simulation to obtain.

2. An iterative procedure is introduced to find the relaxation temperature (T_{relax}) that will approximately produce the desired target temperature field. The iterative equation for the relaxation temperature is

$$T_{\text{relax}}(t+\delta t) = \overline{T_{\text{relax}}(t) + \frac{T_{\text{target}} - T(t)}{\alpha}}, \tag{2.2}$$

   where α is dimensionless number chosen empirically, $T_{\text{relax}}(t+\delta t)$ denotes the relaxation temperature at time $t+\delta t$, where δt is one time step of the model, and $\overline{A}$ is a zonal average of a field A.

3. The relaxation temperature field ($T_{\text{relax}}(t)$) obtained from the simulation is time averaged. This averaged field is time independent and used later in the idealized GCM experiments as the relaxation temperature. In our experiments we set $\alpha = 1500$, but the value has no importance as long as the relaxation temperature obtained produces a final temperature field similar to the target temperature.

This method can produce the relaxation temperature that will simulate any mean temperature profile with a very good accuracy. Furthermore, using this method allows producing the same temperature profiles for different model parameters. For example, it is possible to use different relaxation temperatures that simulate the same temperature profile, where each relaxation temperature corresponds to a different set of model parameters, such as the relaxation time (τ) or convection scheme. Fig. 2.2 shows the temperature, zonal wind and the EKE for three simulations with similar temperature distribution. The left column in Fig. 2.2 describes the result of a simulation with the Held and Suarez (1994) parameters including a convection scheme ($\gamma = 0.7$). The middle and right columns are simulations obtained by using the method described in this section such that their target temperature (T_{target}) in equation 2.2 is the

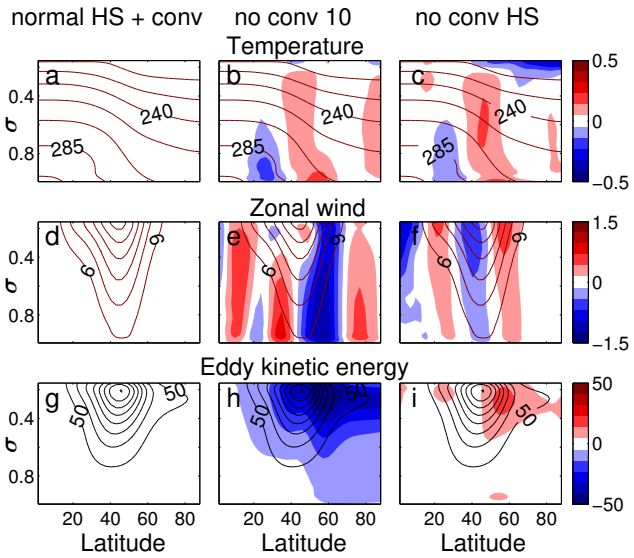

Figure 2.2: The temperature (a-c), zonal wind (d-f) and EKE (g-i) for simulations that the HS forcing was used with convection scheme and two simulations used that have the (almost) same temperature field but when using different relaxation times and no convection scheme. Contours show the fields of the simulation using the normal HS parameters while colors show the deviation from this run. Contours intervals are 15 K for the temperature, 6 m s^{-1} for the zonal wind and 50 m^2 s^{-2} for the EKE.

temperature field of the simulation in left column of Fig. 2.2. The simulations in the middle and right column do not include a convection scheme.

The difference between the simulations in the middle and right column are the relaxation times which are a uniform 10 days and the Held and Suarez (1994) relaxation time respectively (with a relaxation time of 40 days in the upper atmosphere and 4 in the equator surface). Although, the temperature distribution in these three simulations is very similar, the EKE differ substantially. Furthermore, the zonal wind in these simulations approximately follows thermal wind balance, and therefore the differences in the zonal wind occur due to surface effects (which cause whole columns to differ by approximately a similar amplitude). The simulations in the middle and right columns are used in the next sections as reference simulations. In all simulations in this paper the friction damping rate is 1 day, as in Held and Suarez (1994).

In chapter 8 where we use a 3D zonally asymmetric realistic temperature distribution it is necessary to integrate the model for a very long time in order to get a time non-dependent relaxation matrix that will produce the target temperatures. To avoid this, we use a time dependent relaxation matrix that is derived in step 2 (without the zonal average), with the parameter $\alpha = 15000$ and use it for the analysis of the results.

2.3.2 Controling the temperature profile - zonal mean fast relaxation

Another heating formulation that allows simulating any zonally symmetric temperature was suggested by Zurita-Gotor (2007). The main difference of this method to other heating formulations used in idealized models, is the usage of different relaxation time scales for the eddies

and the zonal mean. The temperature equation in this formulation can be written as

$$\partial_t T = ... - \alpha_T((T - \bar{T})) - \alpha_T\gamma(\bar{T} - T_{\mathrm{R}}), \tag{2.3}$$

where $\bar{T}$ is the zonal and time-mean of field T, α_T is the relaxation time of eddies, and is chosen to be as in Held and Suarez (1994), $\alpha_T\gamma$ is the relaxation time for the mean state, where we take $\gamma = 100$ and T_{R} is the relaxation temperature, which is also the target temperature. The fast relaxation for the zonally mean state is chosen to allow reproduction of any chosen target profiles with a good accuracy, such that the zonal and time mean temperature in a simulation is approximately the relaxation temperature. This allows systematically changing different aspects of the temperature field (e.g., the meridional temperature gradient and the vertical temperature gradient), in different regions of the atmosphere and investigate how these changes affect the eddy fields. This method is used in sections 5, 6.

2.3.3 Controlling the diabatic forcing

A third approach we took to change the vertical structure of the meridional temperature gradient is adding diabatic sources at different heights (section 3), which modify the temperature field. The radiative diabatic forcing in the dry GFDL GCM is parametrized by two variables (Appendix B), a relaxation temperature and a relaxation time (τ in Eq. 2.1). As discussed in section 2.2, in order to produce a similar change in the diabatic forcing at different levels it is necessary to account for the two. A simple way of adding a similar amplitude of diabatic heating is to change the relaxation temperature at different levels while taking a uniform relaxation time (e.g., $\tau = 10$ days).[2]

[2]The diabatic forcing in the thermodynamic equation is $\frac{T-T_{\mathrm{relax}}}{\tau}$ (excluding friction) itself depends on the temperature field. The mean temperature field in our simulations is known only after the simulation is performed. Therefore, the diabatic forcing change in our simulations is not equal in different simulations even when the relaxation time is uniform. This is because the temperature change magnitude is different in each simulation as a result of the advection terms.

Chapter 3

Eddy sensitivity to the vertical structure of the meridional temperature gradient

This chapter focuses on understanding the effect of the vertical structure of baroclinicity on eddy activity, and more specifically evaluating if baroclinic growth is dominated by the upper or lower level tropospheric baroclinicity. To do so, the vertical structure of the meridional temperature gradient is modified, and the response of eddies to such changes is investigated. As demonstrated in the next sections, we find that EKE and eddy heat and momentum fluxes respond in a similar manner to modifications in baroclinicity and therefore, throughout this chapter we interchangeably use the terms EKE, eddy fluxes and eddy activity. In general, eddy fluxes and EKE do not have the same response and in some cases can even have opposite trends (e.g., Ferrari and Nikurashin, 2010).

In this chapter two different approaches are taken to control the vertical structure of the meridional temperature gradient:

(a) Changing the temperature field at different levels while keeping the temperature fixed at other levels (model setup is discussed in section 2.3.1). In this method the relaxation temperature is prescribed to produce a desired temperature field. In order to keep the temperature constant in all regions except in a chosen region, the relaxation temperature is modified in many regions and not only in the region where the temperature is modified. This method is similar in spirit to an eddy-mean flow interaction problem, where the mean state is (loosely) determined and the eddy response is investigated.

(b) Changing the diabatic forcing with similar amplitude at different levels (as explained in section 2.3.3). This is achieved by conducting experiments where the relaxation time τ is taken to be uniform in space, and modifying the relaxation temperature at different levels.

As both approaches are valid, in the next sections we take both approaches to investigate the effect of the vertical structure of baroclinicity on eddy activity. Both approaches show that eddy activity is affected significantly more by changes in the upper tropospheric baroclinicity than lower tropospheric baroclinicity. The relaxation temperature we use are described in sections 3.1.1 and 3.1.2. In section 3.2, the results of the simulations are shown where we demonstrate that eddies are more sensitive to changes in the upper-tropospheric temperature

gradient. In section 3.3, a possible relation between our results to the MWM in EKE observed above the Pacific Ocean is presented. In section 3.5 we summarize the results for these simulations.

3.1 Heating profiles

3.1.1 Prescribed temperature changes

In order to study the effect of the vertical structure of the temperature gradient on the eddy activity the heating scheme described in section 2.3.1 was used. The meridional temperature gradient of a reference run ($\partial_y T_{\rm ref}$) was modified in the extratropics, poleward of latitude 24°, in the following manner (Fig. 3.1(d-f)),

$$T_{\rm target}(\vec{r},|\phi|>24) = T_{\rm ref}(\vec{r}) + x(T_{\rm ref}(\vec{r}) - T_{\rm ref}(\vec{r},|\phi|=24))\exp[-\frac{(\sigma-\sigma_c)^2}{2\delta\sigma^2}], \qquad (3.1)$$

and unchanged at lower latitudes ($T_{\rm target}(\vec{r},|\phi|<24) = T_{\rm ref}(\vec{r})$). $T_{\rm target}$ is the desired time mean temperature field, $\vec{r}$ is latitude and height dependent, σ is the vertical coordinate, σ_c is the vertical level where the maximal meridional temperature gradient is changed, $\delta\sigma$ determines the vertical interval of the temperature change, x determines the percentile change in magnitude of the meridional gradient and $T_{\rm ref}(\vec{r},|\phi|=24)$ is the reference temperature at latitude 24°.[1] In our simulations, $T_{\rm ref}$ is taken from a reference simulation using the Held and Suarez (1994) forcing including a convection scheme (see left panels in Fig. 2.2).

Unless stated differently the parameters used in the simulations of this section are $x = \pm 0.02, \pm 0.05$ for $\sigma_c = 0.45, 0.65, 0.85$ and $\delta\sigma = 0.1$ (see table 3.1). These parameters allow us to study the effect of increased/decreased meridional temperature gradient in the extratropics at different levels on eddy activity. The reference simulation used when we compare the results of different simulations that the temperature profile was controlled in the next sections is a simulation in which the parameter $x = 0$ was used. This produces a similar temperature profile to the desired Held and Suarez (1994) temperature profile, and is presented in right column of Fig. 2.2. The simulations presented in this section and in section 3.2 do not include a convection scheme (except the simulations in Fig. 2.1 and the left panel of Fig. 2.2).

Fig. 3.1(a-c) shows the temperature difference $\bar{T} - T_{\rm ref}$, the target temperature difference (d-f) and the relaxation temperature (g-i). The similarity between the target temperature and the mean temperature from the simulation confirms that this method can be used to simulate the desired changes from the reference simulation.

In the scheme described in this section, the vertical interval of the modifications applied to the temperature field were taken in σ coordinates. This choice changes the temperature for same amount of mass in different levels. Another possibility is to change the temperature

[1] The reason the temperature field was modified poleward of latitude 24° is that we wanted to minimize changes in the tropical circulation which can also affect the extratropical circulation and focus on the question how the vertical structure of baroclinicity in the extratropics plays a role in the extratropical circulation.

Experiment		
Controlling tempera-ture (relax-ation as in HS)	σ_c	percentile change (x)
	0.45	$\pm 0.02, \pm 0.05$
	0.65	$\pm 0.02, \pm 0.05$
	0.85	$\pm 0.02, \pm 0.05$
	-	0, (reference)
Controlling heating (uniform relaxation 10 days)	σ_c	amplitude change (A)
	0.45	$\pm 1, \pm 2$
	0.65	$\pm 1, \pm 2$
	0.85	$\pm 1, \pm 2$
	-	0, (reference)
	0.1, 0.15... 0.9	± 2

Table 3.1: Different parameters used in the presented simulations. Controlling temperature refers to the method described in section 2.3.1. Controlling heating refers to method described in section 2.3.3.

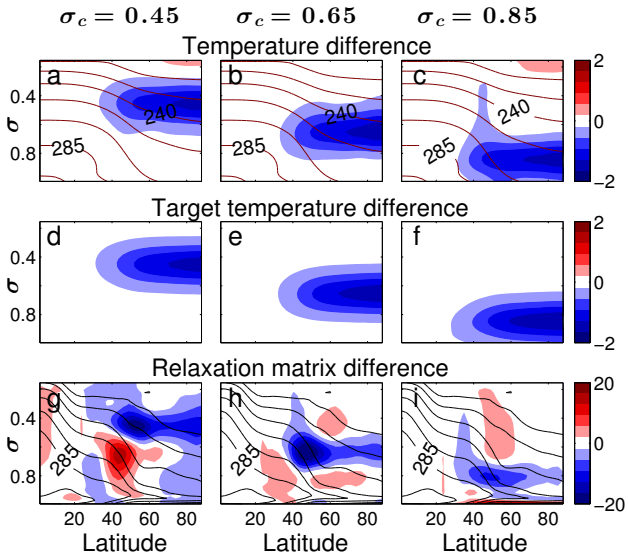

Figure 3.1: In all plots contours are values of the reference simulation and color denotes the deviation from reference. In all panels the parameters used are $\delta\sigma = 0.1$, $x = 0.05$ and $\sigma_c = 0.45, 0.65, 0.85$. (a-c) Temperature (d-f) the theoretical desired temperature difference ($T_{\text{final}} - T_{\text{ref}}$) calculated from Eq. 3.1 and (g-i) is the modification in the relaxation temperature. Contours intervals are 15 K for the temperature plots.

profile in such a way that the vertical interval of change will be similar in z coordinates. For a discussion and results of simulation using z coordinate interval see Appendix C.

3.1.2 Prescribed diabatic heating changes

In order to study the effect of the vertical structure of the temperature gradient on the eddy activity the heating scheme described in section 2.3.3 with a uniform relaxation time of 10 days was used. Our reference run for this method is a run that have a similar temperature profile to Held and Suarez (1994) but with a uniform relaxation time of 10 days. In order to produce such a simulation, the scheme described in section 2.3.1 is used to find the relaxation temperature that produces this temperature profile with a uniform relaxation time. This simulation is

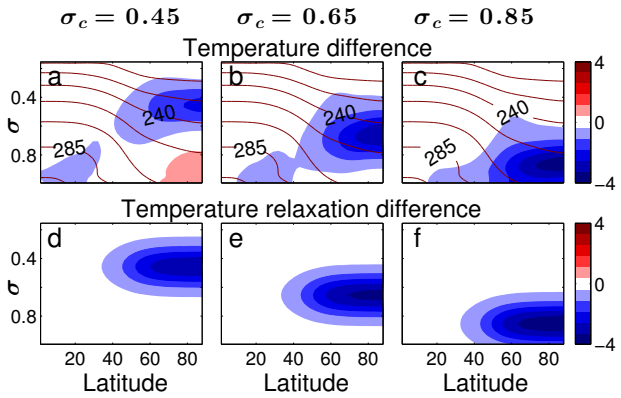

Figure 3.2: contours are values of reference run while colors represent deviation from reference (a-c) temperature for simulations with different σ_c and $A = -2$ K (d-f) modification in the relaxation temperature. Contours intervals are 15 K for the temperature.

presented in the middle column in Fig. 2.2.

The reference relaxation temperature was modified in the following way

$$\delta T_{\text{relax}} = A(1 + \tanh[\frac{3(|\phi| - \phi_b)}{\delta\phi}]) \times \exp[\frac{(\sigma - \sigma_c)^2}{2\delta\sigma^2}](\frac{p}{p_{\text{ref}}})^{\kappa}. \tag{3.2}$$

In the above, ϕ is latitude, ϕ_b controls the latitude where the change in the relaxation temperature saturates, $\delta\phi$ determines how sharp is the gradient in the relaxation temperature, σ_c determines the level where the change in the relaxation temperature is maximal and A determines the amplitude change in that relaxation temperature. The factor $(\frac{p}{p_{\text{ref}}})^{\kappa}$ is present in order to modify the diabatic forcing in a similar magnitude in the thermodynamic equation. The results presented in the next sections are for the parameter choice of $\phi_b = 50$, $\delta\sigma = 0.1$, $\delta\phi = 45$, $A = \pm 1, \pm 2$[K] and $\sigma_c = 0.45, 0.65, 0.85$ unless stated differently. Fig. 3.2 shows the relaxation temperature change (d-f) and the response of the temperature field to this change (a-c). This choice of parameters adds heating sources only in the extratropics and does not change the heating in the tropics. Different numerical values for the parameters were examined ($\phi_b = 60, 33$, $\delta\phi = 0.25, 0.90$, $\delta\sigma = 0.05, 0.2$), but the conclusions presented are invariant to the exact numerical values as long as the change in the relaxation temperature is concentrated at midlatitudes.

3.1.3 Spinup details

Every simulation presented ran for 5000 days and averaged over the last 4500 days where during each day the fields were taken 4 times a day. Hemispherically symmetric simulations were also averaged over the two hemispheres such that the presented plots of the NH are actually an average over the two hemispheres. Each experiment in the simulations that was used to obtain a relaxation temperature, ran for 8000 days and the relaxation temperature was obtained by averaging over the last 6000 days of the simulation.

3.2 The circulation response to changes in baroclinicity

In this section the response of the circulation and in particular the response of eddy activity to changes in the vertical structure of the meridional temperature gradient is investigated. Eddy field are defined as the deviation from time and zonal mean, $A = \hat{\bar{A}} + A'$ where $\hat{A}$ is the time mean and $\bar{A}$ is the zonal mean of the field A. The modifications in the Eady growth rate and static stability caused by the temperature modifications are discussed in section 3.2.1 and the meridional barotropic shear response is discussed in section 3.2.2. The eddy activity response to changes in the vertical structure of baroclinicity are discussed in section 3.2.3, and in section 3.2.4 the changes in surface wind are discussed. We mostly concentrate on the differences between changes induced in the lower, mid and upper troposphere and therefore, the plots show in color the deviations from the reference simulations. In this section we use two different reference simulations for the two different methods described in section 2.3.1 and 2.3.3 (see reference simulations in the right and middle columns of Fig. 2.2, respectively). Furthermore, the simulations are conducted for both cases of increased and decreased temperature gradient.

3.2.1 Eady growth rate

When changing the meridional temperature gradient at specific levels, the static stability changes as well. This is important since the baroclinicity is affected by both the meridional temperature gradient and the static stability. A simple approximate measure for the maximum baroclinic growth rate is given by Eq. 1.1.

Although originating from linear theory, the Eady growth rate has been used extensively in the literature as a measure of baroclinicity (e.g., Ioannou and Lindzen, 1986; Hoskins and Valdes, 1990; Lorenz and Hartmann, 2001; Merlis and Schneider, 2009; Thompson and Barnes, 2014). Figures 3.3 and 3.4 show the Eady growth rate (a-c), buoyancy frequency (d-f) and the vertically integrated Eady growth rate variation (g-i), defined as $\int \lambda d\sigma - \int \lambda^{\mathrm{ref}} d\sigma$ for simulations that the temperature gradient was modified at different levels (Fig. 3.3), and that the diabatic forcing was modified (Fig. 3.4). When increasing (decreasing) the meridional temperature gradient at certain levels the buoyancy frequency is modified such that above the maximal level of temperature change (σ_c), the buoyancy frequency is increased (decreased) and below this level it is decreased (increased) — see Fig. 3.3(d-f) and Fig. 3.4(d-f). As a result, the Eady growth rate is significantly increased (decreased) below the level of maximum change (σ_c) because both, the meridional temperature gradient and the buoyancy frequency, are contributing to increase (decrease) the Eady growth rate. Above σ_c the meridional temperature gradient and the buoyancy have an opposite effect on the Eady growth rate, and therefore its relative change is smaller. In the next sections it is shown that the vertically integrated change of the Eady growth rate (Figs. 3.3g-i and 3.4g-i) is not predicting very well the net response of the eddies.

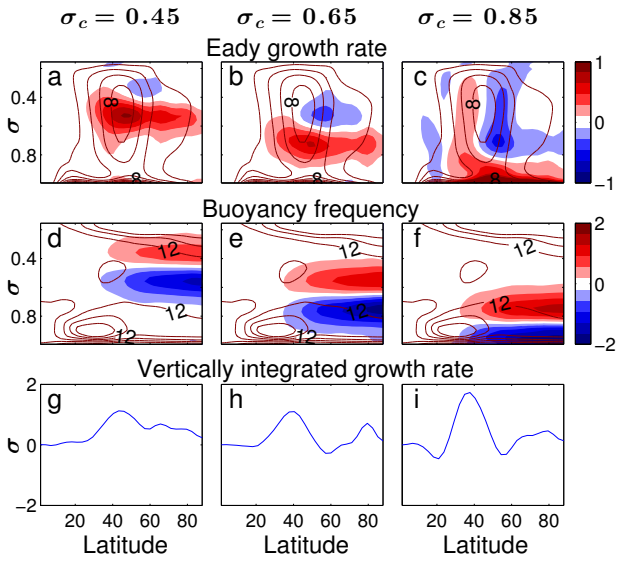

Figure 3.3: The Eady growth rate (a-c), buoyancy frequencey (d-f) and vertically integrated Eady growth rate change (g-i) for three different simulation where the level at which the meridional temperaure gradient was modified with a percentile change of $x = 0.05$ (method described in section 2.3.1). Contours show the reference fields and colors show the deviation from the reference. Contours intervals are 2×10^{-6} s^{-1} for the Eady growth rate and 4×10^{-3} s^{-1} for the buoyancy frequency.

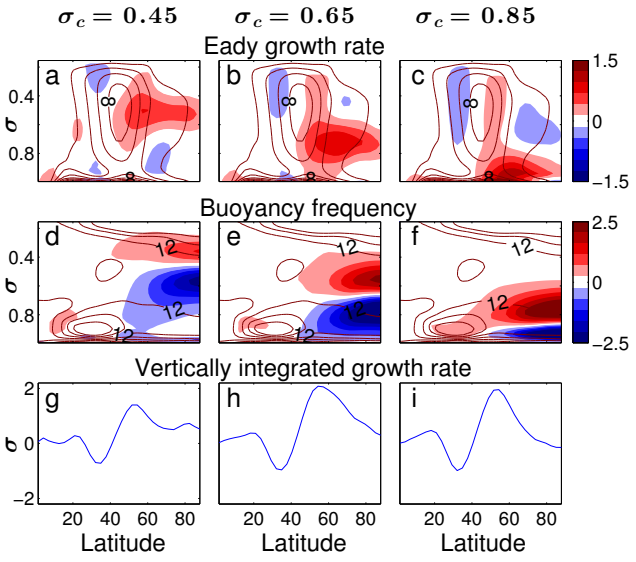

Figure 3.4: The Eady growth rate (a-c), buoyancy frequencey (d-f) and vertical mean Eady growth rate (g-i) for three different simulation where the level at which the diabatic heating was modified with $A = -2$ K (method described in section 2.3.3). Contours show the reference fields and colors show the deviation from the reference. Contours intervals are 2×10^{-6} s^{-1} for the Eady growth rate and 4×10^{-3} s^{-1} for the buoyancy frequency.

3.2.2 Changes in the meridional shear - the barotropic governor

When the vertical structure of the temperature profile is modified in our experiments, also the meridional shear of the wind is modified. It was demonstrated in many studies that changes in the barotropic meridional shear of the flow can affect baroclinic growth and barotropic conversion of eddies (e.g., James and Gray, 1986; James, 1987; Hartmann and Zuercher, 1998;

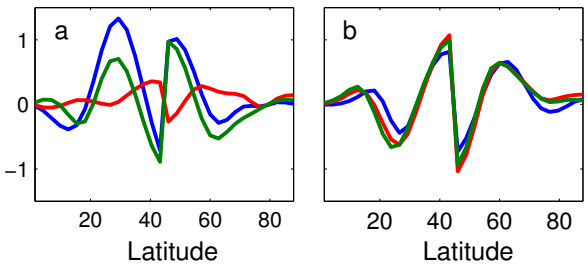

Figure 3.5: The mean change in the barotropic (mean) shear magnitude (10^{-6} s^{-1}) for (a) simulation where the temperature gradient was modified in different σ_c levels and a precentile change $x = 0.05$ and (b) simulation where the diabatic heating was applied in different σ_c levels and $A = -2$ K. Blue, red and green are experiments using $\sigma_c = 0.45, 0.65$ and 0.85, respectively.

Chen et al., 2007). In order to understand if the eddy response in the experiments presented in this paper is mainly as a result of changes in the vertical structure of baroclinicity or as a result of changes in the meridional shear of the flow, the change in the amplitude of the barotropic (mean) shear ($|\int \partial_y u dp/\int dp|$ - $|\int \partial_y u^{\text{ref}} dp/\int dp|$) is shown in Fig. 3.5. In the case where the temperature profile was modified (Fig. 3.5a), the mean shear magnitude increase is largest when the upper troposphere is modified, which according to the barotropic governor mechanism, it is expected to weaken the eddies. This mechanism is competing with the fact that the vertical shear was increased in these simulations. If the barotropic governor is playing an important role, it is expected that in the case of upper baroclinicity changes the eddy activity changes will be less than in the case of lower/mid tropospheric baroclinicity changes since the increased barotropic shear tend to decrease eddy activity. As demonstrated in the next sections, the changes in eddy activity are largest when the upper baroclinicity is modified (Fig. 3.6), implying that the barotropic governor plays a less important role than the changes in the vertical structure of baroclinicity. In case that the diabatic heating was controlled (Fig. 3.5b) the magnitude change in the barotropic shear in all simulations is very similar. As demonstrated in the next sections, the changes in eddy activity are significantly larger when the heating in the upper troposphere is modified (Fig. 3.7), implying again, that in the simulations presented in this chapter, the changes in the barotropic shear play a smaller role in the eddy response than the vertical structure of baroclinicity.

3.2.3 Eddy fluxes and eddy kinetic energy

In figures 3.6 and 3.7 , the eddy kinetic energy (a-c), eddy momentum flux (d-f) and eddy heat flux (g-i) are plotted for simulations where the temperature gradient was modified at different levels (Fig. 3.6), and for simulations where diabatic sources where added at different levels (Fig. 3.7).

When the temperature gradient (Fig. 3.6) or the diabatic heating gradient (Fig. 3.7) is increased in the upper troposphere, the eddy activity is modified significantly more than in cases where the temperature gradient/the diabatic heating is increased in the mid/lower troposphere.

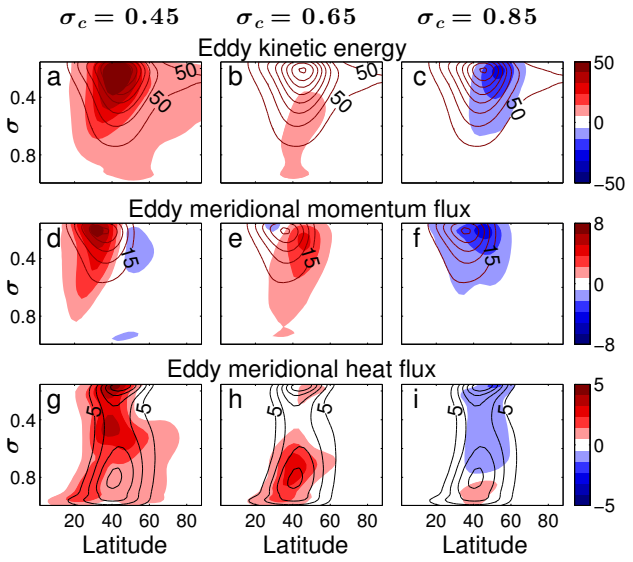

Figure 3.6: The EKE (a-c), eddy momentum flux - $\overline{u'v'}$ (d-f) and eddy heat flux - $\overline{v'T'}$ (g-i) for three different simulation where the level at which the meridional temperaure gradient was modified with a percentile gradient change $x = 0.05$ (method described in section 2.3.1). Contours show the reference fields and colors show the deviation from the reference. Contours intervals are 50 m^2 s^{-2} for the EKE, 15 m^2 s^{-2} for the momentum flux and 5 K m s^{-1} for the heat flux.

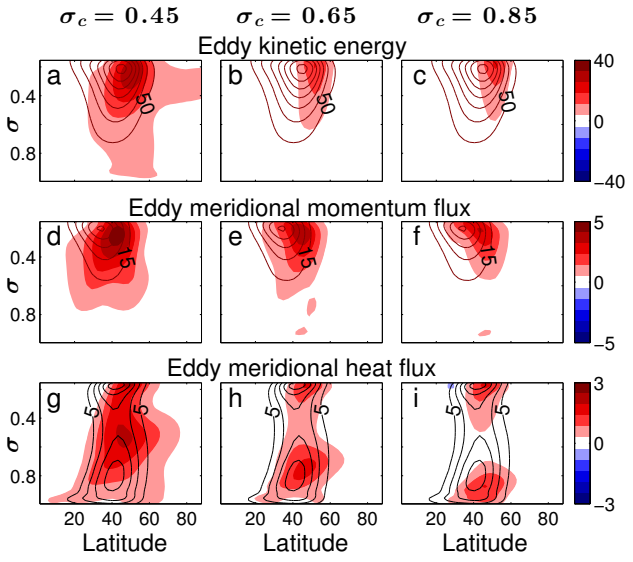

Figure 3.7: The EKE (a-c), eddy momentum flux - $u'v'$ (d-f) and eddy heat flux - $v'T'$ (g-i) for three different simulation where the diabatic heating was applied in different σ_c levels and $A = -2$ K. Contours show the reference fields while colors show the deviation from the reference. Contours intervals are 50 m^2 s^{-2} for the EKE, 15 m^2 s^{-2} for the momentum flux and 5 K m s^{-1} for the heat flux.

Furthermore, the change in the eddy activity does not always follow the amplitude change of the Eady growth rate (Fig. 3.3(g-i), Fig. 3.4(g-i)). For example, the eddy activity change is significantly larger when the diabatic sources are added in the upper troposphere than in the mid troposphere (compare Fig. 3.7a,d,g to Fig. 3.7b,e,h), but the vertically integrated Eady growth rate is larger when the diabatic sources are added in the mid troposphere than in the upper troposphere (3.4g,h). This implies that the vertical structure has a significant effect on eddy activity.

Interestingly, when the baroclinicity is modified in the mid/lower levels, the EKE response and eddy momentum flux response is maximal in the upper troposphere where it was maximal before the modification, and not at the level that the gradient was modified (see also discussion in Ait-Chaalal and Schneider, 2015). On the other hand, the eddy heat flux response is maximal at the level where the gradient was modified, although the response is generally more barotropic than the changes in EKE and momentum flux.

Surprisingly, for the case where the temperature change is prescribed (Fig. 3.6), when the temperature gradient is increased in the lower troposphere, the EKE is decreased. This reduction in EKE as a response to increase in meridional temperature gradient is not a robust effect and does not occur for all choices of the parameter $\delta\sigma$. This response also occurs in cases where the diabatic forcing is modified (as in section 2.3.3) for certain parameter choices (e.g., $\phi_d = 90$, not shown). Why a decreased temperature gradient in lower levels causes in certain cases an increased EKE requires further investigation, and might be related to different factors, such as modification in the jet characteristics, static stability changes or changes in the barotropic shear.[2] Nonetheless, such a decrease in EKE despite an increase in temperature gradients is also observed in nature during midwinter over the Pacific. This is further discussed in sections 3.3 and 3.5.

We next look at the change in the mean EKE over the baroclinic zone as a function of the level where the diabatic forcing was applied (Fig. 3.8), and as a function of the heating amplitude for simulations where the diabatic heating gradient was modified (Fig. 3.9).[3] When the heating is applied at the lower levels ($\sigma_c > 0.65$), the mean EKE slowly increases with decreasing σ_c (Fig. 3.8). As the heating is applied at higher levels in the troposphere, the change of the EKE increases rapidly with decreasing σ_c untill the EKE reaches maximum when $\sigma_c = 0.35$ (a little below tropopause level). As the heating level is further increased above the tropopause ($\sigma_{\text{tropopause}} \approx 0.25$) the change in the EKE is reduced significantly. The EKE dependence on the diabatic heating amplitude in the amplitudes tested is roughly linear for a certain choice of σ_c (Fig. 3.9).

3.2.4 Zonal surface wind

Deviations from thermal wind balance appear mostly near the ground where surface friction is present. In the Ferrel cell, the surface wind is predicted to be proportional to the integrated eddy momentum divergence (Vallis, 2006). Fig. 3.10 shows the relation between the maximum of eddy momentum divergence change to the change of the surface wind for simulations where the temperature or diabatic heating was added at different levels.[4] The figure shows that there

[2] Changes in the barotropic shear are largest in the case that the upper troposphere is modified (Fig. 3.5), though the decrease in eddies is present when the lower baroclinicity is modified. Therefore, it is reasonable to assume that the barotropic shear is playing a smaller part than the vertical structure of baroclinicity in the changes of the eddy activity.

[3] The baroclinic zone is defined between the edge of the Hadley cell in our reference simulation (latitude 27°) and latitude 68°. The results of presented are not sensitive to changes in the definition of the baroclinic zone.

[4] The surface wind is defined as an average over the lower 3 levels of the model, and calculating the zonal wind and the momentum divergence as a meridional average of ±7.5° around the maximum in the divergence.

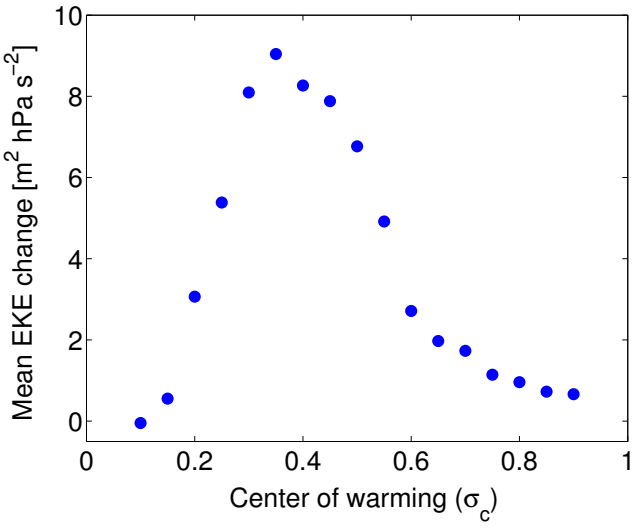

Figure 3.8: The mean EKE change over the baroclinic zone ($\int\int(u'^2+v'^2)-(u'^2_{\text{ref}}+v'^2_{\text{ref}})d\phi dp$) as a function of σ_c. The amplitude change in the diabatic heating is $A=-2$ K (see description in section 2.3.3).

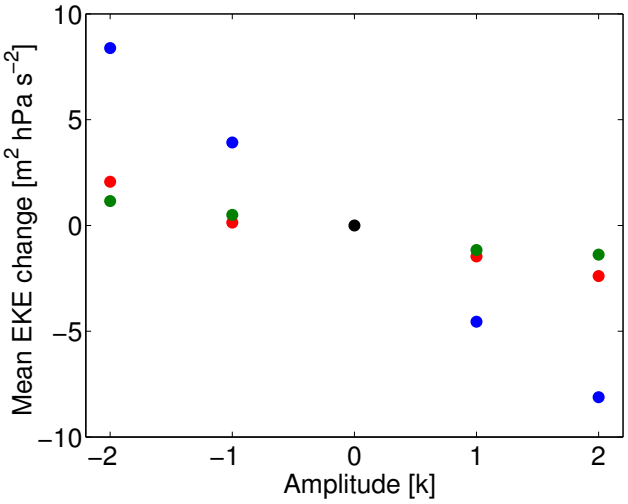

Figure 3.9: The mean EKE change over the baroclinic zone ($\int_{27^\circ}^{68^\circ}\int(u'^2+v'^2)-(u'^2_{\text{ref}}+v'^2_{\text{ref}})d\phi dp$) as a function of the amplitude change in the diabatic heating (see description in section 2.3.3). The black dot represents the reference run. Blue, red and green are experiments using $\sigma_c=0.45, 0.65$ and 0.85, respectively.

is a linear relation between the surface wind change and the vertically integrated momentum flux divergence change. Furthermore, it shows that in cases where the upper tropospheric baroclinicity is modified, the response of the surface wind is larger (compare the blue asterisk/dots to the red/green asterisk/dots). These results indicate that the surface zonal wind is mostly affected from upper tropospheric changes since the eddy activity is affected mostly from upper meridional temperature gradient.

3.3 Possible relation to the Pacific midwinter minimum

The results presented in section 3.2.3 showed that in some cases when the temperature gradient increases (decreases) in the lower troposphere, a decrease (increase) in the EKE is seen. This is opposed to what is predicted from linear theory, where instabilities (and hence EKE) are

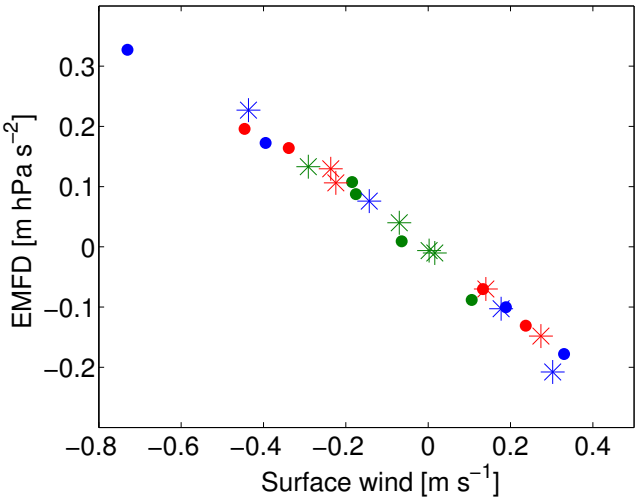

Figure 3.10: Integrated eddy momentum flux divergence change ($\int \partial_y(v'u')dp - \int \partial_y(v'_{\text{ref}}u'_{\text{ref}})dp$) as a function of surface wind change at the lattitude of maximal wind divergence. The asterics symbols are from predetermine temperature experiments (section 2.3.1) and dots are from diabatic heating modifications experiments (section 2.3.3). Blue, red and green are experiments using $\sigma_c = 0.45, 0.65$ and 0.85, respectively.

expected to strengthen with increased temperature gradient and jet strength (see Eq. 1.1). Nevertheless, such an increased temperature gradient that is accompanied with a decrease in EKE is observed on Earth during midwinter above the northern Pacific Ocean (Nakamura, 1992). This is counter-intuitive since the meridional temperature gradient is largest in January, but the EKE is at a local minimum during midwinter. There have been several proposed mechanisms for this phenomena, e.g., Chang, 2001; Harnik and Chang, 2004; Penny et al., 2010; Park et al., 2010.

We investigate in this section a possible connection between the midwinter minimum and the results presented in Fig. 3.6, which show that in certain cases an increased temperature gradient might lead to a decrease in the EKE. First, it is verified that the midwinter minimum can be reproduced using our idealized GCM. This is done by using the method described in section 2.3.1, which allows simulating the observed mean temperature profile above the Pacific Ocean in November, January and April (Fig. 3.11a-c).

The target temperature profiles for the different months were determined by averaging the NCEP /NCAR reanalysis temperature data between the years $1981 - 2010$ separately for each month of the climatology. Focusing on the Pacific basin we zonally averaged the data over longitudes above the Pacific ($160°\text{E} - 138°\text{W}$) such that the target temperature is zonally symmetric. The temperature profiles we got are very similar to the target temperature (maximal deviation from the target temperature is less than 1 K). The relaxation time in these simulation was $k_s = \frac{1}{4}\text{days}^{-1}$ as in Held and Suarez (1994) and $k_a = \frac{1}{20}\text{days}^{-1}$ which is twice than the Held and Suarez (1994).[5] Furthermore, A dry convection scheme with $\gamma = 0.9$ was used. The

[5] Also a uniform 7 days relaxation time and the relaxation time used in Held and Suarez (1994) were simulated and produced similar trends. The reason the relaxation temperature from Held and Suarez (1994) was modified is that one needs to run a much longer simulations in order to produce the target temperature profile accurately when using a long relaxation time in the upper troposphere as in Held and Suarez (1994). When using a uniform

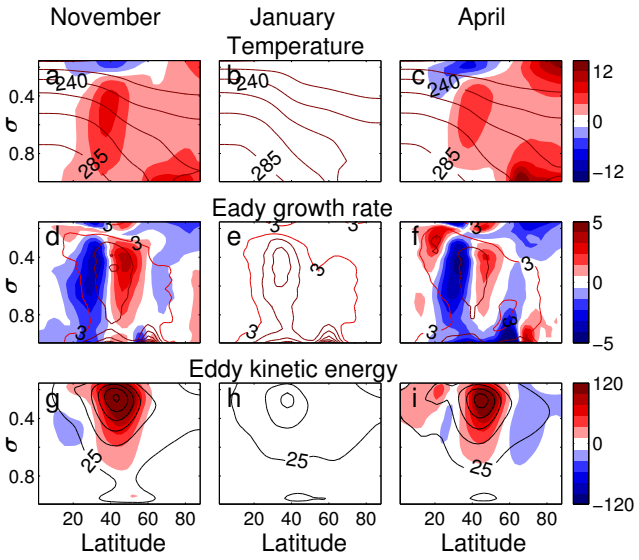

Figure 3.11: . The temperature (a-c), Eady growth rate (d-f) and the EKE (g-i) for November, January and April. Contours represents the value of the presented month while colors show the difference from January. Contours intervals are 15K for the temperature, 3×10^{-6} s^{-1} for the Eady growth rate and 50 m^2 s^{-2} for the EKE.

reason convection scheme is used in these simulations is because the mean temperature profile in the simulations that include a convection scheme had a better agreement with the target temperature. When a convection scheme is not included, the qualitative conclusions are similar though there are larger deviations from the target temperature.

When the different temperatures profiles above the Pacific are simulated, a minimum in the EKE is present in January (Fig. 3.11g-i). The fact that a minimum in the EKE appears in our simulations when using a January temperature profile, is an indication that the diabatic heating, which creates this temperature profile, is a key factor to the presence of the minimum in our simulations. We stress that though the temperature field in our simulations reproduce the mean temperature profile above the northern Pacific very accurately, the wind profile is different from observations due to surface winds which are not reproduced (away from the ground wind obey thermal wind relation). Furthermore, the EKE amplitude we obtain is different in magnitude from the observed one. When comparing the 3-10 band-pass filter of the EKE calculated from reanalysis data to the simulations presented in this paper (not shown), we find that the EKE obtained from the reanalysis data is larger (by a factor $1.5 - 2$). Chang (2006) found a similar trend and explained it by the fact that the mean state is neutrally stable (Hall and Sardeshmukh, 1998), and therefore eddies are relatively weak in the simulations. It is worth to mention that the magnitude of the EKE is strongly dependent on the choice of relaxation time and different choices of relaxation times, tend to change the frequencies at which the EKE peaks. Despite these differences, the main conclusion here relies on the fact that the trend in the EKE in our simulations shows a similar trend as in observations.

Next, in order to study the role of the lower/upper temperature gradient change in the

relaxation time of 7 days, the temperature in the simulation is more similar to the target temperature (less than 0.5K difference) but the EKE is much smaller due the fast relaxation in the upper troposphere.

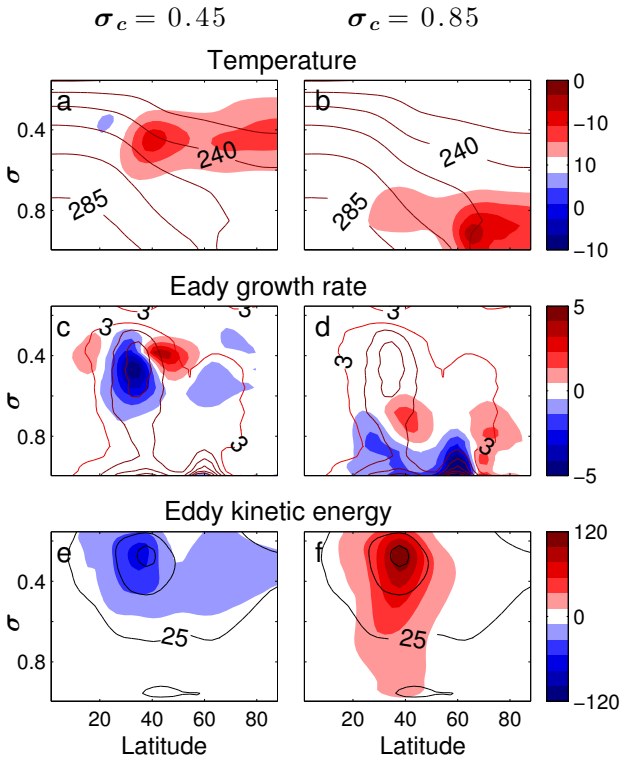

Figure 3.12: . The temperature (a-c), Eady growth rate (d-f) and the EKE (g-i) using the target temperature from equation 3.3 with $\sigma_c = 0.45, 0.85$. Contours represents the value of January fields and colors show the difference from January. Contours intervals are 15 K for the temperature, 3×10^{-6} s^{-1} for the Eady growth rate and 50 m^2 s^{-2} for the EKE.

emergence of the minimum, the January temperature profile is modified, such that the lower or upper temperature field is taken to be April-like. Namely,

$$T_{\text{target}} = T_{\text{Jan}} + (T_{\text{Apr}} - T_{\text{Jan}}) \exp[\frac{(\sigma - \sigma_c)^2}{2\delta\sigma^2}], \tag{3.3}$$

where T_{Jan}, T_{Apr} are the mean temperature fields above the Pacific in January an April respectively. When $\sigma_c = 0.85$ ($\sigma_c = 0.45$), the lower (the upper) temperature field is modified to be April-like while the other levels are January-like. Fig. 3.12 shows the temperature profile, Eady growth rate and EKE for simulations using the target temperature from equation 3.3. Notice that the EKE is increased when the lower tropospheric temperature gradient is decreased, and it is decreased when the upper temperature profile is modified (compared to normal January). This result is consistent with the results shown in Fig. 3.6 where the EKE decreased (increased) when the temperature gradient increased in the lower (upper) tropospheric levels. The results from Fig. 3.12 suggest that a possible contribution to the midwinter minimum is an increased temperature gradient in lower tropospheric levels during midwinter (or alternatively, the modification in the lower tropospheric temperature field). The increase in lower tropospheric temperature gradient is probably not the sole reason for the minimum seen in our simulations, and other contributions such as increased static stability and the fact that in some regions the temperature gradient increases (although the mean decreases), might play an important role.

3.4 Sensitivity to diabatic heating

The method presented in this chapter permits simulating a prescribed temperature field. However, it is possible that simulations with different parameters have the same temperature field but different eddy activity (see EKE in Fig. 2.2). Therefore, an essential issue is to determine to what extent the temperature profile determines the circulation. In classical eddy-mean flow problems the temperature profile is assumed to be given and the circulation properties are derived from the given temperature field (e.g., the Eady problem). The approach used in this chapter was similar. Eddy activity responses to different temperature profiles were studied. This approach was motivated by the assumption that eddy activity differences are primarily caused due to the different temperature profiles, with the underlying assumption that the diabatic forcing plays a direct role in determining the temperature profile, but the diabatic forcing does not play a direct role in determining the eddy properties. If the diabatic forcing has a direct effect on the circulation, the knowledge regarding temperature distribution alone is not enough to deduct robust conclusions regarding the circulation. For example, the result that in some of our simulations, the EKE was decreased (increased) as a response to increased (decreased) lower tropospheric temperature gradient suggests that the temperature gradient (or Eady growth rate) may not be a sufficient measure for instabilities, and the diabatic heating plays an important role as well.

We note that the result that the upper tropospheric temperature gradient affects eddy activity more than the lower temperature gradient occurs also when using a the standard Held and Suarez (1994) relaxation temperature profile. Fig. 2.1(a-c) shows the temperature profile change to the relaxation temperature change plotted in Fig. 2.1(d-f). Fig. 2.1(g-i) shows the EKE response to these changes. Despite the fact that the temperature changes were much larger in the simulations where the mid or lower tropospheric temperatures were modified, the EKE response is on the same order of magnitude in all simulations. This implies that also in these simulations, where our method for determining the relaxation temperature was not used, the eddy activity is affected mostly from the temperature gradient in the upper troposphere.[6]

3.5 Summary and discussion

In this chapter the relative importance of the upper and lower tropospheric meridional temperature gradient for the magnitude of the EKE and eddy fluxes are investigated. The response of eddies to changes in the vertical structure of the temperature gradient is especially interesting since global circulation models suggest that as a result of greenhouse warming the lower tropospheric temperature gradient will decrease, where as the upper tropospheric temperature gradient will increase.

[6]Notice that the temperature response to modifications in the relaxation temperature is much larger in the lower troposphere than the upper troposphere (Fig. 2.1). Since the diabatic heating is $\propto \frac{T_{\text{relax}}-T}{\tau}$, the diabatic forcing added will be larger in the upper troposphere because the difference $T_{\text{relax}} - T$ is larger in the upper troposphere than the lower troposphere. An assumption that eddy activity is affected also by the diabatic heating and not only by the temperature field, could be consistent with most of our results.

An idealized GCM with a Newtonian cooling scheme allowed controlling the temperature profile to a good degree, which in turn allowed a comparison between cases where the lower and upper tropospheric temperature gradient was modified separately. Consistently, it was found that the eddy activity is affected mostly by changes in the upper temperature gradient changes. The results described in this chapter suggest that in a global warming scenario, the effects of increased upper-troposphere meridional temperature gradient will dominate the response of eddy activity resulting in a larger EKE. This is consistent the results of Wu et al. (2010) who used a more complex GCM. It should be noted that our conclusions rely on idealized temperature changes, while the temperature changes that are predicted to occur in global warming scenario have a more complicated structure (see chapter 8).

Chapter 4

Eddy sensitivity to upper-level baroclinicity: a linear model perspective

In this chapter we try to understand the results of chapter 3 and concentrate on the question of why upper-level baroclinicity affects more eddy activity. This question is crucial in order to understand whether the results of chapter 3, which showed that eddies are more sensitive to changes in the upper tropospheric gradient, are robust.

In order to understand whether the results of chapter 3 are robust, some general relation between the vertical structure of the shear and eddy quantities is needed. In atmospheric sciences as in other fields, the physical intuition we have is usually based on simple toy models that relate meaningful physical quantities. In order to get a relation between the vertical structure of the shear to eddy amplitudes we use a modified 1D Eady-like model that has a non uniform vertical shear (section. 4.1). In section 4.2 we expand the results to the case that the β effect is present. Furthermore, we show that the framework we use is consistent with the results of chapter 3 as well as with the results of previous studies (Held and O'Brien, 1992), that showed that the linear growth rate is more sensitive to lower level shear.

4.1 A linear model relating growth rate to non-uniform shear

The Eady growth rate[1] of the reference simulations used in chapter 3 is plotted in Fig. 3.3a and 3.4a. The maximum Eady growth rate of our reference state occurs at midlatitudes at a height of $\sigma \approx 0.45$. Fig. 4.1 shows that also on Earth's atmosphere the Eady growth rate is maximal in the mid-upper troposphere (the surface is excluded since the static stability is close to zero).

One possible reason for the large effect of the upper baroclinicity on eddy activity is that when modifying the temperature gradient at upper tropospheric levels, the region with maximal Eady growth rate is modified. If the most important region for growth of instabilities is the

[1] In the following discussion we refer to the Eady growth rate as the growth rate calculated from the standard Eady problem for every grid point as calculated in Eq. 1.1. In the previous chapter the Eady growth rate was used as a baroclinicity measure.

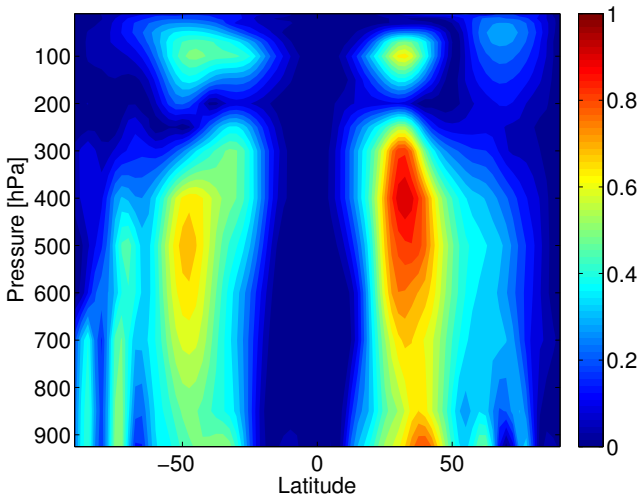

Figure 4.1: The zonal mean and time mean over DJF of the Eady growth rate$\times 10^5$ calculated from NCEP reanalysis data between 1981-2010.

region where the Eady growth rate is maximal locally, then we expect that the largest effect on eddy activity will be when this region's baroclinicity is modified. On the other hand, according to this hypotheses, modifying the temperature gradient at mid/lower tropospheric levels, modifies the Eady growth rate at tropospheric levels where the Eady growth rate is small, and therefore there is a weaker eddy response. To test this hypothesis, we develop a simple 1D Eady-like problem with piecewise linear shear, and demonstrate that indeed changes in the regions of maximal shear (i.e., maximal Eady growth rate) are those that have the largest effect on the growth rate.

One-dimensional Eady-like models were shown to be useful in various cases, for example, to study the effect of stratospheric shear on instabilities (Wittman et al., 2007; Muller, 1991), and the effect of changes in the static stability on instabilities (Blumen, 1979). Here it is demonstrated that if the shear is not uniform across the atmosphere, shear modifications in the layer that has a larger shear, has a larger effect on the growth rate than shear modifications in the layer that has a smaller shear. In section 3.2.1 it was demonstrated that changes in the temperature gradient in upper levels of the troposphere, where the Eady growth rate is larger, affect more eddy activity than temperature gradient changes in lower levels where the Eady growth rate is smaller. Although baroclinicity measures (such as the Eady growth rate) depend on both the shear and the static stability, in the Eady-like problem solved here only the wind shear is modified. Since the buoyancy frequency is constant in this 1D Eady-like problem, shear modifications are analogous to Eady growth rate changes in the GCM simulations. Furthermore, the calculated growth rate in the 1D Eady-like problem is analogous to the eddy activity in the simulations.

We consider two atmospheric sections, equal in depth, in which the static stability (N), density and wind shear are constant in each one of them. The two levels represent the upper and lower troposphere, and they differ only in their wind shear (γ_l, γ_u where subscript l and u are for the lower and upper levels, respectively). Since the Eady problem is well known, and a comprehensive mathematical development of the 1D quasi-geostrophic (QG) Eady problem

is given in standard textbooks (e.g., Pedlosky 1987; Vallis 2006) we give here only a short description of the mathematical equations. The troposphere is bounded below at $z = 0$. The two levels share a free interface at $z = h_1$, and the troposphere is bounded from above at $z = h_2$. We write the equations in terms of non-dimensional parameters which, are the horizontal coordinate $x^* = \frac{f_0}{Nh_1}x$, time $t^* = \frac{f_0\gamma_l}{N}t$, vertical coordinate $z^* = \frac{1}{h_1}z$, non-dimensional shear parameter $\gamma^* = \gamma_u/\gamma_l$ and a non-dimensional height parameter $h^* = h_2/h_1$, where f_0 is the Coriolis parameter and the starred parameters are dimensionless. The streamfunction in each layer obeys the QG potential vorticity equation, which can be expressed as the Laplace equation

$$\Psi_{x^*x^*} + \Psi_{y^*y^*} + \Psi_{z^*z^*} = 0, \tag{4.1}$$

where subscripts are derivatives. The surface ($z = 0$) and top ($z^* = h^*$) boundary conditions are that the vertical velocity is zero (Eqs. 4.2,4.3). The boundary conditions on the surface between the levels ($z^* = 1$) are that the pressure and vertical velocity are continuous (Eqs. 4.4,4.5). The boundary conditions are expressed as

$$(\Psi_{z^*t^*} - \Psi_{x^*})|_{z^*=0} = 0 \tag{4.2}$$

$$(\Psi_{z^*t^*} - \Psi_{z^*x^*} - \gamma^*\Psi_{z^*x^*} + h^*\gamma^*\Psi_{z^*x^*} - \gamma^*\Psi_{x^*})|_{z^*=h^*} = 0 \tag{4.3}$$

$$\Psi|_{z^*=1^-} = \Psi|_{z^*=1^+} \tag{4.4}$$

$$(\Psi_{z^*t^*} + \Psi_{z^*x^*} - \Psi_{x^*})|_{z^*=1^-} = (\Psi_{z^*t^*} + \Psi_{z^*x^*} - \gamma^*\Psi_{x^*})|_{z^*=1^+}. \tag{4.5}$$

In Fig. 4.2a the zonal velocity profiles of three different cases are plotted, and in Fig. 4.2b the corresponding growth rates are plotted. The solid line has a uniform shear as in the Eady problem ($\gamma = 0.002$ s^{-1}), while the dotted line and dashed lines show the solutions for cases that the mean shear is equal to the solid line, but the shear in the upper and lower levels are different ($\gamma_u = 0.002 \pm 0.0005$ s^{-1}, and $\gamma_l = 0.002 \mp 0.0005$ s^{-1}). The growth rates of the two cases of non-uniform shear are identical, hence it does not assist in differentiating between the contribution of the upper and lower level shear. Furthermore, this example shows that the mean shear does not determine the growth rate since the non-uniform cases has a larger growth rate than the uniform shear case.

In order to understand better the relative importance of the lower and upper levels we choose a reference state that has non-uniform shear (solid line in Fig. 4.2c). This case is analogous to the atmosphere state where the Eady growth rate is larger in the upper troposphere as in our simulations. The reference was modified such that the shear was reduced by 0.0005 s^{-1} in each layer separately, thus the mean shear for the two cases is equal, but in one case the upper level has the same shear as the reference (Fig. 4.2c, dashed line), and in the second case the lower section has the same shear as the reference (Fig. 4.2c, dotted line). Fig. 4.2d shows that the upper layer change affects the growth rate significantly more (the maximum of the dotted line is below the maximum of the dashed line). For wide range of parameters tested, it was found that when the shear is not uniform in the two regions, changing the shear in the region where

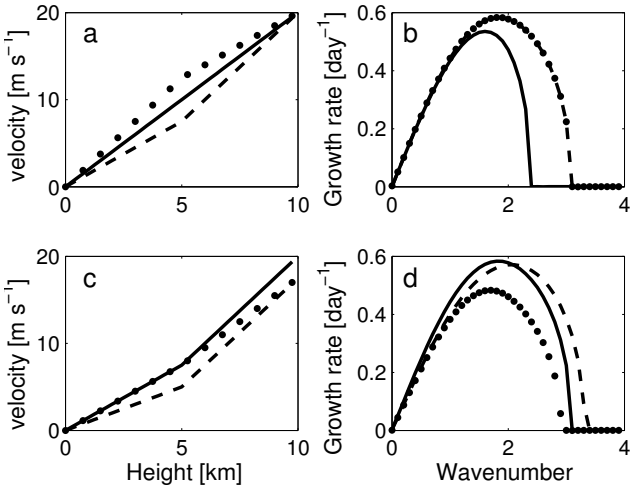

Figure 4.2: The vertical profile of the zonal wind specified to the 1D Eady-like problem (a and c). Growth rate as a function of rescaled wavenumber ($k* = \frac{NH}{f}k$) for the 1D modified problem (b are the results corresponding to the velocities in panel a and d to panel c). The solid, dashed and dotted lines are the reference shear, decreased lower shear and decreased upper shear, respectively.

the shear is larger affects the growth rate more than changing the shear in the region where the shear is smaller.[2]

We stress that the 1D problem can assist understanding the linear dynamics, but does not take into account any non-linear dynamics. Furthermore, the results presented here are different than previous results by Held and O'Brien (1992) and Pavan (1996), which used a QG model and found that EKE and eddy fluxes are more sensitive to changes in lower level baroclinicity. In the three level linear model used by Held and O'Brien (1992) they show that the growth rate of disturbances increases as the shear is more concentrated in the lower level, and decreases as the shear is more concentrated in the upper level, and they demonstrate that their QG model follows this result. The reason that their linear model gives a different prediction than the piecewise Eady model presented here is that they included the β effect. The β effect leads to a behavior that near linear shear, the growth rate increases as the shear is more concentrated in the lower level, and decreases as the shear is more concentrated in the upper level. However, in section 4.2 we show that this qualitative behavior of the growth rate is only correct in cases that there is no large concentration of shear (close to linear shear), which are the cases they investigated. In cases where the shear (or baroclinicity) is far from vertically uniform, one can show in a linear model that the growth rate increases as the shear is more concentrated in a specific region - as was shown qualitatively in the simple Eady model. The qualitative reason that the EKE is more sensitive to changes in upper baroclinicity in the simulations presented in chapter 3 is that the baroclinicity of the reference state we use is concentrated in the upper troposphere.

[2]The reason we choose to show the results in terms of the real parameters is that when rescaling the variables, the phase velocity is rescaled by the shear of one layer. Since we want to change each shear separately, the scale of the phase velocity would be different for different cases.

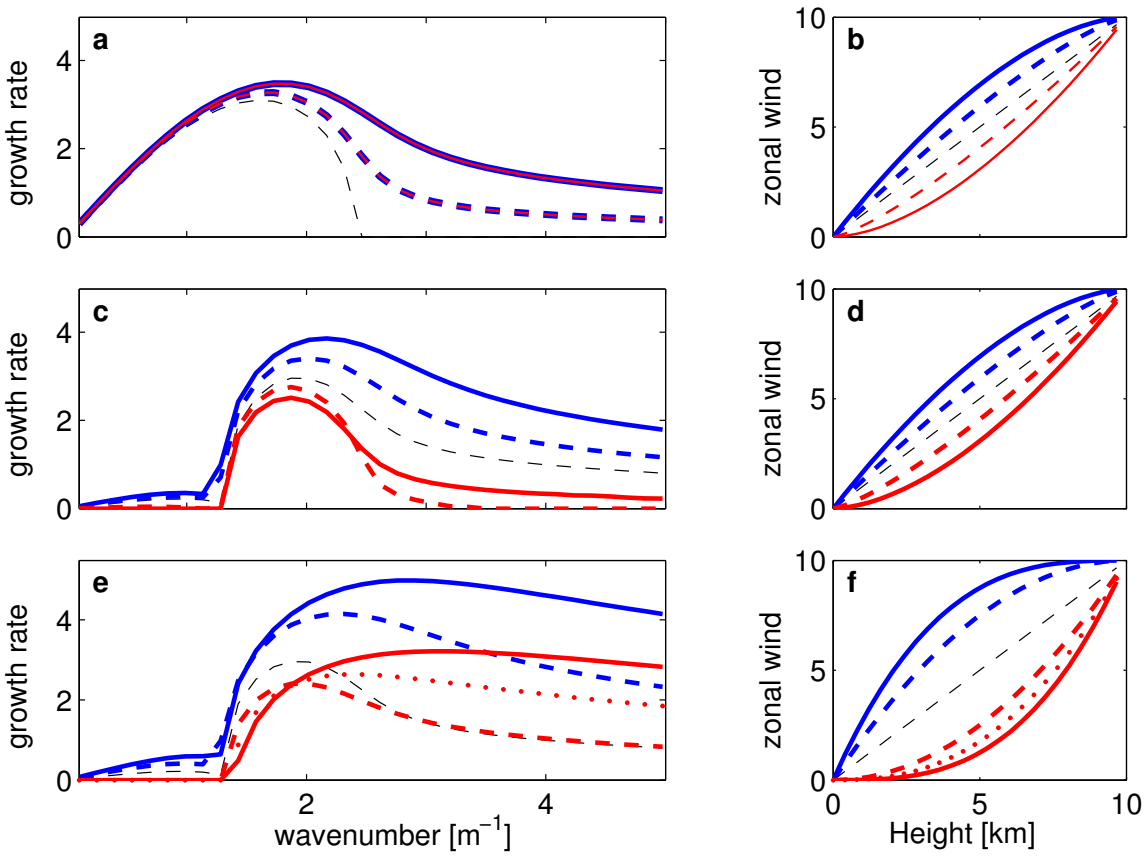

Figure 4.3: The growth rate as a function of the zonal wavenumber for different choices of shear and β (left) and the wind profiles as a function of height (right). Linear shear is in black ($n = 1$), lower shear concentration is in blue and upper shear concentration is in red. (a,b) $n = 1.3$ (dashed), $n = 1.7$ (solid) and $\beta = 0$; (c,d) $n = 1.3$ (dashed), $n = 1.7$ (solid) and $\beta = 10^{-11}\mathrm{s}^{-1}\mathrm{m}^{-1}$;(e,f) $n = 2$ (dashed), $n = 2.5$ (dotted), $n = 3$ (solid) and $\beta = 10^{-11}\mathrm{s}^{-1}\mathrm{m}^{-1}$.

4.2 Sensitivity of the linear growth rate to the vertical structure of wind shear

Held and O'Brien (1992) used a three layer QG model with the β plane approximation to study how eddies respond to changes in the vertical structure of the wind shear. Using linear instability analysis they showed that for wind shear that is concentrated in the lower layer of their model the growth rate is larger than when it is concentrated in the upper layer for the same mean shear. On the other hand, in section 4.1 (and in Yuval and Kaspi, 2016) we showed that the maximal growth rate for an Eady-like model with stepwise shear, is mostly sensitive to shear concentration, and demonstrated that when the shear is predominantly concentrated in the upper level, the growth rate is more sensitive to changes in the upper level shear.

Here it is demonstrated in a simple 1D Eady-like model, that the results of Held and O'Brien (1992) and section 4.1 can coexist. The invicid QG potential vorticity (PV) equation, linearized about the local mean state characterized by the zonal mean $U = U(z)$ is used with a constant static stability N^2. The mean PV gradient can be written as $\partial_y Q = \beta - \partial_z(\frac{f^2}{N^2}U_z)$ with $\beta = 2\Omega R\cos(\theta)$ where R is the radius, Ω is the rotation rate and subscripts denote derivatives.

In order to solve the linear growth rate for different mean states, the method introduced by Smith (2007) is used, and details of the numerical scheme can be found there. All the mean states used depend only on the vertical coordinate, and the obtained growth rates are for a 1D problem.

To take into account shear profiles that are concentrated in the lower/upper region of the troposphere, the following wind profiles are considered:

$$U_{\rm up} = U_{\rm top}\frac{z^n}{H^n} \tag{4.6}$$

and

$$U_{\rm low} = U_{\rm top} - U_{\rm top}\frac{(H-z)^n}{H^n}, \tag{4.7}$$

where H is the upper level of the model, which is taken it to be $H = 10$km, $U_{\rm top} = 10\,{\rm m\,s^{-1}}$ is the wind at the upper level. $U_{\rm up}$ is the case that the shear is concentrated in the upper atmosphere and $U_{\rm low}$ is the case the wind is concentrated in the lower atmosphere. The parameter n controls the shear concentration, and is taken to be larger or equal to 1. The constant shear problem (Eady problem) is the case where $n = 1$.

Fig. 4.3(a,b) shows the growth rates and wind profiles for different choices of shear, with $\beta = 0$. It is evident that the growth rate is sensitive to the concentration of baroclinicity, but the growth rate is affected similarly for lower and upper concentration. This result is qualitatively similar to the result obtained by section 4.1, where for an Eady-like model with two different shears and $\beta = 0$, the growth rate was increased when the shear was more concentrated, regardless of the layer it was concentrated at.

Fig. 4.3(c,d) shows the growth rates for shear profiles that are concentrated in the upper and lower levels, with $\beta = 10^{-11}{\rm s^{-1}m^{-1}}$. The figure shows that for moderate shear concentration (n close to one), in the presence of the β effect, a larger shear concentration at the lower levels increases the maximal growth rate, while larger shear concentration in the upper levels decreases the maximal growth rate.[3] This result is similar to the result introduced in Held and O'Brien (1992) (see figure 1 there). For all the cases tested, it was found that for similar mean shear, an increase in the shear concentration in the lower levels leads to increase in the maximal growth rate.

On the other hand, the reduction in the growth rate as we concentrate the shear more and more in the upper level does not hold when the shear concentration becomes larger. Fig. 4.3(e,f) shows that when the shear is largely concentrated in the upper region, an increased shear in the upper levels tends to increase the growth rate. To see this, we take the red dots in Fig. 4.3e as the reference state ($n = 2.5$), and increase the upper shear to a state described by the solid red line ($n = 3$), which has a larger maximal growth rate (Fig. 4.3e,f). On the other hand, an increase in the lower level shear concentration (described by the dashed red line, $n = 2$) has a smaller maximal growth rate than the dotted line. Finally, we conclude that

[3]The existence of a region that an increased shear in the upper regions decreases the growth rate depends on the exact parameters used in the model - see also Fig. 4.4.

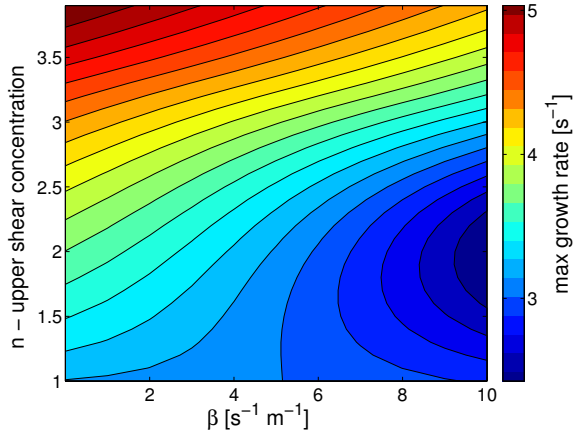

Figure 4.4: The maximal growth rate ($\times 10^6$) as a function of β ($\times 10^{12}$) and the upper shear concentration n (see equation 4.6).

for a state that has a large shear concentration in the upper levels, a further increase in the upper shear concentration in the upper levels (while keeping a constant mean shear, meaning a decrease in the lower level shear) will increase the growth rate, while an increase in the lower level shear concentration in the lower levels (accompanied with a decrease in the upper level shear) will decrease the maximal growth rate.

To sum up the results, Fig. 4.4 shows the maximal growth rate as a function of the upper shear concentration (the power n in Eq. 4.6) and β for thirty different values of n and eleven different values of β. This figure demonstrates that in the presence of large enough β, the concentration of shear in the upper levels has a non-monotonic relation with the growth rate. The values of β at Earth's extratropics ($\beta \approx 10^{-11}\mathrm{m}^{-1}\ \mathrm{s}^{-1}$ at latitude $\phi = 60°$) are in the regime where the growth rate is a non-monotonic function of the shear concentration (Fig. 4.4), and this non-monotonicity explains the discrepancy between the two models. For a constant height (H), the ratio between the upper level wind and β is the dominant factor that determines if the growth rate is a non-monotonic function of the upper shear. The results shown here demonstrate that when the vertical mean shear is constant, upper shear concentration can decrease the maximal growth rate as obtained by Held and O'Brien (1992) in cases that the shear concentration is relatively small (Fig. 4.3c). On the other hand, in cases where the upper shear concentration is large and the mean vertical shear is constant, the maximal Eady growth rate increases when the upper shear is increased even more and decreases when lower shear is increased (similar to section 4.1).

Chapter 5

The effect of vertical baroclinicity concentration on atmospheric macroturbulence scaling relations

Studies by Schneider and Walker (2008) and O'Gorman and Schneider (2008) showed that for a wide range of parameters, idealized GCM simulations follow semi-empirical scaling laws relating linearly the EKE and eddy fluxes to the MAPE derived by Lorenz (1955). In this chapter, the validity of this linear scaling, and the response of eddies to changes in the vertical structure of the lapse rate and the meridional temperature gradient are investigated.

In order to investigate how a meridional temperature gradient concentration affects eddies and the relation between EKE, eddy fluxes and MAPE, the meridional temperature gradient was systematically modified at different latitudinal regions in the baroclinic zone. This allows the meridional temperature gradient to be modified, while keeping the lapse rate constant and the vertical structure unchanged, testing the sensitivity of eddies to changes in the meridional gradient alone in regions where baroclinicity is large. This chapter broadens the results introduced in chapter 3 that studied the sensitivity of eddies to changes in the vertical structure of baroclinicity as a result of changes in the meridional temperature gradient, but did not study the response of eddies to changes in the lapse rate or meridional structure changes in the meridional temperature gradient.

Since MAPE is not a local quantity (Lorenz, 1955), and the temperature modifications introduced to the simulations are local, a local measure of instability is needed in order to discuss how the structure of the temperature field affects eddies. As in other studies, the Eady growth rate is used as a local baroclinic instability measure to evaluate changes in baroclinicity of the mean state (e.g., Hoskins and Valdes, 1990; Lorenz and Hartmann, 2001; Wu et al., 2010). The use of the Eady growth rate as a baroclinicity measure assists in discussing qualitative changes in the simulations, and it is not expected that a local large Eady growth rate would necessarily mean a large local EKE. The use of the Eady growth rate is problematic because (a) it is a linear growth rate of an idealized one dimensional problem with no horizontal spatial dependence, and the real growth rate might differ from the Eady growth rate; (b) in the simulations we

calculate the saturated EKE and not the growth rate, and there is no a priory reason that the linear growth rate is necessarily correlated with the saturated EKE that depends on nonlinear processes. Despite these limitations we find the Eady growth rate as a useful local measure of instability. Other measures of instability such as supercriticality (Held and Larichev, 1996), which are also a function of the meridional temperature gradient divided by static stability ($\propto \frac{\partial_y T}{N}$, where N is the Brunt-Väisälä frequency), will not make a qualitative difference since the Eady growth rate has similar dependence on the meridional temperature gradient and static stability.

The chapter is organized as follows. The relaxation temperatures we use are described in sections 5.1.1, 5.1.2 and 5.1.3. The details of MAPE and eddy fields calculations are found in section 5.1.4. In section 5.2 - the results of the simulations are presented, particularly focusing on the relation between EKE, EHF, EMF and changes in the mean temperature profile and MAPE, and in section 5.3 the results are discussed and summarized.

5.1 Temperature profiles in the simulations

In order to study how the vertical structure of baroclinicity changes the relation between MAPE, EKE and eddy fluxes, the meridional and vertical temperature gradient are modified systematically using the diabatic heating scheme described in section 2.3.2. The temperature modifications simulated are of three types:

- Changes in the meridional temperature gradient at different levels of the troposphere (see section 5.1.1). These temperature changes also induce changes in the lapse rate.
- Changes in the vertical temperature gradient (i.e., lapse rate) at different levels of the troposphere, while keeping the meridional temperature gradient constant (see section 5.1.2).
- Changes in the meridional temperature gradient at different latitudes within the baroclinic region, while keeping the lapse rate unchanged (see section 5.1.3).

Throughout this section, the reference temperature (T_{ref}) is the equilibrium temperature structure of a simulation performed using Held and Suarez (1994) forcing including a dry convection scheme that relaxes the atmosphere to a lapse rate of 0.7 Γ_{dry}, where $\Gamma_{\mathrm{dry}} = g/c_p$ is the dry adiabatic lapse rate. The reference temperature profile is obtained using a simulation with a convection scheme in order to enable changing the lapse rate without creating statically unstable sections of the atmosphere. There is no convection scheme in any other simulation in this study.

5.1.1 Changes in the vertical structure - changes in meridional gradient and lapse rate

The meridional temperature gradient of the reference run ($\partial_y T_{\mathrm{ref}}$) was modified only outside of the tropical region (poleward of latitude 24°), as described in section 3.1.1.

The parameters used in the simulations are $x = 0, \pm 0.05, \pm 0.10, \pm 0.15, \pm 0.20, \pm 0.25$ for $\sigma_c = 0.45, 0.65, 0.75, 0.85$ and $\delta\sigma = 0.1$ and $\delta\sigma \to \infty$ (when $\delta\sigma \to \infty$ the temperature gradient modifications are in all atmospheric levels). In Fig. 5.1(a-d) the temperature changes are presented in color for simulations where the temperature gradient was increased by 10 percent in the upper, mid, and lower troposphere (Fig. 5.1a-c), and when the temperature gradient was modified in all atmospheric levels (Fig. 5.1d). Results are presented relative to the reference.

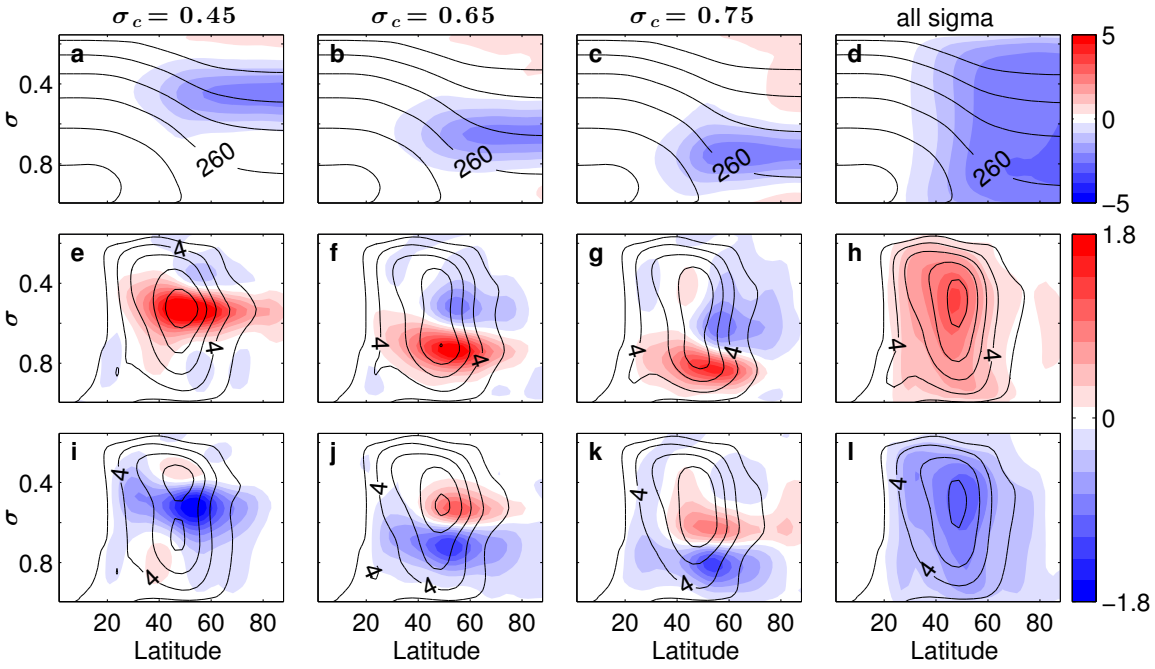

Figure 5.1: The temperature (a-d) and the Eady growth rate $\times 10^6$ (e-l) for simulations where the temperature gradient was increased (a-h)/decreased(i-l) by 10 percent in the upper (a,e,i), mid (b,f,j), lower troposphere (c,g,k) and in all levels of the atmosphere (d,h,l). Contours show the temperature and the Eady growth rate, and colors show the deviation from the reference simulation. The contour intervals are 15 K (temperature), and 2 s^{-1} (Eady growth rate).

Since the meridional temperature gradient is modified by an amount which is proportional to the reference over the target region, regions with larger temperature gradient will be modified more, and this might play a role in the results. It was verified with another set of simulations (not shown) that the results of this study remains qualitatively the same also when the absolute value of the meridional temperature gradient is modified poleward of $\phi = 24°$.

5.1.2 Changes in the vertical structure - changes in the lapse rate

The temperature profile was modified such that the lapse rate was changed in chosen vertical levels in the following manner:

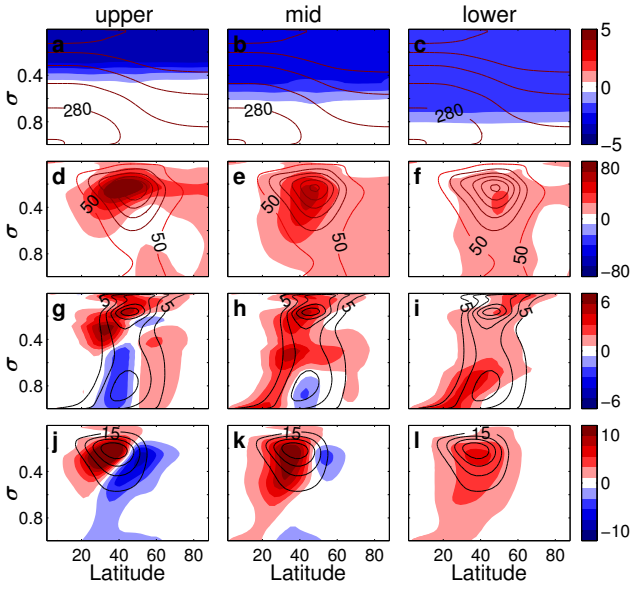

Figure 5.2: Temperature (a-c), EKE (d-f), EHF (g-i), EMF (j-l) for simulations where the lapse rate was modified in the upper ($0.25 < \sigma < 0.45$), mid ($0.45 < \sigma < 0.65$) and lower ($0.65 < \sigma < 0.85$) troposphere by 1 K km^{-1}. Contours show the reference run values and the colors represents deviation from the reference. The contour intervals are 20K (temperature), 50 m^2 s^{-2} (EKE), 5 m K s^{-1} (EHF) and 15 m^2 s^{-2} (EMF).

$$
\begin{aligned}
&T_{\mathrm{R}}(\phi,\sigma) = \\
&T_{\mathrm{ref}}(\phi,\sigma) && \text{for } \sigma > \sigma_1 \\
&T_{\mathrm{ref}}(\phi,\sigma) - A(z(\sigma) - z(\sigma_1)) && \text{for } \sigma_1 > \sigma > \sigma_2 \\
&T_{\mathrm{ref}}(\phi,\sigma) - A(z(\sigma_2) - z(\sigma_1)) && \text{for } \sigma < \sigma_2,
\end{aligned}
$$

where $z(\sigma)$ is the averaged geopotential height of a σ surface and A is the change in the lapse rate between the levels σ_1 to σ_2. The parameters used in this study are $A = \pm 0.5, \pm 1, \pm 1.5, \pm 2$K km^{-1} for $(\sigma_1, \sigma_2) = [(0.45, 0.25), (0.55, 0.35), (0.65, 0.45), (0.75, 0.55), (0.85, 0.65), (0.95, 0.75), (0.99, 0.25)]$.[1] In Fig. 5.2(a-c) the changes in the temperature profiles (color) are plotted for cases where the lapse rate was modified in upper, mid and lower tropospheric levels. These temperature profile changes modify only the lapse rate and the mean temperature but not the meridional temperature gradient. The changes in the mean profile, occur above the level of σ_1.

To verify that changes in the mean temperature in upper levels of the simulations do not lead to qualitative changes in the results, temperature profiles where the mean temperature in the upper troposphere was constant and only the levels below σ_2 were modified were used,

[1] for $(\sigma_1, \sigma_2) = (0.99, 0.25)$ the simulations where $A = 1.5$, 2 are not plotted since the change in the MAPE for these simulations is much larger than the rest of the simulations, although the qualitative conclusions of this work apply also if these simulations are taken into consideration.

namely

$$
\begin{aligned}
&T_{\mathrm{R}}(\phi,\sigma) = \\
&T_{\mathrm{ref}}(\phi,\sigma) + A(z(\sigma_2) - z(\sigma_1)) && \text{for } \sigma > \sigma_1 \\
&T_{\mathrm{ref}}(\phi,\sigma) - A(z(\sigma) - z(\sigma_2)) && \text{for } \sigma_1 > \sigma > \sigma_2 \\
&T_{\mathrm{ref}}(\phi,\sigma) && \text{for } \sigma < \sigma_2.
\end{aligned}
$$

Since the modification in the mean temperature did not change the qualitative results of this study, these results are not shown.

5.1.3 Changes in the meridional structure - changes in the meridional temperature gradient alone

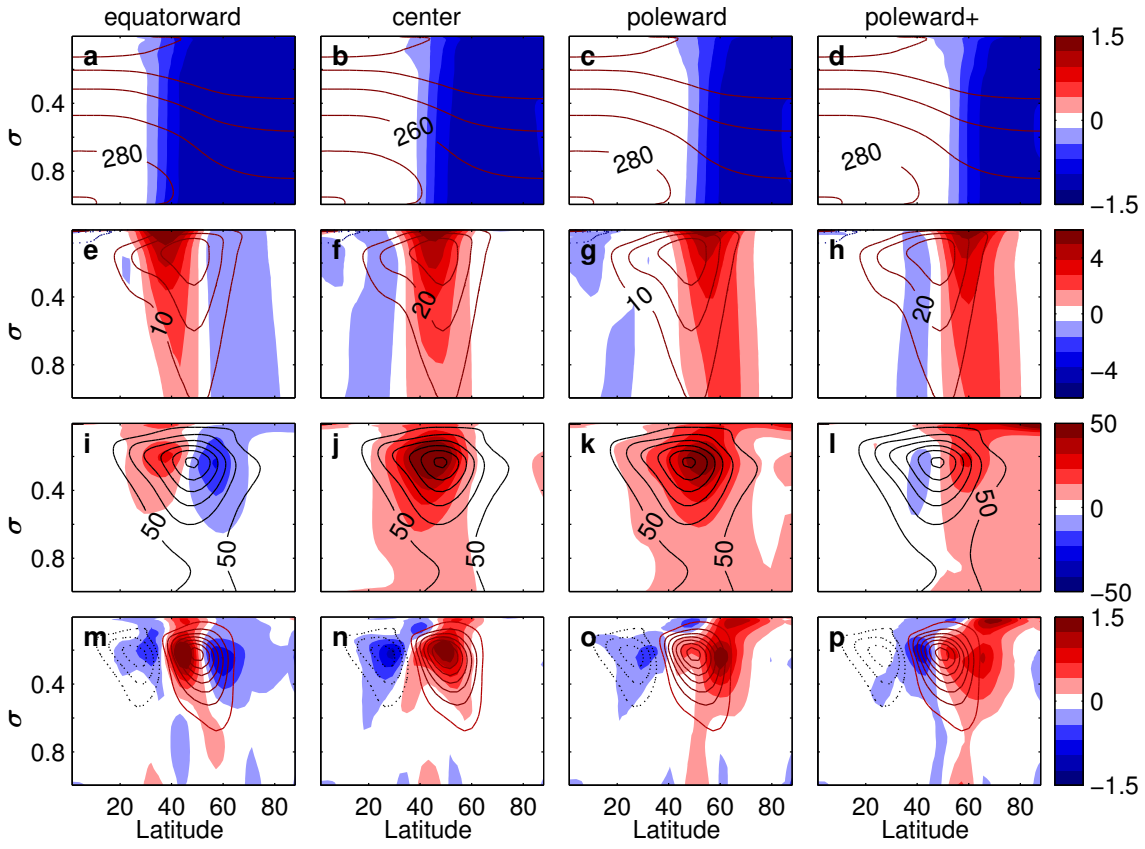

Figure 5.3: Temperature (a-d), zonal wind (e-h), EKE (i-l), EMF convergence $\times 10^5$ (m-p) for simulations that the meridional temperature gradient was modified equatorward of the center of the baroclinic zone $(29°, 40°)$, in the center of the baroclinic zone $(38°, 49°)$, poleward of the baroclinic zone center $(46°, 57°)$ and significantly poleward of the baroclinic zone center $(51°, 62°)$ by $\pm 1/11$ K degree^{-1}. Contours show the reference (dashed contours for negative values) run values and the colors represents deviation from the reference. The contour intervals are 20 K (temperature), 10 m s^{-1} (zonal wind), 50 m^2 s^{-2} (EKE) and 1 m s^{-2} (EMF convergence).

To isolate the effect on eddies of changes in the meridional temperature gradient from the changes in the lapse rate, the temperature gradient at different latitudes in the baroclinic zone

was modified in the following manner:

$$
\begin{aligned}
&T_{\mathrm{R}}(\phi,\sigma) = \\
&T_{\mathrm{ref}}(\phi,\sigma) && \text{for } \phi < \phi_1 \\
&T_{\mathrm{ref}}(\phi,\sigma) - B(\phi-\phi_1) && \text{for } \phi_1 < \phi < \phi_2 \\
&T_{\mathrm{ref}}(\phi,\sigma) - B(\phi_2-\phi_1) && \text{for } \phi > \phi_2,
\end{aligned}
$$

where ϕ is latitude, B is the change in the meridional temperature gradient between latitudes ϕ_1 to ϕ_2. The parameters used in this study are $B = \pm 1/11, \pm 2/11$K degree^{-1} and $(\phi_1, \phi_2) \approx [(29°, 40°),\ (35°, 46°),\ (38°, 49°),\ (40°, 51°),\ (43°, 54°),\ (46°, 57°),\ (48°, 59°),\ (51°, 62°)]$. In Fig. 5.3(a-d), 5.3(e-h) the changes in the temperature profiles and zonal wind (color) are plotted for cases where the temperature gradient was modified equatorward of the center of the baroclinic zone $(29°, 40°)$, in the center of the baroclinic zone $(38°, 49°)$, poleward of the baroclinic zone center $(46°, 57°)$ and significantly poleward of the baroclinic zone center $(51°, 62°)$.

Unlike the temperature modifications in sections 5.1.1 and 5.1.2, the vertical structure of the troposphere is not modified when applying these temperature changes. These temperature changes, modify the meridional structure of the temperature gradient without affecting the lapse rate. This allows for an investigation of how changes in the meridional temperature gradient structure affect eddies, and if the relation between EKE, eddy fluxes and MAPE is sensitive to the meridional structure of the temperature gradient.

5.1.4 Calculation of the MAPE

MAPE is calculated using the quadratic approximation of Lorenz (1955) in sigma coordinates. MAPE and integrated eddy quantities (EKE and eddy fluxes) are calculated in the baroclinic zone, which is defined as the region within 15° latitude of the maximum of the vertically integrated eddy heat flux, where the integral is performed from the level $\sigma_s = 0.95$, which is close to the surface, up to the tropopause ($\int_{\sigma_s}^{\sigma_t} \overline{v'\theta'}\cos(\phi)\mathrm{d}\sigma$).[2] The baroclonic zone, which is the region over which MAPE is calculated will vary slightly between experiments as the latitude of maximum vertically integrated eddy heat flux varies. Choosing the baroclinic zone to be fixed between $26° - 65°$ or $30° - 60°$ does not qualitatively change the results. The resulting expression for the MAPE per unit area is

$$
\mathrm{MAPE} = \int_{\sigma_\mathrm{t}}^{\sigma_\mathrm{s}} \frac{\mathrm{c_p p_0}}{2\mathrm{g}} \Gamma \left(\frac{\langle \bar{\mathrm{p}} \rangle}{\mathrm{p_0}}\right)^{\kappa} (\langle \bar{\theta}^2 \rangle - \langle \bar{\theta} \rangle^2) \mathrm{d}\sigma, \tag{5.1}
$$

where $\langle A \rangle$ is the average over the baroclinic zone of field A, c_p is the heat capacity, g is the gravitational acceleration, σ_t is the tropopause height in the baroclinic region, θ is the potential temperature, $p_0 = 10^5$ Pa is a reference pressure and $\Gamma = -\frac{\kappa}{\langle \bar{p} \rangle} \left\langle \frac{\partial \bar{\theta}}{\partial p} \right\rangle^{-1}$ is an inverse measure of static stability.

[2] The tropopause is defined as a level with zonal and time mean temperature lapse rate of 2K km^{-1}.

5.2 Results

The response of the eddy fields to changes in the vertical and meridional structure of baroclinicity is investigated, focusing mainly on the relation between the MAPE, EKE and eddy fluxes. Ideally, we would like to isolate the effects of changes in the vertical structure of the meridional and vertical temperature gradient on eddy fields. Modifying the vertical gradient (lapse rate) at chosen vertical levels without changing the meridional temperature gradient is possible, but changing the vertical structure of the meridional temperature gradient, leads to changes in lapse rate, and it is not possible to isolate the changes in the vertical structure of the meridional temperature gradient. Therefore, the effects of changes in the meridional temperature gradient on eddy fields are investigated in two different manners. The results are divided into three sections; (a) changes in the vertical structure of baroclinicity (section 5.2.1), where the meridional temperature gradient is changed at some atmospheric levels, and consequently also the vertical structure of the lapse rate is modified, but not the mean lapse rate (b) changes in the vertical structure of the lapse rate alone (section 5.2.2) and (c) changes in the meridional structure of the temperature gradient (section 5.2.3), where the meridional temperature gradient is modified without modifying the lapse rate, but the vertical structure of baroclinicity is not modified. The last section also reveals how changes in the meridional temperature gradient at different latitudes leads to very different changes in the eddy fields.

Throughout this chapter, eddies are defined as the deviation from zonal and time mean, and eddy energies and fluxes are calculated using an integral over the baroclinic zone. The EHF and EMF contain a $\cos\phi$ factor i.e., EHF $= \overline{v'\theta'\cos\phi}$ and EMF $= \overline{u'v'\cos\phi}$, where prime denotes the deviation from zonal and time mean.

5.2.1 Modifying the baroclinicity at chosen vertical levels

In Fig. 5.4 the EKE (a-c), EHF (d-f) and EMF (g-i) are plotted against the temperature gradient percent change, MAPE and EAPE for simulations where the meridional temperature gradient was modified at different levels. Several interesting features are seen in the figure: (a) Fig. 5.4(a,d,g) shows that eddies are more sensitive to changes in the meridional temperature gradient in the upper levels (blue dots) than in the mid-lower troposphere (red, magenta, and orange dots); (b) Fig. 5.4(a) shows that changing the temperature gradient in all vertical levels (grey dots), changes the EKE on the same order of magnitude as changing only the upper tropospheric levels (blue dots); (c) Fig. 5.4(a) shows that increasing (decreasing) the meridional temperature gradient in mid-lower tropospheric levels (red and magenta dots) cause a non-intuitive decrease (increase) in EKE, which is seen in Fig. 5.4(b) as a negative slope between EKE and MAPE; (d) Fig. 5.4(b) shows that each color has an approximate linear relationship between MAPE and EKE, but with a different slope, implying no universal relationship between MAPE and EKE. For example, the blue and grey dashed lines are the best linear fit for the blue and grey dots, and the slopes of these lines have almost a factor two difference (1.86 and 1.01); (e) Fig. 5.4(c) shows that the EKE and EAPE have an approximate linear relation;(f)

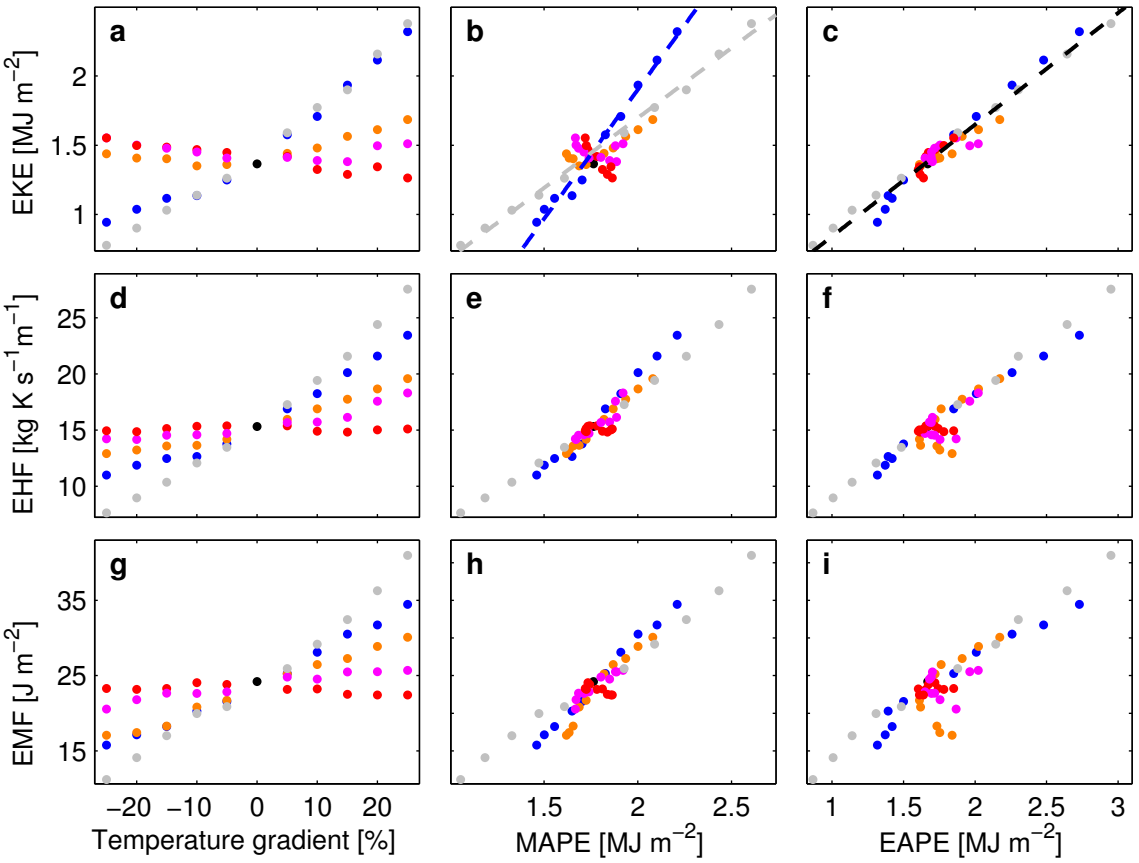

Figure 5.4: The EKE (a-c), EHF$\times 10^{-4}$ (d-f), EMF $\times\ 10^{-4}$ (g-i) as a function of the percent change in the meridional temperature gradient, MAPE and EAPE. The colors show different vertical levels of meridional temperature gradient change for the upper ($\sigma_c = 0.45$, blue), mid ($\sigma_c = 0.65$, orange), mid-lower ($\sigma_c = 0.75$, magenta), lower ($\sigma_c = 0.85$, red) and all levels of the troposphere (grey). The grey and blue dashed lines in panel b are linear fits for the grey and blue dots and have slopes of 1.01 and 1.86, respectively. The black dashed line in panel c is a fit to all the points and has a slope of 0.80.

Fig. 5.4(e,h) shows that eddy fluxes and MAPE have an approximate linear relation;(g) 5.4(f,i) shows that eddy fluxes and EAPE have noticeable deviations from linear scaling.

In order to understand the changes in the eddy fields, the changes in the local Eady growth rate ($\lambda = 0.31\frac{g}{NT}\left|\frac{\partial T}{\partial y}\right|$, Lindzen and Farrel, 1980), which is used as a measure for baroclinicity, are plotted in Fig. 5.1(e-l) for cases where the temperature gradient was modified by ± 10 percent (e-h, $x = 0.1$; i-l, $x = -0.1$). The Eady growth rate and the MAPE are affected by changes in both the static stability and the meridional temperature gradient. Increasing or decreasing the temperature gradient only in some levels of the troposphere (Fig. 5.1a-c), causes the static stability to increase in some regions and decrease in others. Therefore, the Eady growth rate can decrease (increase) in some regions even if the temperature gradient is increased (decreased), see Fig. 5.1(e-g) (decreased, i-k). Increasing (decreasing) the temperature gradient in all atmospheric levels, leads to an increase (decrease) in the Eady growth rate at all levels of the atmosphere since the static stability is approximately unchanged while the temperature gradient increases (decreases) at all levels (Fig. 5.1(h,l)).

In the reference simulation, the baroclinicity is concentrated in the mid-upper troposphere

(see Fig. 5.1h,l for the Eady growth rate when the gradient is modified at all levels, and the vertical structure is nearly unmodified). When changing the temperature gradient in the upper troposphere, the baroclinicity is modified in the region of maximal baroclinicity (Fig. 5.1e,i), which causes the largest change in the MAPE compared to other levels, and the response of the EKE and eddy fluxes is largest (blue dots in Fig. 5.4b).[3] When comparing two simulations with modified gradients, a larger MAPE change in one of the simulations does not necessarily mean a larger change in EKE of the simulation (e.g., compare the blue and grey dots in Fig. 5.4b). For example, in the simulation set considered in this section, the EKE is most sensitive to changes in MAPE when the upper tropospheric temperature gradient is modified. We conclude that there is no linear scaling with a unique slope relating between MAPE and EKE even when all parameters in the simulations (except the relaxation temperature) are similar. In Appendix D it is shown that the deviation from linear relation occurs also in the relation between EAPE and MAPE, implying that the closure suggested by Schneider and Walker (2008) is not robust for these simulations.

The decrease in EKE in response to an increase in the meridional temperature gradient in the mid-lower levels is surprising, although a decrease in EKE when the meridional temperature gradient increases is seen also in observations of the northern Pacific winter (Nakamura, 1992). Increasing the temperature gradient in the mid or lower troposphere (Fig. 5.1b-c), leads to an increase in the Eady growth rate on average, but it increases in the mid-lower levels where the reference baroclinicity is smaller, and decreases at higher levels where the reference baroclinicity is larger (Fig. 5.1e-f). On the other hand, decreasing the temperature gradient in the mid-lower troposphere, leads to a decrease in the mean baroclinicity, but the regions where it increases are of larger baroclinicity (Fig. 5.1j-k). Therefore, we hypothesize that the reason for the small increase in EKE when reducing the temperature gradient in the lower troposphere is the increased concentration of baroclinicity in the mid-upper levels.

Interestingly, the vertically integrated EHF and EMF have a smaller dependence on the changes in the vertical structure of baroclinicity and scale almost linearly with MAPE with the exception of modifying the gradient in lower levels (red dots, Fig. 5.4e,h). As shown in the next section, when changing the vertical structure of the lapse rate, the MAPE and eddy fluxes do not have linear relation.

5.2.2 Modifying the lapse rate at chosen vertical levels

In many studies that relate eddy fields to mean fields, the vertical structure of the lapse rate is not taken into account, and only the vertically averaged lapse rate is taken (e.g., Stone, 1972; Held, 1978). This is typically done because it enables one to deduce simple scaling relations. To understand to what extent the vertical structure of the lapse rate plays a role in affecting eddies and whether using the vertically mean lapse rate is sufficient when deriving scaling relations between eddies and mean quantities, the lapse rate was modified at different vertical levels

[3] When increasing (decreasing) the temperature gradient, the largest increase (decrease) in baroclinicity happens below this level because of the changes in the static stability (Fig. 5.1e-l).

separately.

In Fig. 5.5 the EKE (a-c), EHF (d-f) and EMF (g-i) are plotted as a function of the lapse rate amplitude change, MAPE and EAPE for simulations where the lapse rate was modified at different vertical levels as described in section 5.1.2. The main results are: (a) Changing the lapse rate with a certain amplitude at different vertical levels results in very different amplitude changes in EKE and eddy fluxes (Fig. 5.5a,d,g). This implies that the vertical structure of the lapse rate plays an important role in determining eddies' amplitude, and knowledge regarding the mean lapse rate is not sufficient in order to determine eddy amplitudes; (b) Fig. 5.5 shows that changing the lapse in all tropospheric levels induces the largest change in eddy quantities. This is expected, but underlined here since when the meridional temperature gradient is changed in all vertical levels, the change in eddies was not larger than when only the upper levels where modified (Fig. 5.4); (c) Increasing the lapse rate induces larger changes in the EKE than decreasing it (Fig. 5.5a)[4]; (d) Changes in the upper tropospheric lapse rate that lead to a large increase in EKE (Fig. 5.5a), do not increase significantly eddy fluxes (Fig. 5.5d,g - blue dots); (e) EKE and MAPE (Fig. 5.5b) as well as EKE and EAPE (Fig. 5.5c) have an approximate linear relation for these simulations; (f) MAPE and eddy fluxes do not have a linear relation in these simulations, and changes in the lower level lapse rate lead to a larger sensitivity in eddy fluxes to MAPE changes (see black dots' slope in Fig. 5.5e,h).

To explain why the EKE response is not symmetric when the lapse rate is modified, one can consider the fact that MAPE $\propto \mathrm{N}^{-1}$. Combining this with the approximate linear relation between the MAPE and the EKE shown in Fig. 5.5b results in the lapse rate increase inducing a larger EKE response than when decreasing it.

The relation between EKE and MAPE is approximately linear for all simulations in this section, regardless of the level that the lapse rate is modified at (see dashed line in Fig. 5.5b). When considering all simulations, the relation between eddy fluxes and MAPE is not linear, but when considering each color separately, there is an approximate linear relation between eddy fluxes and MAPE, where each color has a different slope relating eddy fluxes and MAPE.[5] As the lapse rate is modified in the upper region of the troposphere, the slope which approximately relates MAPE to eddy fluxes is smaller. This is most pronounced when the lapse rate is modified in the upper part of the troposphere (blue and dark green dots in Fig. 5.5e,h), where at certain simulations, eddy fluxes even reduce, though the MAPE has increased. The opposite response of EKE and eddy fluxes was also shown to be present in the ocean (Ferrari and Nikurashin, 2010).

To understand why the mean EHF and EMF have a weak response to changes in the lapse rate in the upper troposphere, the zonal mean EKE, EHF and EMF are plotted in Fig. 5.2 for simulations where the lapse rate was modified by 1 K km^{-1} in the lower, mid and upper troposphere. When the lapse rate is modified at the mid-upper levels, the eddy fluxes have

[4] Also eddy fluxes are more sensitive to increase in the lapse rate than its decrease in most cases (Fig. 5.5d,f).

[5] Schneider and Walker (2008) showed that the surface eddy heat flux ($\overline{v_s' \theta_s'}$) scales linearly with MAPE (see Eq. 9 in Schneider and Walker, 2008). Also plotting the surface EHF as a function of the MAPE does not give a linear relation between the two.

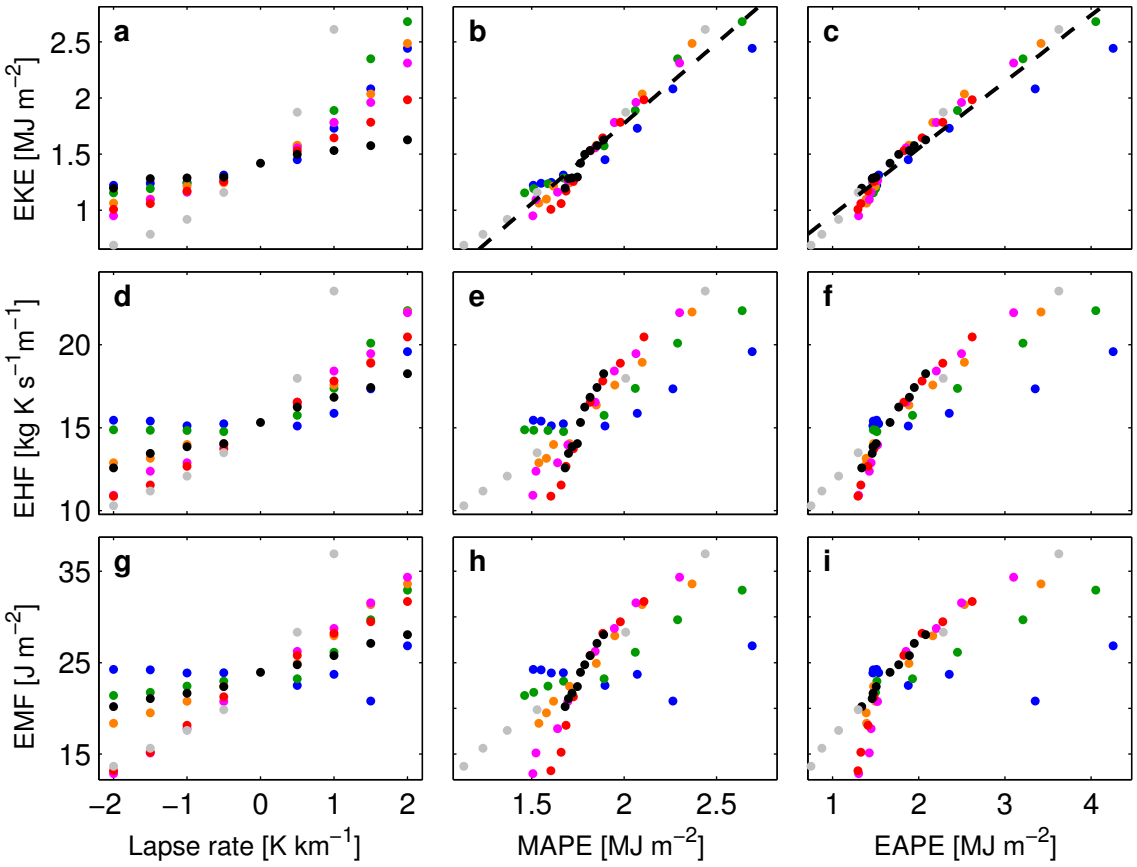

Figure 5.5: EKE (a-c), EHF$\times 10^{-4}$ (d-f) and EMF$\times 10^{-4}$ (g-i) as a function of the lapse rate change, MAPE and EAPE for different simulations where the lapse rate was modified at different vertical levels. The colors show different vertical levels of lapse rate change - in the upper ($0.25 < \sigma < 0.45$, blue; $0.35 < \sigma < 0.55$, dark green), mid ($0.45 < \sigma < 0.65$; orange, $0.55 < \sigma < 0.75$, magenta), lower ($0.65 < \sigma < 0.85$; red, $0.75 < \sigma < 0.95$, black), and throughout the troposphere ($0.25 < \sigma < 0.99$, grey). The black dashed line in panel b is the best linear fit for all the dots and has a slope of 1.42. The black dashed line in panel c is a fit to all the points and has a slope of 0.59.

a mixed response (weaken in some regions and strengthen in others). For example, when the lapse rate is modified at chosen sigma levels, EHF tends to increase at these levels and above them, while below these levels, it tends to decrease or to have a mixed response. Therefore, the integrated response of the EHF and EMF is relatively weak when the lapse rate is modified in the upper levels of the troposphere.

5.2.3 Changes in the meridional structure of the temperature gradient

In section 5.2.1 the vertical structure of the meridional temperature gradient was modified, and consequently also the lapse rate was modified. In this section only changes in the meridional temperature gradient at different latitudes are induced, but the vertical structure is not modified and the lapse rate remains unchanged (see also discussion on this in chapter 6). These changes allow investigation into how the meridional structure of the meridional temperature gradient

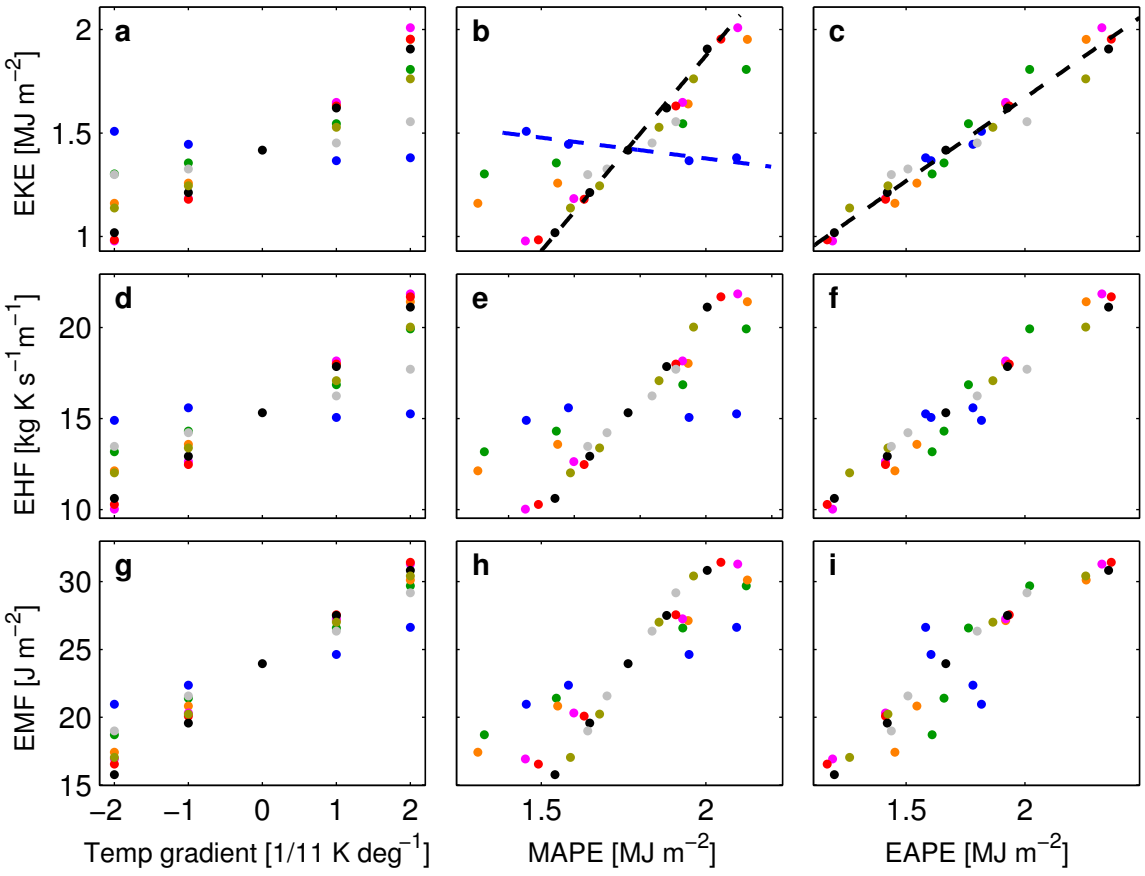

Figure 5.6: EKE (a-c), EHF$\times 10^{-4}$ (d-f), EMF$\times 10^{-4}$ (g-i) as a function of the meridional gradient change, MAPE and EAPE for different simulations where the gradient was modified at different latitudes. The temperature gradient was modified between different latitudes ($(29°, 40°)$ blue, $(35°, 46°)$ dark green, $(38°, 49°)$ orange, $(40°, 51°)$ magenta, $(43°, 54°)$ red, $(46°, 57°)$ black, $(48°, 59°)$ dark gray, $(51°, 62°)$ grey). The black and blue dashed lines in panel b are the best linear fit for the black and blue dots and have a slope of 1.88 and -0.2. The black dashed line in panel c is a fit to all the points and has a slope of 0.80.

alone affects eddies. In Fig. 5.6 the EKE (a-c), EHF (d-f) and EMF (g-i) are plotted as a function of the meridional gradient change, MAPE and EAPE for the simulations described in section 5.1.3. The center of the baroclinic zone is defined here to be the maximal vertically integrated EHF, and is found at latitude 43° in the reference simulation (and in most of the other simulations as well). It is found that EKE and eddy fluxes are more sensitive to changes in the meridional temperature gradient in the vicinity and slightly poleward of this latitude. Namely, the change in EKE and eddy fluxes is relatively small (and can be even negative) when the temperature gradient is concentrated equatorward of this region (blue dots), or if the change in the gradient is significantly poleward of this region (grey dots).

The simulations in this chapter are in a mixed subtropical-eddy driven jet regime, where the EMF convergence is negative a few degrees equatorward of the jet maximum decelerating it, and positive at the jet peak and at the poleward flank of the jet accelerating it (see Fig. 5.3). One possible explanation for the weak eddy response to increased temperature gradient at the equatorward flank of the jet, is that the shear is increased in regions where the jet is more

subtropical and the EMF diverge and decelerate the jet (or have a mixed effect on the jet, Fig. 5.3m). On the other hand, when the temperature gradient is increased close to the jet peak or slightly poleward (Fig. 5.3f,g), where the jet is more eddy driven, the baroclinicity is increased where eddies accelerate the jet, and the increased baroclinicity, tends to increase baroclinic eddies more (Fig. 5.3j,k,n,o). This explanation is consistent with the idea of Held (2000) that is based on the concept that the Hadley cell edge (which is similar to the subtropical jet core) is at the point the atmosphere becomes baroclinically unstable. Therefore, when increasing the temperature gradient in the region of the subtropical jet, where the atmosphere is stable, the effect on eddies is minor. These results are consistent with previous studies that showed that stronger sea surface temperature (SST) gradients close to the jet center, leads to a stronger eddy response than stronger SST gradients in regions that are significantly equatorward or poleward of this region (Brayshaw et al., 2008; Sampe et al., 2010), or other studies that showed that a strong subtropical jet is associated with a tendency to hamper eddies (Lachmy and Harnik, 2014). When the temperature gradient is increased significantly poleward from the jet peak, the increase in EMF convergence is mostly poleward of the baroclinic zone and so is the (small) increase in EKE.

Fig. 5.6(b,e,h) shows that eddies are less sensitive to changes in MAPE in regions where the gradient was changed in more equatorward regions (blue, green and orange dots), and similar in other simulations. Furthermore, it is found that when the change in the gradient appears poleward of the baroclinic region center, eddy fluxes and EKE scale linearly with MAPE. As other simulations in this paper, in these simulations the EAPE and EKE have an approximate linear relation (Fig. 5.6c). These results show that the latitudinal region where the temperature gradient is modified plays an important role in determining eddy amplitudes, and this can have implications on how to define the baroclinic zone.

5.3 Summary and discussion

To systematically simulate changes in the temperature field of the simulations, an idealized GCM was used with a Newtonian cooling scheme that relaxes the zonal mean temperature with a short time scale to a chosen relaxation temperature, while the relaxation time for eddies was 100 times longer. This allowed for an accurate comparison of three types of temperature changes: (a) meridional temperature gradient changes at different vertical levels, with changes in the lapse rate's vertical structure, (b) lapse rate changes at different vertical levels alone and (c) meridional temperature gradient changes at different latitudinal sections.

In addition to the relationship between MAPE and eddy fields, the sensitivity of eddies to the different temperature modifications was studied. We point out that this question is different from the relation between MAPE and eddy fields since similar amplitude changes in the temperature field at different sections of the atmosphere modify the MAPE differently, and therefore a large increase in eddies for a certain temperature change does not necessarily imply larger eddy sensitivity to MAPE changes. The main results and conclusions of the chapter are:

- MAPE is a nonlinear function of the meridional temperature gradient and of the lapse rate (MAPE $\approx \frac{(\partial_y T)^2}{\partial_z T}$), and therefore in regions where the meridional temperature gradient or lapse rate are large, a similar amplitude change in them will cause larger change in MAPE. Thus, if EKE and eddy fluxes scale linearly with MAPE it implies that eddies are more sensitive to meridional temperature gradient and lapse rate changes where the baroclinicity is large.

- Using changes in MAPE as a first order approximation to EKE response to changes in the temperature field is qualitatively useful since there is a good correlation between changes in MAPE and EKE in most simulations (Figs. 5.4b, 5.5b, 5.6b). On the other hand, the slope which relates between MAPE and EKE is not constant implying that there is no universal relation between EKE and MAPE, and in some of the simulations shown in Fig. 5.4b and 5.6b there is even a negative slope relating EKE to MAPE (increase in MAPE can be accompanied by EKE decrease). Therefore, it is not quantitatively reliable to estimate EKE changes based on MAPE changes alone.

- It is found that when the vertical structure of the temperature gradient or lapse rate is modified, the largest response in EKE occurs when the baroclinicity is modified in regions where baroclinicity is predominantly large (Fig. 5.4a,5.5a).

- In all simulations EKE and EAPE show an approximate linear relation, but different types of changes in the temperature field result in different slopes relating EAPE to EKE (see slopes of linear fits in Figs. 5.4c, 5.5c, 5.6c).

- When the lapse rate is modified at different vertical levels it is found that the EKE scales approximately linearly with MAPE (Fig. 5.5b). Since similar amplitude changes in the lapse rate at different levels of the troposphere cause very different MAPE changes, this result implies that the vertical structure of the lapse rate has a large effect on eddies. Therefore, the vertical mean lapse rate that is commonly used in theoretical considerations, might not be a sufficient measure for theoretical considerations for a troposphere with a lapse rate that changes significantly with altitude.

- When the meridional temperature gradient is modified at different latitudes in the baroclinic zone, it is found that eddies are less sensitive to changes at the equatorward regions of the baroclinic zone, which tends to strengthen the subtropical jet, and more sensitive to changes in the gradient at the center/poleward of the jet where momentum convergence drives the (eddy driven) jet (Fig. 5.6a,d,h). These results are consistent with previous studies that showed that eddies are more sensitive to an increase in the SST gradient at the center of the jet than at regions that are significantly poleward or equatorward of the jet center (Brayshaw et al., 2008; Sampe et al., 2010).

The baroclinic adjustment hypothesis (Stone, 1978; Schneider, 2004) suggests that baroclinic eddies maintain the extratropical troposphere neutral with respect to linear baroclinic

instability when averaging on the extratropical troposphere. A possible interpretation of the increased eddy activity as a result of increased baroclinicity concentration, is that when there is a local concentration of baroclinicity, there is a region that stores a large amount of potential energy that is highly unstable, and in this region, stronger eddy fluxes are needed to maintain a neutral mean flow. This explanation is similar to the adjustment hypothesis, but this hypothesis implies that the adjustment occurs on smaller scales.

Chapter 6

Eddy response to changes in jet characteristics

The purpose of this chapter is to investigate the eddy sensitivity to jet amplitude and location changes in different circulation regimes (a merged jet regime and a double jet regime). This chapter follows on the results of chapter 5 that studied the relation between the MAPE and EKE when the vertical and meridional temperature structure of the atmosphere changes. There it found that MAPE changes in the vicinity of the STJ cause relatively small changes in EKE, compared to changes in the vicinity of the EDJ.

It is shown that in the extratropical region eddies are most sensitive to changes in the temperature gradient in the vicinity of the EDJ, and less sensitive to change in the poleward flank of the STJ, or significantly poleward of the EDJ core. In the tropical region we find that eddies are also sensitive to changes in temperature gradient in the equatorward flank of the STJ (inside the tropics), though large temperature gradients inside the Hadley cell are not probable because of the large heat transport of the mean circulation that flattens efficiently the temperature gradient. Furthermore, it is demonstrated that when an atmospheric jet changes its characteristics and shifts equatorwad (becomes more STJ like), eddies tend to decrease, and we link this behavior to the presence of the Pacific mid-winter minimum (MWM) in EKE in chapter 7.

The GCM and the specific modifications to the Newtonian relaxation scheme used in the model are discussed in section 2.3.2. In section 6.1 the temperature profiles of the reference states are discussed and the induced temperature profile modifications we study are discussed in section 6.2. In section 6.3, we present the results of the simulations, where we focus on the response of eddies to changes in the jets' amplitude and location. In section 6.4, the results and their implications are summarized.

6.1 Reference states of the atmosphere

Two different reference simulations are investigated in this chapter, one that has a single merged jet, and another with two separated jets. It is beneficial to study two different reference

simulations because it allows to test the robustness of the results for different mean states.

The first reference temperature ($T_{\rm HS}$) is the equilibrium temperature structure of a simulation performed using the Held and Suarez (1994) forcing that includes a dry convection scheme. The convection scheme relaxes the atmosphere to a lapse rate of 0.7 $\Gamma_{\rm dry}$, where $\Gamma_{\rm dry} = g/c_p$ is the dry adiabatic lapse rate on a short time scale of 4 hours in cases the lapse rate exceeds this value. There is no convection scheme in any other simulation in this chapter. The eddy relaxation time which is used for these simulations is the same as in Held and Suarez (1994).

The left panels of Fig. 6.1 show the temperature, wind, mass streamfunction, absolute angular momentum, EKE, eddy heat flux (EHF) and EMFC of this reference. In this reference a single merged jet is obtained (see colors in Fig. 6.1a). This jet can be classified as a merged jet because it has two different driving mechanisms. In it's center/poleward flank there is significant EMFC and it is located in the Ferrel cell (Fig. 6.1c,e), implying that in this region it is an EDJ. On the other hand, its equatorward flank is found near the Hadley cell edge, it has a very baroclinic structure and EMF divergence occurs there (Fig. 6.1e), which implies that at low latitudes it is a subtropical-like jet.[1] The jet in this reference is quantitatively similar to the jet over the northern Pacific in January (Fig. 1.3b). Fig. 6.1c shows that an air parcel that flows poleward in the Hadley cell does not conserve its angular momentum since stream lines cross absolute angular momentum lines, and in addition there is significant EMF divergence that occurs inside the Hadley cell.

The second reference temperature ($T_{\rm April}$) is obtained by zonally averaging the multi-annual (1979-2010) NCEP/NCAR (National Centers for Environmental Prediction/ National Center for Atmospheric Research) reanalysis April temperature above the northern Pacific basin (160°E − 138°W).[2] This (zonally symmetric) reference temperature is chosen because it simulates an atmospheric state with two separated jets. We stress that the use of a realistic temperature does not mean that other fields will be quantitatively realistic due to the idealized framework we use (lack of moisture, ocean, orography etc.). The eddy relaxation time used in the simulations with this reference is 20 days (uniform in space). The right panels of Fig. 6.1 show the NH temperature, wind, mass streamfunction, absolute angular momentum, EKE, eddy heat flux (EHF) and EMFC of this reference. Two separated jets are present in this simulation (Fig. 6.1b, colors), a STJ which peaks at latitude 21° close to the edge of the Hadley cell (Fig. 6.1d), and an EDJ which peaks in the middle of the Ferrel cell at latitude 41°, where EMFC occurs (Fig. 6.1f, colors). Note that the jet in this reference is quantitatively similar to the jet over the northern Atlantic in January (Fig. 1.3a). The eddy fields of this reference shown in Fig. 6.1f,h,j are weaker than the eddy fields in the merged jet reference, which are plotted in the three bottom panels in the left column of Fig. 6.1. The weak eddies, and specifically weak EMFC, lead to relatively weak surface winds in this reference. Fig. 6.1d shows that the upper branch of the Hadley circulation is close to be angular momentum conserving since it does not

[1] Lachmy and Harnik (2014) discuss the fact that EMFC changes sign at the region where the mean meridional wind changes sign. Since the meridional wind changes sign at the edge of the Hadley cell, it is expected that EMF will diverge inside the Hadley cell (at the equatorward flank of the STJ).

[2] Since the vertical resolution of the GCM used in this chapter has different vertical resolution than the NCEP/NCAR reanalysis data, the temperature fields are interpolated to the levels of the model.

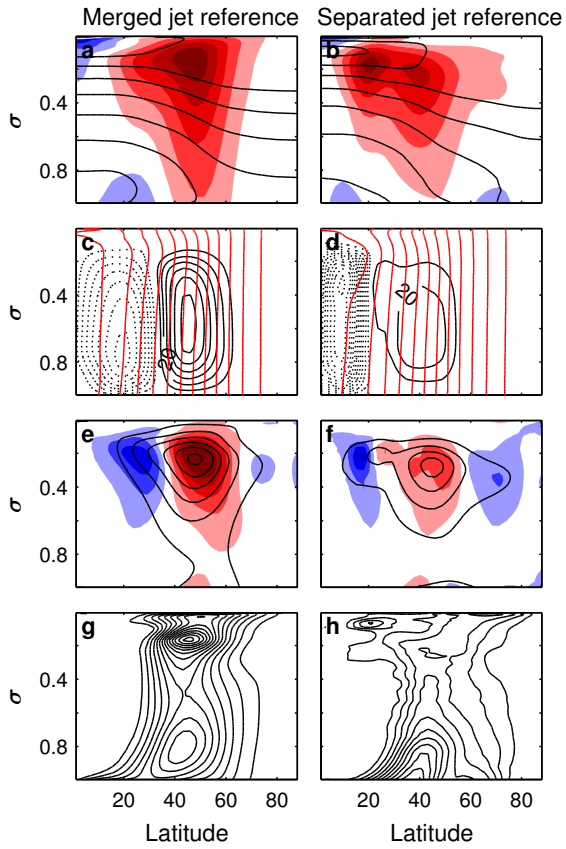

Figure 6.1: Contours of the temperature (a-b), mass streamfunction (black) and total angular momentum (red) (c-d), EKE (e-f) and EHF (g-h) for the merged jet reference (left column), and separated jet reference (right column) simulations. The zonal wind is plotted in colors in panels a-b (color spacing 8 m s^{-1}) and the meridional EMFC$\times 10^6$ is plotted in color in panels e-f (color spacing 12 m s^{-2}). The contour intervals are 15 K (temperature), 10 kg $s^{-1} \times 10^9$ (mass streamfunction), $0.1\Omega a^2$ (total angular momentum), 50 m^2 s^{-2} (EKE) and 2 K m s^{-1} (EHF).

cross total angular momentum contours (red).

6.2 Temperature profile modifications in the simulations

In order to study how changes in the zonal wind at different latitudes affect eddies, the meridional temperature gradient was modified at different latitudes. Changing the meridional temperature gradient leads to changes in the wind shear (thermal wind balance), and therefore we are able to modify the zonal wind at different latitudes systematically. The reference temperature was modified in the following ways:

- The temperature gradient was increased or decreased at a chosen latitudinal band. This causes change in the mean temperature gradient and tends to decrease or increase the wind shear at the proximity of these latitudes.

- The mean temperature gradient was increased at a chosen latitudinal band and decreased at a different latitudinal band simultaneously, such that the gradient was locally modified but its global mean value is approximately unmodified.

For the case that the gradient of the relaxation temperature was modified by a constant over a latitudinal band, the relaxation temperature can be written as $T_{\text{relaxation}}(\phi,\sigma) = T_{\text{ref}}(\phi,\sigma) + \delta T(\phi,\sigma,\phi_1,\phi_2,B)$, where

$$\delta T(\phi,\sigma,\phi_1,\phi_2,B) = \begin{cases} 0 & \text{for } \phi < \phi_1 \\ -B(\phi-\phi_1) & \text{for } \phi_1 < \phi < \phi_2, \sigma > 0.2 \\ -B(\phi_2-\phi_1) & \text{for } \phi > \phi_2, \sigma > 0.2 \\ -B(\phi-\phi_1)e^{-\frac{(\sigma-0.2)^2}{0.1^2}} & \text{for } \phi_1 < \phi < \phi_2, \sigma < 0.2 \\ -B(\phi_2-\phi_1)e^{-\frac{(\sigma-0.2)^2}{0.1^2}} & \text{for } \phi > \phi_2, \sigma < 0.2, \end{cases}$$

and ϕ is latitude, σ is the vertical coordinate and B is the change in the meridional temperature gradient between latitudes ϕ_1 to ϕ_2. The exponential decay at the high levels where $\sigma < 0.2$ is present to limit the temperature changes to the troposphere. In all experiments the gradient amplitude used was $B = \pm 2/8.5$ K degree^{-1}. The latitudes ϕ_1 and ϕ_2 used in section 6.3.1,6.3.2 are described in row a of Table 6.1. In the merged jet reference simulation, which is hemispherically symmetric, the gradient was modified in both hemispheres and in the separated jet reference simulation, that is not symmetric, only the NH was modified. The difference in the temperature profiles and zonal wind compared to the separated jet reference are plotted in color in the two upper rows of Fig. 6.2 for cases where the temperature gradient was increased at different latitudes.

To consider changes in the structure of the meridional temperature gradient without changes in the mean gradient, relaxation profiles with the temperature structure $T_{\text{relaxation}}(\phi,\sigma) = T_{\text{ref}}(\phi,\sigma) + \delta T(\phi,\sigma,\phi_1,\phi_2,B) - \delta T(\phi,\sigma,\phi_3,\phi_4,B)$ were used with the parameters $B = \pm 2/8.5$K degree^{-1}. To investigate the eddy response to a latitudinal shift of the EDJ, the parameters $\phi_1,\phi_2,\phi_3,\phi_4$ were chosen such that the EDJ was strengthened in one of its flanks and weakened on its other flank, and are described in row b of Table 6.1.

6.3 Result - Eddy response to changes in jet characteristics

Eddy amplitudes are evaluated by three different vertical mean eddy quantities: the EKE, the meridional component of the Eliassen-Palm flux (EP_y) and the vertical component of the EP flux (EP_z). They can be explicitly expressed as (Andrews et al., 1983):

$$EP_y = a\cos\phi(-\overline{u'v'} + \psi\partial_p\overline{u}) \tag{6.1}$$

and

$$EP_z = a\cos\phi(-\overline{u'w'} - \psi(\frac{\partial_\phi(\overline{u}\cos\phi)}{a\cos\phi} - f)), \tag{6.2}$$

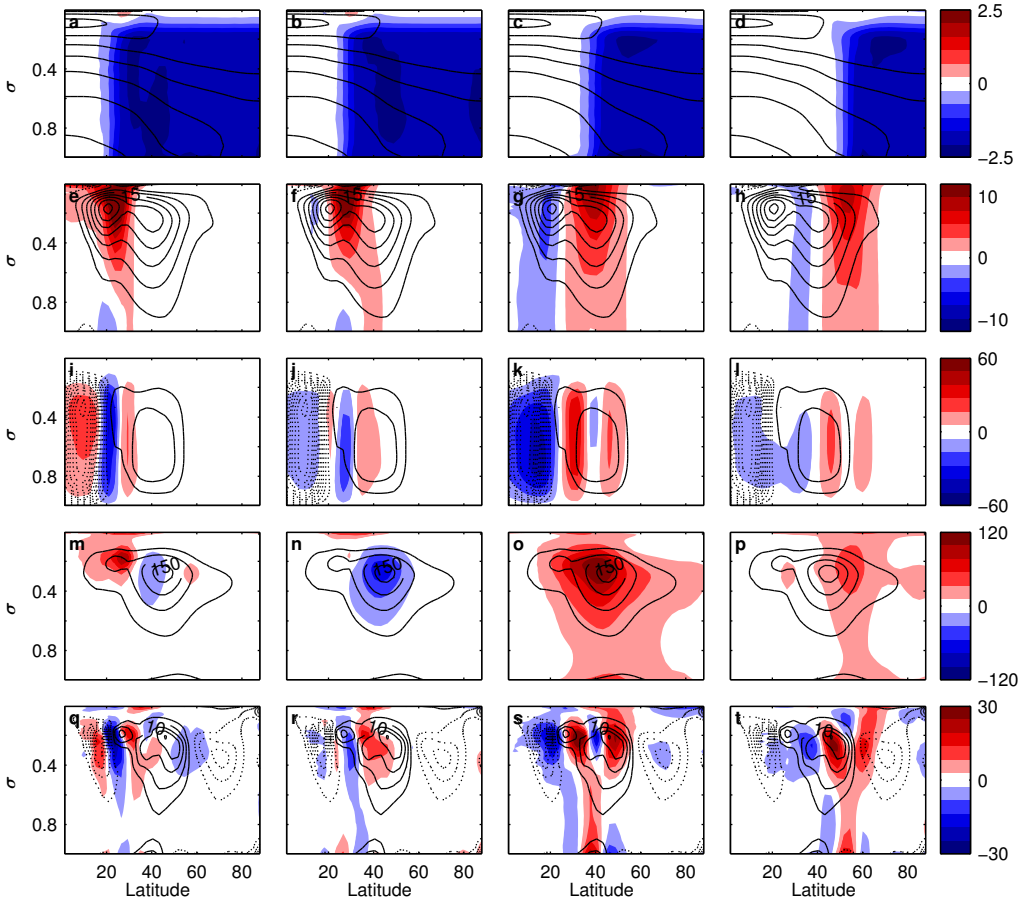

Figure 6.2: Temperature (a-d), zonal wind (e-h), mass streamfunction (i-l), EKE (m-p) and EMFC$\times 10^6$ (q-t) for simulations where the meridional temperature gradient was in the vicinity of the STJ (latitudes $18°, 26°$, first column), at the region between the jets (latitudes $24°, 32°$, second column), at the EDJ region (latitudes $35°, 43°$, third column) and poleward of the EDJ (latitudes $49°, 57°$, fourth column). Contours show the separated jet reference (dashed contours for negative values) and the colors represent deviation from this reference. The contour intervals are 15 K (temperature), 5 m s^{-1} (zonal wind), 10 kg s^{-1} $\times$ 10^9 (mass streamfunction), 50 m^2 s^{-2} (EKE) and 5 m s^{-2} (EMFC).

where $\psi = \frac{\overline{v'\theta'}}{\partial_p \theta}$, θ is the potential temperature, p is the pressure, ϕ is the latitude, f is the Coriolis parameter, a is the planetary radius, u, v and w are the zonal, meridional and vertical velocities, respectively. All vertically mean quantities in this section are averaged in sigma coordinates between $0.2 < \sigma < 1$.

6.3.1 Case I: Separated jets reference

The temperature, zonal wind, mass streamfunction and EKE are plotted in Fig. 6.2 for simulations where the temperature gradient was increased in the vicinity of the STJ (left column), between the jets (second column), in the vicinity of the EDJ (third column) and poleward of the EDJ for the separated jet reference. Contours show the reference state and colors show deviation from the reference. The EKE and EMFC are more sensitive to gradient changes in the vicinity of the EDJ than to changes in the vicinity of the STJ (Fig. 6.2m,o,q,s). For an increase in the temperature gradient in the vicinity of the EDJ (third column in Fig. 6.2), the

	Experiment description	Latitude changes at:
a	Increasing/decreasing the mean gradient at latitudes (ϕ_1, ϕ_2)	For both references: $(13°, 21°)$, $(15°, 23°)$, $(18°, 26°)$, $(21°, 29°)$, $(24°, 32°)$, $(26°, 34°)$, $(29°, 37°)$, $(32°, 40°)$, $(35°, 43°)$, $(37°, 45°)$, $(40°, 48°)$, $(43°, 51°)$, $(46°, 54°)$, $(49°, 57°)$, $(52°, 60°)$, $(55°, 63°)$, $(57°, 65°)$, $(60°, 68°)$
b	Shifting jet simulations - changes at latitudes $(\phi_1, \phi_2, \phi_3, \phi_4)$	For both references: $(27°, 35°, 38°, 46°)$, $(29°, 37°, 41°, 49°)$, $(32°, 40°, 43°, 51°)$, $(35°, 43°, 46°, 54°)$, $(38°, 46°, 49°, 57°)$, $(41°, 49°, 51°, 59°)$
c	Changing jet's amplitude simultaneously - changes in latitudes $(\phi_1, \phi_2, \phi_3, \phi_4)$	Separated jet reference: $(18°, 26°, 35°, 43°)$, $(24°, 32°, 32°, 40°)$, $(18°, 26°, 32°, 40°)$ Merged jet reference: $(24°, 32°, 40°, 48°)$

Table 6.1: The experiments performed in this chapter. Numbers indicate the latitudes where the meridional temperature gradient was modified in the simulations.

surface wind increases at midlatitudes as a result of an increase in the EMFC (and decreases in lower latitudes where EMF divergence increases). When the meridional temperature gradient is increased in the vicinity of the EDJ (two left columns in Fig. 6.2), there is no increase in surface winds at low latitudes since EMF does not converge in low latitudes. The small increase in surface wind in these simulations occurs at higher latitudes where there is an increase in EMFC.

To test if the large eddy response to changes in the meridional temperature gradient in the vicinity of the EDJ is dependent on the exact latitudinal location of the modification in the gradient, a set of simulations was conducted where the meridional temperature gradient was modified at different latitudinal bands. The northern hemispheric mean of the EKE and EP fluxes differences between the separated jet reference and these simulations are plotted in Fig. 6.3(a-d), where panels a,b are for the case the gradient was increased and panels c,d for a decreased gradient. The x axis shows the center latitude that the gradient was changed (defined as $\frac{\phi_1+\phi_2}{2}$, where ϕ_1, ϕ_2 are the boundaries of the latitudinal band that is changed, and the latitudinal width of the change is always about 8.5°), and the y axis shows the change in magnitude. When the meridional temperature gradient is increased in the vicinity of the EDJ, the change in EKE is maximal (Fig. 6.3a). The EKE is less sensitive to increase in the equatorward flank of the STJ, even less sensitive to changes poleward of the EDJ and least

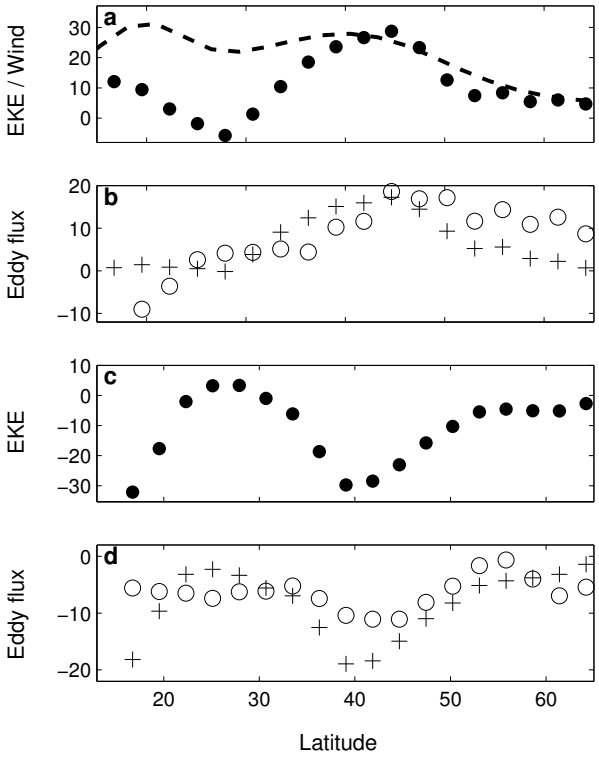

Figure 6.3: (a) EKE averaged over the NH where each dot represents a simulation. The ordinate is the difference of the mean EKE from the separated jet reference simulation, and the abscissa shows the center latitude where the temperature gradient was increased (black dots, panel c for a decreased gradient). The dashed line in panel (a) shows the zonal wind at $\sigma = 0.25$ of the reference simulation. (b) like in (a) for the horizontal (circles) and vertical (plusses) EP flux. Panels c,d show similar plots as in a,b for simulations with a decreased gradient.

sensitive (and can even have a decrease in EKE) when the gradient is increased at the latitudes between the jets. In Appendix A we show that when the amplitudes of the two jets is modified simultaneously but with opposite signs, the eddy fields response is similar to the change in the EDJ (if the jet is stronger, also eddy fields are stronger).

These results are consistent with the results of Brayshaw et al. (2008) that showed that eddies are most sensitive to changes in SST gradient below the EDJ, less sensitive to changes in the SST at low latitudes, and least sensitive to changes at high latitudes (significantly poleward of the jet maximum).

In general, the response of the EP fluxes is similar to the response of the EKE (Fig. 6.3b), but with the exception that when the gradient is increased at lower latitudes the response in the meridional EP flux is opposite to the EKE response, and the response of the vertical EP flux is relatively weak. The negative meridional EP flux tendency occurs because at lower latitudes the EMF reduces (see EMFC in Fig. 6.2q) and it tends to concentrate in a smaller region, but its maximal value tends to increase in these simulations. We note that a strong meridional temperature gradient is not probable to occur within the Hadley cell since the mean circulation tends to flatten the temperature gradient very efficiently. The response of eddies to a decreased temperature gradient is quantitatively similar, though a decreased gradient deep in the tropics results in similar magnitude eddy response as changes near the EDJ (Fig. 6.3c,d).

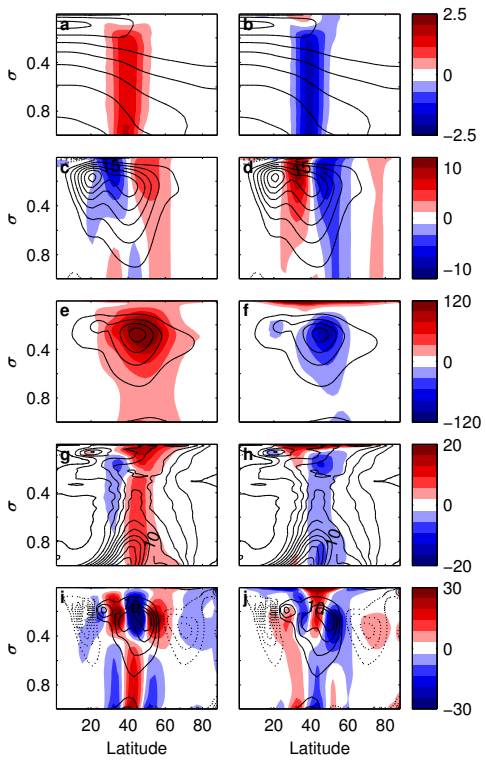

Figure 6.4: Temperature (a-b), zonal wind (c-d), EKE (e-f), EHFC$\times 10^6$ (g-h) and EMFC (i-j) for simulations where the EDJ was shifted poleward (left column) and equatorward (right column). The meridional temperature gradient was changed at latitudes $30° - 38°$ and $41° - 49°$. Contours show the separated jet reference (dashed contours for negative values), and the colors represent deviation from this reference. The contour intervals are 15 K (temperature), 5 m s^{-1} (zonal wind), 50 m^2 s^{-2} (EKE), 2 m s^{-1}K (EHF) and 5 m s^{-2} (EMFC).

In Fig. 6.4 the temperature, zonal wind, EKE, EMFC and EHF are plotted for simulations that the temperature gradient was modified such that the EDJ is shifted at latitude. When the EDJ is shifted poleward (left column) eddy fields tend to increase (Fig. 6.4e,g,i, though the EMFC shows a mixed response), and when the EDJ is shifted equatorward the eddy fields tends to weaken (Fig. 6.4f,h,j). In chapter 7 we use this conclusion and apply it to a real atmospheric phenomena. These results imply that when the jet becomes more EDJ-like (poleward shift), eddies tend to increase, and when it becomes more STJ-like (equatorward shift), eddies tend to decrease. The sensitivity of these results to the exact location of the center of the shift was examined in a series of simulations. It was found that when the jet is shifted polewards, if the latitude of the shift's center is equatorward of latitude 43° the eddies tend to strengthen and otherwise they weaken (the cases the eddies weaken are cases that the shear decrease occurs close to the peak of the EDJ). When the jet is shifted equatorward the eddies tend to weaken if the latitude of the shift's center is poleward of latitude 40° and otherwise they tend strengthen.

6.3.2 Case II: Mixed jet

The temperature, zonal wind, mass streamfunction and EKE are plotted in Fig. 6.5 for simulations that the temperature gradient was modified at different latitudes for the merged jet background reference. Contours show the reference state and colors show deviation from this

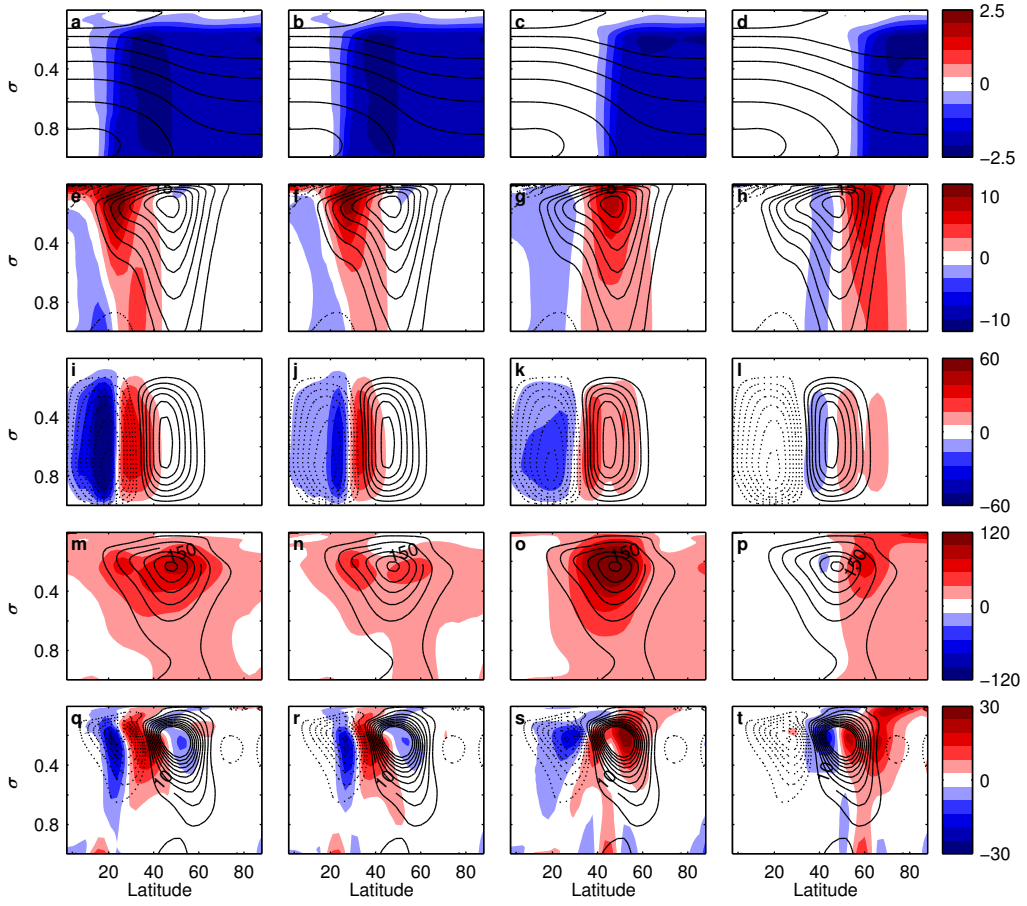

Figure 6.5: Temperature (a-d), zonal wind (e-h), mass streamfunction (i-l), EKE (m-p) and EMFC$\times 10^6$ (q-t) for simulations where the meridional temperature gradient was increased in the tropics (latitudes $15°, 23°$, first column), equatorward flank of the jet (latitudes $21°, 29°$, second column) at the jet center (latitudes $41°, 49°$, third column), and at the poleward flank of the jet (latitudes $55°, 63°$, fourth column). Contours show the merged jet reference (dashed contours for negative values) and the colors represent deviation from this reference. The contour intervals are 15 K (temperature), 5 m s^{-1} (zonal wind), 10 kg s^{-1} $\times$ 10^9 (mass streamfunction), 50 m^2 s^{-2} (EKE) and 5 m s^{-2} (EMFC).

reference. This figure shows that EKE is most sensitive to changes in the gradient in the vicinity of the EDJ (the EKE response in Fig. 6.5o is largest). Furthermore, when the temperature gradient is increased inside the Hadley cell (two left columns in Fig. 6.5), the Hadley cell strengthens and contracts. In this reference an air parcel that moves poleward in the Hadley cell does not conserve its angular momentum (Fig. 6.1c) and EMF divergence acts to weaken the zonal wind. The increase of the Hadley cell amplitude with the increase of EMF divergence is consistent with the results of Walker and Schneider (2006) that showed that in cases that eddies play an important role in the Hadley cell, its strength is proportional to the EMF divergence. Furthemore, when the increase in temperature gradient occurs at low latitudes (Fig. 6.5, two left columns), the increase in surface winds (and in EMFC) occurs poleward of this region, where the Ferrel cell strengthens. This implies that even when the temperature gradient is increased inside the Hadley cell, the increase in surface winds (and EMFC) will not occur inside the Hadley cell (see also Lachmy and Harnik, 2014 for a discussion why inside the Hadley cell there is EMF divergence).

Fig. 6.6(a-b) shows the EKE and EP flux differences between simulations where the temperature gradient was increased (decreased gradient on c-d panels) at different latitudes and the merged jet reference simulation as a function of the latitude that the temperature gradient was changed. The results shown in Fig. 6.6a are qualitatively similar to the results of section 6.3.1. Eddies are found to be more sensitive to changes in the temperature gradient (or wind shear) in the vicinity of the EDJ, less sensitive to temperature gradient changes inside the Hadley cell, even less sensitive to changes in the gradient at high latitudes (poleward of the EDJ), and least sensitive (and can even show an opposite response) to changes on the equatorward flank of the EDJ (which is equivalent to the region between the jets that was found in section 6.3.1 to be least sensitive). In the merged jet reference simulation, the Hadley cell's edge is at latitude $\phi_{\text{Hadley}} \approx 30°$, and when the temperature gradient is modified deep in the tropics (below latitude 20°) the change in the EKE can be as big as the change in EKE when the temperature gradient is modified in the vicinity of the EDJ (Fig. 6.6a). This implies that changes in the temperature gradient deep in the tropics can have a significant impact on eddies.

A significant difference between the results of the two references is the response of the EP fluxes when the temperature is increased at low latitudes (i.e., inside the Hadley cell). In the merged jet reference, the response of eddy fluxes are similar to the response of the EKE (when the EKE increases more, so do the fluxes), and in the separated jet reference, an increase in the EKE is not always accompanied by an increase in the fluxes. The different eddy response is possibly related to the different nature of the Hadley cell in each of the reference simulations. In the merged jet reference eddies are dominant, the mean angular momentum is not conserved on a poleward moving air parcel and EMF divergence occurs inside the cell, while in the separated jet reference the upper branch of the Hadley cell is almost angular momentum conserving and eddies are not playing a big role in the Hadley cell circulation (Fig. 6.1c,d). This possibly also results in the different response of the Hadley cell when the temperature gradient is modified at low latitudes; in the separated jet reference the mass streamfunction of the Hadley cell weakens and expands in a response to increased gradient at low latitudes (Fig. 6.2i), while in the merged jet reference the response is opposite (Fig. 6.5i,j).

The temperature, zonal wind, EKE, EMFC and EHF are plotted in Fig. 6.7 for simulations that the temperature gradient was modified such that the EDJ is shifted at latitude. A poleward shift of the EDJ results in an increase in eddies, while an equatorward shift results in a decrease in eddy fields. These results are similar to what was shown in section 6.3.2 for the separated jet reference. The sensitivity of these results to the exact location of the center of the shift was examined in a series of simulations, and it was found that when the jet is shifted poleward, if the latitude of the shift's center is equatorward of latitude 48° the eddies tend to strengthen and otherwise to weaken. When the jet is shifted equatorward, the eddies weaken if the latitude of the shift's center is poleward of latitude 43° and otherwise they tend strengthen.

When the temperature gradient is modified in a certain latitudinal band, the EKE response is over a broad range of latitudes. This effect is most obvious when the temperature gradient changes are found inside the Hadley cell, and the EKE response happens in all midlatitudes

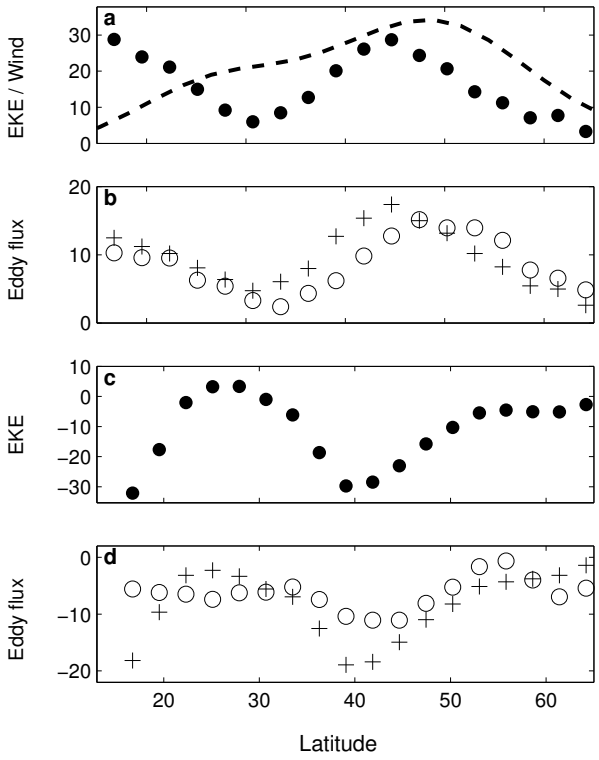

Figure 6.6: (a) Globally averaged EKE where each dot represents a simulation. The ordinate is the difference of the mean EKE from the reference simulation, and the abscissa represents the center latitude where the temperature gradient was increased (black dots, panel c for a decreased gradient). The dashed line in panel (a) shows the zonal wind at $\sigma = 0.25$ of the merged jet reference simulation. (b) like in (a) for the horizontal (circles) and vertical (plusses) EP flux. Panels c,d show similar plots as in a,b for simulations with a decreased gradient.

(Fig. 6.5m). This implies that local bariclinicity measures are not sufficient to understand the local EKE response to changes in the meridional structure of the temperature gradient. In general, eddy fluxes, and especially EHF show a more localized response than EKE when the temperature gradient is modified, though their response is not confined to the region where the gradient was changed.

6.3.3 Strong STJ inhibits eddy momentum flux in high mid-latitudes

Lee and Kim (2003) showed in a numerical study that when the STJ is relatively weak eddies grow $20° - 30°$ poleward of the STJ, eventually creating a second jet (an EDJ). On the other hand, for a strong STJ, they showed that eddies tend to grow in the vicinity of the STJ, which leads to an atmospheric state with a single (merged) jet. To test this hypothesis, the meridional temperature gradient was increased significantly to strengthen the STJ, and investigate if this could inhibit eddy growth at higher latitudes, where the EDJ is found.

Fig. 6.8 shows the zonal wind (a-b), mass streamfunction (c-d), EKE (e-f), EMFC (g-h), EHF (i-j) for simulations where the STJ temperature gradient was significantly increased ($5°$K/$8.5°$) in latitudes $18° - 26°$ in the separated jets reference (left column) and the merged jet

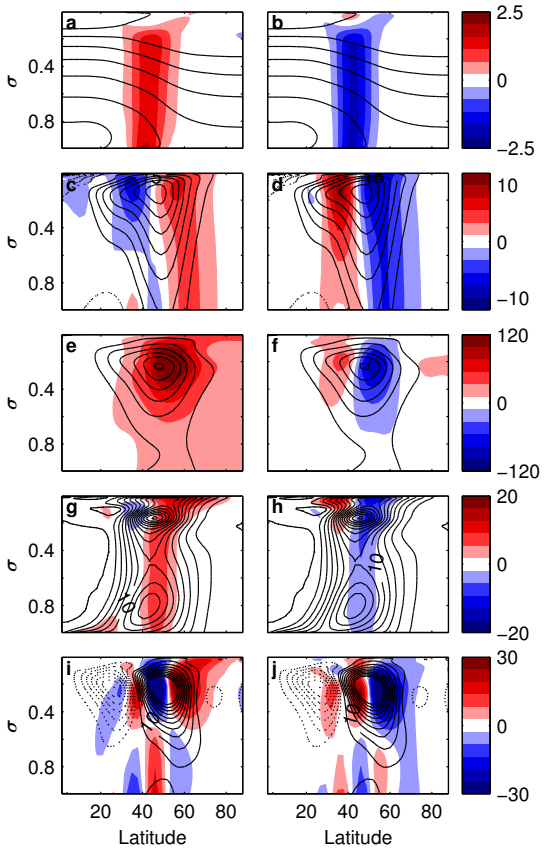

Figure 6.7: Temperature (a-b), zonal wind (c-d), EKE (e-f), EHFC$\times 10^6$ (g-h) and EMFC (i-j) for simulations where the EDJ was shifted poleward (left column) and equatorward (right column). The meridional temperature gradient was changed at latitudes $32° - 40°$ and $43° - 51°$. Contours show the merged jet reference (dashed contours for negative values) and the colors represent deviation from this reference. The contour intervals are 15 K (temperature), 5 m s^{-1} (zonal wind), 50 m^2 s^{-2} (EKE), 2 m s^{-1}K (EHF) and 5 m s^{-2} (EMFC).

reference (right column). When significantly strengthening the STJ, EMFC tends to decrease in midlatitudes where the EDJ was present in the reference (Fig. 6.8g,h). Furthermore, the Ferrel's cell mass streamfunction as well as EMFC tends to be more concentrated at lower latitudes (Fig. 6.8c,d). The decrease in EMFC and streamfunction at higher latitudes implies that the role of eddies in accelerating the jet at higher latitudes is decreased.[3] Furthermore, the contraction of the Ferrel cell, implies that a two jet state is less favorable since there is little latitudinal separation between the Hadley and the Ferrel cell. On the other hand, EHF and EKE do not decrease in high latitudes, and the large EHF in high latitudes implies that baroclinic growth still occurs at these latitudes. These results are consistent with the results of Lee and Kim (2003) and Son and Lee (2005) in the sense that in the presence of a strong STJ the EMFC occurs closer to the STJ (leading to a single jet), but, the reduction in EMFC at high latitudes is not accompanied by a decrease in EKE or EHF at high latitudes and eddy activity increases in high latitudes.

[3]The diabatic heating used in this work enforces the vertical shear of the zonal wind in midlatitudes to remain unchanged because thermal wind balance approximately holds. Nevertheless, the fact that the EMFC decreases at higher latitudes, implies that the acceleration of the zonal wind by the eddies decreases. This is most pronounce in Fig. 6.8d that the surface winds in high latitudes decrease by more than 5m s^{-1}.

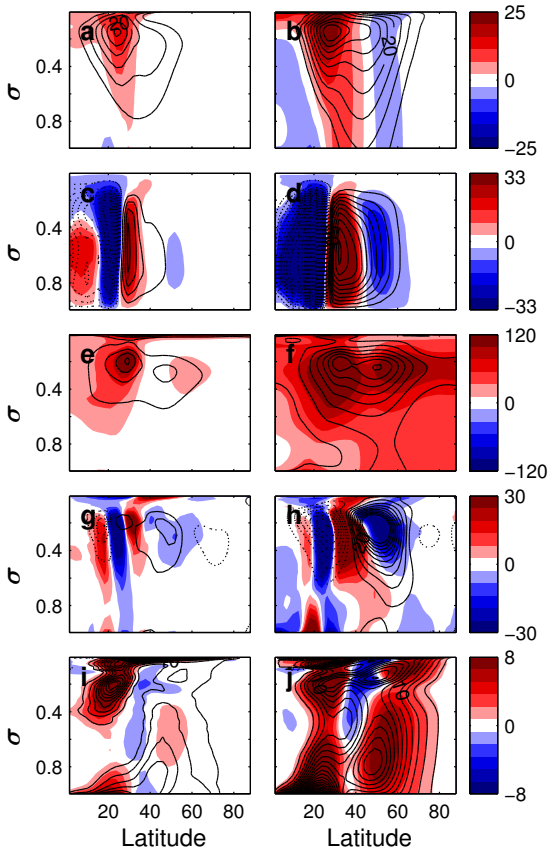

Figure 6.8: Zonal wind (a-b), mass streamfunction (c-d), EKE (e-f), EMFC$\times 10^6$ (g-h), EHF (i-j) for separated jet reference (left column) and the merged jet reference (right column) with significantly increased gradient (5°K/8.5°) at latitudes $18° - 26°$. Contours show the field values of each run and colors represent deviation from the relevant reference. The contour intervals are 10m s^{-1} (wind), 10kg s^{-1} $\times 10^9$ (mass streamfunction), 50 m^2 s^{-2} (EKE), 15 m s^{-2} (EMFC) and 2 m K s^{-1} (EHF).

6.4 Summary and discussion

In this chapter the eddy response to changes in the vertical wind shear at different latitudes was investigated. We especially focus on the eddy sensitivity to jet amplitude changes in the vicinity of the STJ and the EDJ, and their response to a jet shift. Understanding how different jet types affect eddy activity is important since it serves as a guideline to characterize how unstable is the atmosphere also by considering the type of the jet, and not only by linear baroclinicity measures.

To methodically modify the jet strength at different latitudes (and keeping the wind shear at other latitudes approximately unchanged), an idealized GCM was used with a Newtonian cooling scheme that relaxes the zonal mean temperature field a hundred times faster than it relaxes eddies. This allows controlling the zonal mean temperature field with high accuracy, and since thermal wind balance approximately holds, to set the vertical wind shear.

In order to investigate the eddy response to changes in the jet structure, two different reference simulations were considered, one with a well separated STJ and EDJ, and the other with a single merged jet. It was found in both references that the eddy fields are most sensitive to changes in the temperature gradient in the vicinity the EDJ, less sensitive to gradient changes

in the equatorward flank of the STJ (latitudes inside the Hadley cell), even less sensitive to gradient changes significantly poleward of the EDJ, and least sensitive in cases where the gradient was modified between the jets (at the poleward flank of the STJ). In addition, it was found that when the STJ weakens and the EDJ strengthens simultaneously, eddies tend to increase (Appendix E). In a different simulation set it was shown that a moderate poleward (equatorward) shift of the EDJ leads to an increase (decrease) eddy fields. Since the qualitative results of the simulations in the two references were similar, it increases the confidence that these results could be generalized and be applicable to other situations.

A potential mechanism that was not discussed so far and might influence baroclinic growth in midlatitudes is the barotropic governor (James and Gray, 1986; James, 1987). According to this mechanism a concentration of barotropic shear could have a damping effect on baroclinic eddies, and therefore sharp jets in the meridional direction could be less favorable for baroclinic eddies than wider jets. This implies that when the jet amplitude is increased near its maximum (and the jet becomes sharper), barotropic shear is more concentrated, and can reduce baroclinic eddies compared to the case that the jet amplitude is increased near its flanks, and the meridional gradient of the zonal wind is less concentrated. However, this effect is not the dominant effect in these simulations, since eddies' response is larger when the gradient is modified in the vicinity of the EDJ maximum, and less sensitive to changes near its flanks (Figs. 6.2o, 6.3a, 6.5o and Fig. 6.6a). If the barotropic governor would be the dominant mechanism, we would expect the result to be opposite.

Chapter 7

Pacific midwinter minimum in a zonally symmetric GCM - the role of poleward jet shift

In this chapter, we extend the work of chapter 3 and demonstrate that a MWM-like EKE pattern can be obtained in an idealized GCM that mimics a realistic zonal symmetric Pacific temperature distribution for different months. The resemblance between the EKE behavior in the simulations of the transition seasons and winter to the one from reanalysis might indicate that the temperature distribution in the different months might be the main contributor to general trends in the EKE. It is demonstrated that the EKE reduction in January is at least partly related to the equatorward jet shift in winter. Furthermore, in chapter 6 we found that a poleward shift of the jet tends to increase eddy fields, and we relate the poleward shift of the jet in transition seasons relative to January, to the presence of the MWM. The poleward shift in transition seasons implies that the jet is more EDJ-like, which tends to strengthen eddies as shown in the previous chapter. Our results suggests that zonally symmetric dry dynamics have the necessary complexity to explain the Pacific MWM, and that zonal asymmetries or moisture are not a necessary condition for the presence of the MWM. Furthermore, the results imply that the poleward jet shift in transition seasons play a large role in the observed minimum.

The section is organized as follows. The "realistic" zonally-symmetric temperature distributions used in the model are discussed in section 7.1. In section 7.2, we present the results of the simulations which shows that a Pacific MWM can be obtained using this GCM configuration. In section 7.3 it is demonstrated that the January jet is more STJ-like and when this jet is shifted polewards in the simulations, there is an increase in the EKE. In section 7.4, different aspects of the results are summarized.

7.1 Temperature profiles in the simulations

To investigate whether in a semi-realistic, zonally symmetric model, a Pacific MWM can be reproduced, the monthly averaged temperature profiles that are taken from NCEP/NCAR

reanalysis data in the northern Pacific and northern Atlantic are simulated for different months. The relaxation temperature profiles for each month are determined by averaging the reanalysis monthly average temperature data between the years $1981-2010$. Focusing on the northern Pacific basin, the temperature is zonally averaged over longitudes of the northern Pacific basin ($160°$E$-138°$W), which leads to a zonally symmetric relaxation temperature. In the simulations where the northern Atlantic temperature profile is used, the reanalysis data is averaged between longitudes $30°$W $-$ $70°$W. Since the vertical resolution of the GCM used in this chapter has different vertical resolution than the NCEP/NCAR reanalysis data, the temperature fields are interpolated to be at the levels of the model.

To obtain a northern Pacific-like temperature profile in different months in the idealized GCM, the diabatic formulation described in section 2.3.2 is used. The simulations are integrated over 2000 days, where the first 1000 days of each simulation are treated as spinup and the results are averaged over the last 1000 days. Simulations in this chapter are not hemispherically symmetric and only the northern hemispheric data is presented.

In Fig. 7.1 the temperature and the zonal wind differences between simulations with this heating formulation and the reanalysis data in November, January and March are plotted. The simulations temperatures of different months are very similar to the reanalysis data and the deviations are less than a degree (Fig. 7.1(a-c)). On the other hand, the wind field has substantial differences Fig. 7.1(d-f). Despite the large wind differences between the simulations and the reanalysis data, the vertical wind shear in the simulations and in the reanalysis data are very similar since thermal wind balance approximately holds, and the wind difference are mainly due to large differences in the surface winds between the simulations and the reanalysis data. Furthermore, these surface winds differences have a similar structure in most of the months (reduced surface winds below the jet peak and increased surface winds both north and south of the jet peak), so the bias is similar in most simulations. We conclude that the method presented above can reproduce with a very good accuracy the wind shear and the temperature profile, but can not reproduce accurately the surface winds.

7.1.1 EKE calculation and reanalysis data

To compare the EKE results of the simulations to observations, the EKE from NCEP/NCAR data using 4 times a day reanalysis data of horizontal winds between 1980-2014 is calculated using a Butterworth bandpass filter with a cutoff period of $3-10$ days. This allows comparing between the zonally symmetric simulations and the zonally asymmetric data. Furthermore, the presence of the MWM in the simulations is present also when the EKE is defined as a deviation from zonal and time mean.

7.2 Results

The latitude-time diagram of the vertically integrated EKE as a function of the month of the year in the northern Pacific from reanalysis data is plotted in Fig. 7.2a and a similar figure for

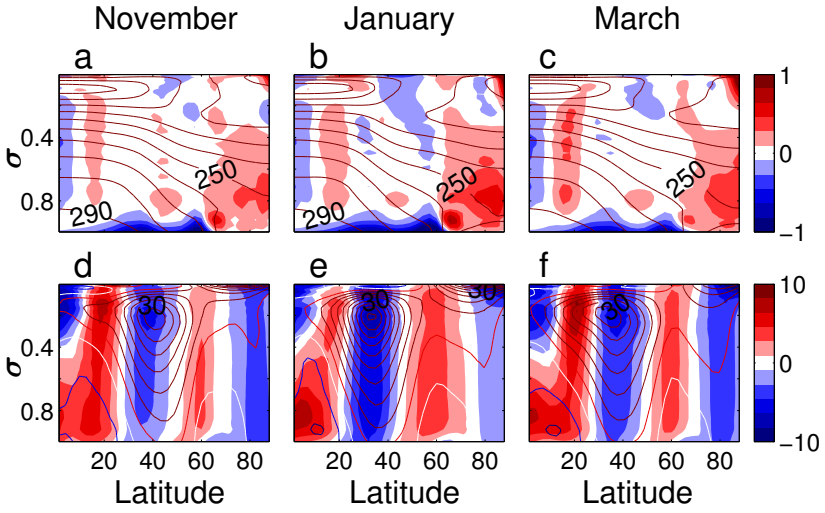

Figure 7.1: The temperature (a-c) and zonal wind (d-f) for November, January and March averaged over the Pacific. Colors indicate the differences between simulation and reanalysis. Contours represent reanalysis data fields. The contours intervals are 10 K (temperature) and 5 m s^{-1} (zonal wind).

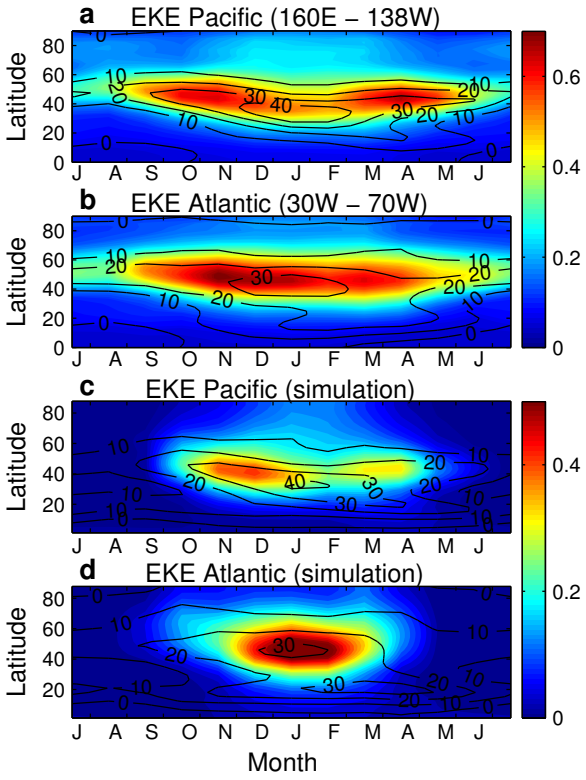

Figure 7.2: The mean EKE ($\frac{1}{2g}\int v^{*2} + u^{*2} dp$) in units of MJ m^{-2} (color), and the zonal wind at 250 hPa (contour) as a function of latitude and the temperature field for different months of the year in NCEP reanalysis data (a-b) and simulations (c-d) for the northern Pacific (a,c) and northern Atlantic (b,d).

the simulations in Fig. 7.2c. The observed pattern of the EKE in the reanalysis data resembles the EKE pattern in the simulations in the sense that there is clear MWM in the EKE in the simulations. The local maximum in the EKE appears in November and December and after midwinter in March and April. In addition, at higher latitudes, poleward of 60°N the EKE is larger in winter than in the transition seasons both in the simulations and in observations.

When comparing the EKE calculated from the simulations to the reanalysis data, it is found that the EKE obtained from the simulations between October and April is smaller by approximately 30 percent. This trend was also found by Chang (2006) and Yuval and Kaspi (2016) when using an idealized GCM with realistic temperature distribution. Chang (2006) suggested that the reduced EKE in the simulations is a consequence of the neutrally stable mean state in winter (Hall and Sardeshmukh, 1998). While the temperature fields in the simulations are similar to reanalysis data, the static stability in the simulations is larger than the observed static stability since the simulations don't include moisture effects (dry static stability is larger than moist static stability for the same temperature profile). In addition, Hayashi and Golder (1981) showed that latent heat release acts to enhance baroclinic energy conversion, and since the GCM does not include moist effects, it is expected that the EKE will be reduced in the simulations compared to reanalysis data.

Furthermore, the EKE magnitude is affected by different model parameters, such as the relaxation time. When the relaxation time is increased, so does the EKE. For example, varying the eddy relaxation time between $10-80$ days leads to EKE changes by more than 30 percent , but nevertheless, a MWM is present when simulating different relaxation time scales (the relaxation times studied are $10, 40$ and 80 days, not shown). Since the idealized GCM is missing a lot of realistic physical aspects, it is not expected to reproduce the quantitative results of the reanalysis, and the focus of this chapter is on the qualitative aspects of the results. From May to September, the EKE in the simulations is almost zero, which is different from observations. It is possible that latent heat effects, zonal asymmetries and zonal mean temperature variability play an important role in exciting and enhancing instabilities in these months, and since these effect are absent in this model the EKE is negligible.

In order to take into account the effects of moisture on the static stability in a simple manner, Chang (2006) suggested that instead of using the observed temperature profile as the relaxation temperature, to use a relaxation temperature profile with a reduced static stability which keeps the meridional temperature gradient as in the observations. This profile can be written as

$$T_{\text{reduced}}(\phi,\sigma) = T_{\text{observed}}(\phi,\sigma) - Az(\sigma), \tag{7.1}$$

where $z(\sigma)$ is the averaged geopotential height of the σ surface and A is the reduction in the static stability. In Fig. 7.3 the EKE is shown for simulations with relaxation temperature profiles taken from Eq. 7.1 with the values $A = 0.4, 0.5, 0.7$ K km^{-1}. The EKE is larger as the lapse rate parameter is increased and when increasing the lapse rate parameter sufficiently, the EKE values are closer to the observed winter EKE values. Furthermore, using the modified temperature fields leads to a single EKE maximum in fall and early winter, and the second maximum in early spring is absent. This result implies that the presence of a MWM in the simulations is sensitive to the lapse rate of the relaxation temperature. The enhancement of the EKE when the static stability is reduced implies that the reduced EKE in the simulations is partly a consequence of the usage of dry static stability. Including a modified static stability

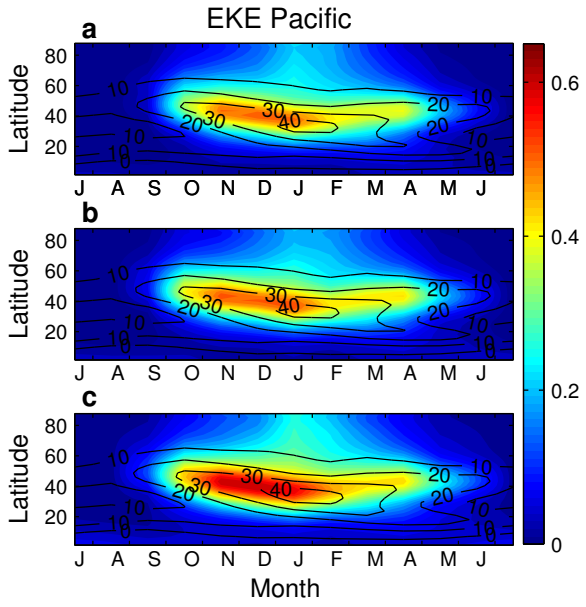

Figure 7.3: Colors show the mean EKE $\frac{1}{2g}\int v^{*2} + u^{*2} dp$ in units of MJ m^{-2} as a function of latitude and the temperature field of different months of the year in simulations of the northern Pacific with a modified temperature field described in Eq. 7.1 with (a) $A = 0.4$ K km^{-1}, (b) $A = 0.5$ K km^{-1} and (a) $A = 0.7$ K km^{-1}. Contours show the zonal wind in each set of simulations at $\sigma = 0.242$.

in the simulations, increases the EKE and quantitatively the EKE is closer to reanalysis data values. Note that in the simulations of Chang (2006) a MWM did not appear, and the target temperature was not the observed temperature but the reduced static stability profile (T_{reduced}). Whether the modification in the static stability is the underlying reason for the MWM not to be present in Chang (2006) is difficult to know since there are other possible reasons, such as non accurate reproduction of the temperature profile or the complexity of the model, which took into account zonal asymmetries, and other effects that are not included in this chapter.

To investigate whether the MWM-like behavior is observed in the simulations of the northern Pacific is unique to the Pacific, the vertically integrated EKE of simulations in which the temperature profiles in the northern Atlantic were used is plotted in Fig. 7.2d. In the Atlantic simulations there is a clear maximum in midwinter (January) in the EKE. The EKE pattern in the Atlantic simulations is different than observations (shown in Fig. 7.2b), where the EKE has similar maximal values along a few months (with even a weak MWM). On the other hand, using NCEP reanalysis with a Butterworth bandpass filter with a cutoff period of $2-6$ days as in Nakamura (1992), the EKE in the Atlantic shows a single maximum in EKE in midwinter (not shown, see also Fig. 2b of Nakamura, 1992), which is similar to the simulations results. The fact that the MWM is not present in the Atlantic simulations, but is present in the Pacific simulations, indicates that the zonally averaged temperatures play an important role in the occurrence of the Pacific MWM.

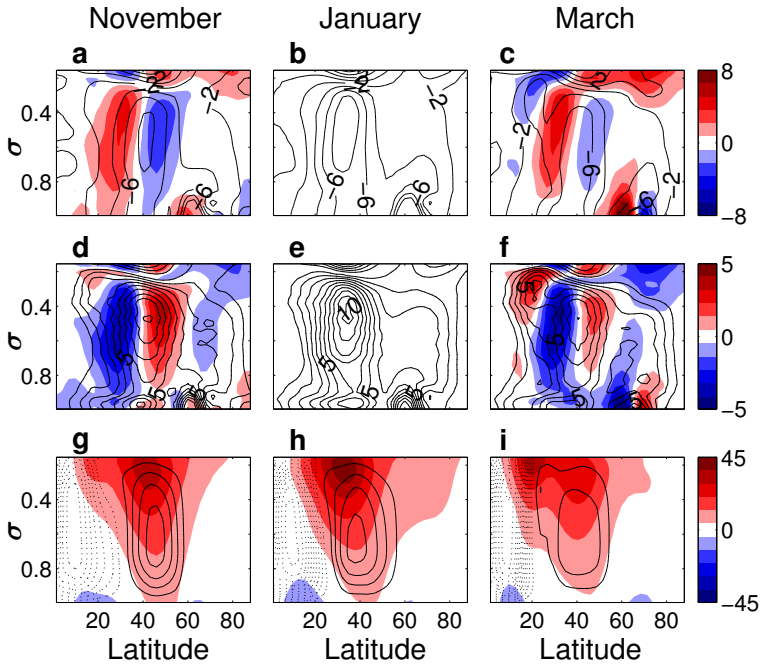

Figure 7.4: The meridional temperature gradient (10^{-6} K m^{-1}) (a-c), and Eady growth rate (10^{-6} s^{-1}) (d-f) for November, January and March. Colors indicate the differences from January and contours are the values of the different fields. The contour intervals are 2×10^{-6} K m^{-1} (temperature gradient) and 1×10^{-6} s^{-1} (Eady growth rate). In panels g-i the streamfunction (contours intervals 10kg s$^{-1} \times 10^{9}$) and wind (colors) are plotted for each simulation separately.

7.3 The poleward shift of the jet in transition seasons

To understand the appearance of a MWM-like behavior in the simulations, the temperature gradient and the Eady growth rate, which is used as a measure for baroclinicity, are plotted in Fig. 7.4 for simulations with the Pacific temperature profile in November, January and March. Interestingly, in both transition seasons, there is a decrease in instability measures at lower latitudes (≈ 30°N), while a local increase in temperature gradient and Eady growth rate in the poleward flank of the jet (Fig. 7.4a,c,d,f), especially in the upper troposphere around latitude 45°N. In January, the baroclinicity is more equatorward than in transition seasons as a result of a strong Hadley cell that creates a strong STJ (Lachmy and Harnik, 2014). The results shown here, which are based on a zonal symmetric model, are consistent with the idea that the MWM is a consequence of the Pacific winter jet being more subtropical while in transition seasons, the jet is more an EDJ-like or a mixed jet (Lachmy and Harnik, 2014).

To consider if a jet is more subtropical or more eddy-driven we consider the distance from the Ferrel's cell center (as the distance is larger, the jet will be more similar to a STJ). Fig. 7.4(g-i) shows that the jet's maximum is closest to the edge of the Hadley cell in January. Furthermore, while the jet peak of the EDJ is found in the middle of the Ferrel cell in both transition seasons, in January the jet peak is shifted equatorward (and the lower level wind maximum is poleward of the jet maximum). Therefore, we conclude that the jet in the January simulation is a more subtropical-like jet than in transition seasons.

To investigate the role of the poleward shift of the jet in transition seasons in comparison

to January, the January temperature profile was modified at midlatitudes to be more similar to the transition seasons in the following way:

$$T_{\text{Jan}-\text{tran}} = T_{\text{Jan}} + (T_{\text{tran}} - T_{\text{Jan}})e^{-\frac{(\phi-\phi_c)^2}{2\phi_d^2} - \frac{(\sigma-\sigma_c)^2}{2\sigma_d^2}} \tag{7.2}$$

where $\phi_c = 36^\circ$ is the center latitude that the change in temperature occurs, $\phi_d = 10^\circ$ is the typical width of the change in degrees, $\sigma_c = 0.63$ is the center height that the change occurs, $\sigma_d = 0.3$ is the width of the change in the vertical, T_{Jan} is the zonally symmetric Pacific January temperature profile, and T_{tran} is the temperature profile in the transition seasons where March, April, October and November are examined separately. The choice of parameter was done such that there will be similarity between the observed gradient differences in midlatitudes and the simulated ones.[1] Fig. 7.5 shows the temperature, wind, mass streamfucntion and EKE differences between January and the modified January profile (equation 7.2). The induced temperature changes lead to a weakening of the jet at its equatorward flank and strengthening at its poleward flank, where the temperature change is larger in fall than in the spring (Fig. 7.5a-d). Therefore, January spring-like simulations have a weak poleward shift of the jet (Fig. 7.5e,f), and consequently only a small change in the mean EKE (Fig. 7.5m,n). Conversely, the January fall-like simulations have a large shift in the temperature gradient and a large increase in EKE (Fig. 7.5o,p). This response of the eddies, which is similar to the response seen in chapter 6 implies that as the jet becomes more eddy-driven like and shifts more poleward, the EKE increases.[2]

7.4 Discussion and Summary

The Pacific MWM is a puzzling phenomena that is counter intuitive, since the EKE is at local minimum in the month where the meridional temperature gradient is largest. Thus, understanding the reasons for the MWM is essential in order to broaden the understanding of the physical mechanisms that control the storm tracks.

The scientific tools used in studies that investigated the MWM have mostly focused on investigating reanalysis data (e.g., Nakamura, 1992; Chang, 2001; Nakamura and Sampe, 2002; Penny et al., 2010, 2011, 2013), realistic GCMs (e.g., Chang, 2001; Park et al., 2010; Lee et al., 2013) and linear or quasi-geostrophic models (e.g. Zhang and Held, 1999; Harnik and Chang, 2004; Deng and Mak, 2005). Despite the progress in the understanding of the MWM possible mechanisms by these models there has been a gap between the success of reproducing the Pacific MWM-like behavior in realistic GCMs and linear models, and the inability to reproduce a MWM in idealized GCMs (e.g., Chang, 2006). Furthermore, many of the suggested mechanisms (e.g. increased advection above areas with large baroclinicity, topographic effects, seeding) as well as

[1] To make sure that the results are not very sensitive to the choice of the ϕ_c, also simulations with the value $\phi_c = 42^\circ$ were performed, and the results remains qualitatively similar.

[2] The modified January-October profile ($T_{\text{Jan}-\text{Oct}}$) has the largest EKE. Note that this does not imply that a simulation with the October temperature distribution has a larger EKE than a simulation with a temperature distribution of November/March.

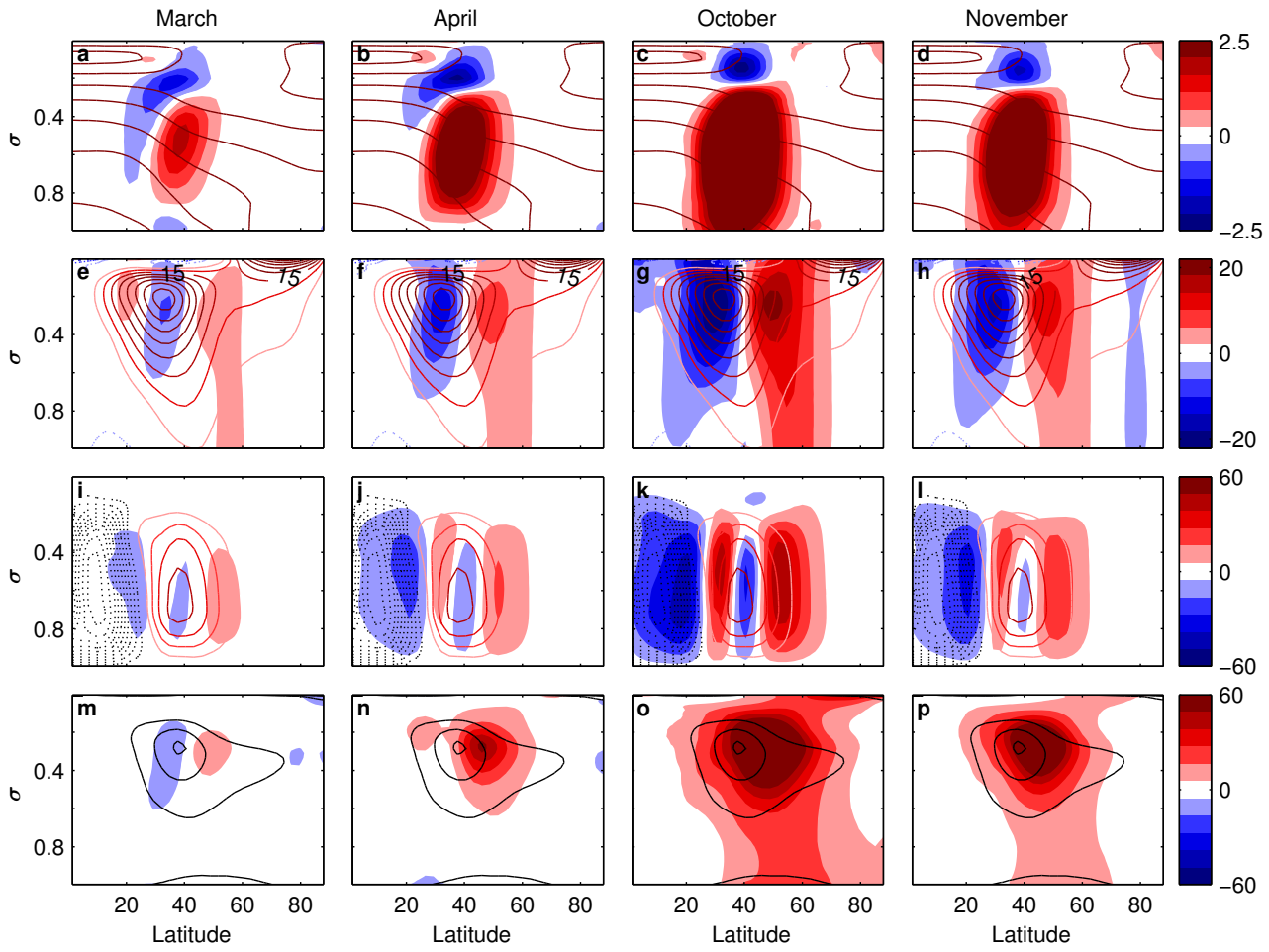

Figure 7.5: Temperature (a-d), zonal wind (e-h), mass streamfunction (i-l) and EKE (m-p) for simulations where the January temperature profile was modified as in equation 7.2. Contours show the January reference (dashed contours for negative values) and the colors represent deviation from this reference. The contour intervals are 15 K (temperature), 5 m s^{-1} (zonal wind), 10 kg $s^{-1} \times 10^9$ (mass streamfunction) and 50 m^2 s^{-2} (EKE).

many of the models for the MWM based their explanation and results on zonal asymmetries.

In this chapter, a zonally symmetric idealized GCM with a Newtonian cooling scheme which relaxes the zonal mean temperature with a fast time scale (4.8 hours), but relaxes eddies with a much longer time scale (20 days) is used. This allows mimicking the zonal mean observed temperature field in different months of the year in the northern Pacific and Atlantic. Keeping the mean relaxation time constant and changing the eddy relaxation time to values of $10, 40$ or 80 days changes the amplitude of eddies, which increase with reducing the relaxation time, but keeps the qualitative picture similar (not shown). The increase of eddies with relaxation time is because the relaxation time of eddies tends to hamper eddies and as the relaxation time is increased, eddies are less hampered by the diabatic term.

It is found that when the mean Pacific temperature field is simulated in different months, the EKE exhibits a MWM-like behavior where the EKE is larger by about 30 percent in transition seasons than in midwinter, which is similar to observation. When simulating the mean temperature fields in the northern Atlantic it is found that there is no MWM and there

is a single EKE maximum in winter.

The MWM-like behavior reproduced in a zonally symmetric idealized dry GCM, using a realistic temperature profile of the Pacific, implies that the temperature structure above the Pacific plays an important role in the MWM occurrence, and the presence of moisture or zonal asymmetries are not a necessary ingredient. Nevertheless, the temperature profile above the Pacific is a consequence of the presence of complicated dynamics, which may be affected significantly by latent heat and zonal asymmetries. An additional interesting point is that despite the vertical wind shear in the simulations being very similar to observations, the surface winds in the simulations are very different from the observed winds (Fig. 7.1(d-f)). As a consequence of this, the meridional wind shear in the simulations near the jet is reduced and the jet is wider (Fig. 7.1). The idealized GCM fails to reproduce realistic surface winds, and tends to decrease the wind below the jet maximal wind and increase the surface winds both south and north of the jet maximum, which tends to broaden the jet. This result weakens the argument that the MWM is a result of the narrow jet in midwinter as suggested by Harnik and Chang (2004) and Deng and Mak (2005), since the MWM is also present when the jet is broadened significantly.

To study the relevance of the conclusion that a poleward jet shift leads to increase in eddy fields to Earth's atmosphere, a realistic (zonally symmetric) Pacific-like January, November and March temperature fields were simulated. The simulations show that a MWM-like behavior in the EKE can be reproduced in the idealized framework used here. We show that in transition seasons (both in observations and simulations), the jet shifts poleward relative to its position during midwinter, and hypothesize that this shift contributes to the presence of the MWM. To verify this hypothesis, it was shown that when the January temperature gradient is modified at midlatitudes to resemble a transition season-like (which tends to shift the jet polewards), EKE increases. This finding is interesting since it suggests that the Pacific temperature structure, and specifically the poleward shift of the jet in transition seasons could have a significant contribution to the presence of the MWM. Note that also in chapter 3 we obtained a MWM in an idealized model and suggested that the vertical structure of baroclinicity plays a role in the presence of the minimum. Here we suggest a clear mechanism that could also lead to a MWM-like behavior. Furthermore, the simulations in this chapter are conducted with a different diabatic heating method, and the fact that the minimum is reproduced in both methods, increases the confidence that the minimum reproduction is method-independent.

Chapter 8

Circulation response to global warming-like temperature changes

Global warming simulations show robust temperature change in some atmospheric regions as a response to increased greenhouse gases concentrations. The most robust responses are tropical warming aloft, surface polar warming and stratospheric cooling (see Fig. 1.1). These temperature trends occur in all IPCC models, though their warming amplitudes are different. The discrepancy between models is especially large at the NH polar surface region, and the amplitude of warming varies significantly between models (Fig. 1.2). These changes might lead to changes in the extratropical atmospheric circulation. Generally, there is some agreement between the CMIP5 models that show a poleward shift in storm tracks and change in their intensity (e.g., Held, 1993; Stephenson and Held, 1993; Hall et al., 1994; Bengtsson and Hodges, 2006; Yin, 2005; O'Gorman and Schneider, 2008; Wu et al., 2010; O'Gorman, 2010b), although these changes do not occur in all models, and eddy fields response to the projected temperatures is not robust across models, especially in the NH (Chang et al., 2012).

Many previous studies that used an idealized GCMs focused on inducing diabatic heating changes that resemble the change in the temperature trends predicted by the IPCC report (e.g., Polvani and Kushner, 2002; Kushner and Polvani, 2004; Lorenz and DeWeaver, 2007; Lim and Simmonds, 2009; Butler et al., 2010; Lu et al., 2014). The challenge in the method used in these papers is that when inducing diabatic warming in certain regions, other regions change their temperature and therefore the temperature field often does not look like the prediction from the IPCC report. Furthermore, These studies used an idealized zonally symmetric temperature distribution. We find that using an idealized zonally symmetric temperature distribution is not suitable to understand the eddy response to global warming-like temperature changes, since the response of eddies is sensitive to the shape of the warming and to the chosen reference (section 8.2). Therefore, we use an idealized approach that allows simulating any 3D zonally asymmetric chosen temperature field (see section 2.3.1), and use a realistic temperature distribution as a target temperature and realistic 3-dimensional temperature changes. This allows investigating the response of eddies to different temperature changes in a realistic temperature distribution, such as upper tropical warming and surface polar warming.

In this chapter we aim to understand the response of eddies to changes in temperatures that resemble global warming like-scenarios. This approach is similar to the approach used by Lunkeit et al. (1998). In section 8.1 the data from a CMIP5 model, which is used to construct the 3D temperature field, and some details about the simulations are described. In section 8.2 we describe problems that limit the use of our previous approach. Nevertheless, in section 8.3 we use this approach to understand better some of the effects of upper tropospheric tropical temperature change and polar surface warming on the circulation. In section 8.4 we compare between a zonally asymmetric idealized model with realistic temperature distribution and a CMIP5 model with historical temperature distribution, and show that the main features of the circulation can be reproduced in the idealized model. In section 8.5 we use the idealized zonally asymmetric model to investigate the effect of the polar amplification (section 8.5.1) and the upper tropospheric warming (section 8.5.2) on the circulation. In section 8.6 we summarize the results.

8.1 Data and Methodology - the GFDL-ESM2G model

In this chapter, we use the GFDL-ESM2G model from the CMIP5 data set to obtain the historical temperature distribution for the NH winter. To do that, the monthly mean temperature data of the historical run is averaged over December-January-February (DJF) between the years 1980-2000. In order to obtain a global warming-like temperature distribution, the data from the RCP8.5 scenario between the years 2080-2100 is used. These mean temperature fields are used as a target temperature in our idealized simulations.

The zonally mean temperature difference, and meridional temperature gradient difference between the RCP8.5 to historical runs for the GFDL-ESM2G model are plotted in Fig. 8.1 as a function of latitude and pressure. In the SH the temperature gradient increases in midlatitudes in all vertical levels, while in the NH the absolute value of the temperature gradient increases in upper levels and decreases in lower levels. Because the temperature gradient change at midlatitudes in the SH is increasing at all levels, it is easier to understand the response of the circulation to these changes, and indeed CMIP5 models agree that the circulation in the SH will shift poleward and strengthen (Chang et al., 2012). This poleward shift can also be seen in simple idealized models as demonstrated in section 8.2.1 (see also Butler et al., 2010). The circulation response in the NH is more complicated due to the different response at different vertical levels, and there are relatively large differences between models (Chang et al., 2012), though in the upper troposphere, the majority of the CMIP5 models predict a poleward shift in the circulation.

While the GFDL-ESM2G model includes orography, the simple idealized model used in this chapter does not. Therefore, in order to obtain a full 3-dimensional target temperature for the idealized simulations conducted in this chapter the temperature is extrapolated downward in regions where there is land in the GFDL-ESM2G model. The target temperature is calculated by extrapolating the temperature downward using the mean lapse rate to estimate the tem-

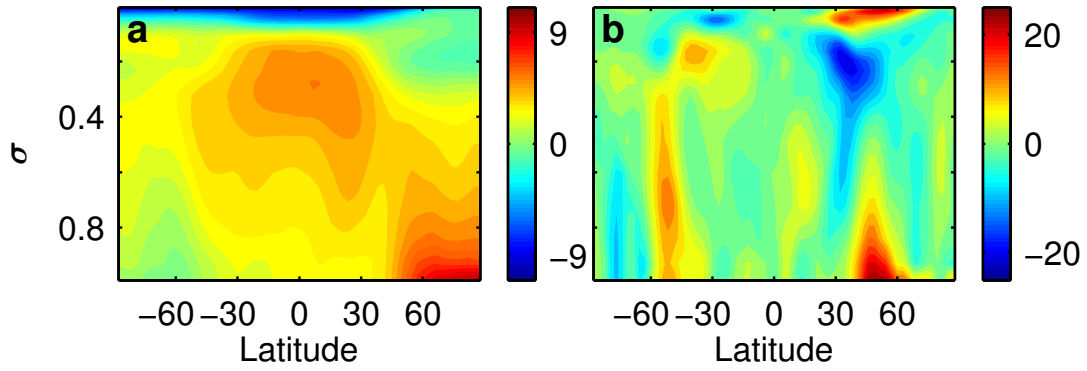

Figure 8.1: (a) The DJF zonal mean temperature difference and (b) The zonal mean meridional temperature gradient between the historical run and the RCP8.5 scenario for the GFDL-ESM2G model.

perature in every missing grid point (the mean lapse rate is calculated on a $15° \times 15°$ region near the point that we extrapolate to). [1] Although the model that is used here does not have a realistic representation of orography, we do take into account land masses by increasing the linear friction relaxation frequency by factor 4 to a value of 6 day^{-1} in regions where there are land masses (Fig. 8.2). Furthermore, the friction frequency is set to 3/2 day^{-1} at every grid point above the "land" and decays to zero 300hPa above it as in Held and Suarez (1994). This manipulation is necessary to obtain a separate storm tracks for the northern Atlantic and Northern Pacific. The relaxation frequency for the temperature in these simulations are $k_s = 1/7$ days^{-1} near the tropical surface and $k_a = 1/30$ days^{-1} in the upper troposphere (see Eq. B.2 for the parametrization of the relaxation time).

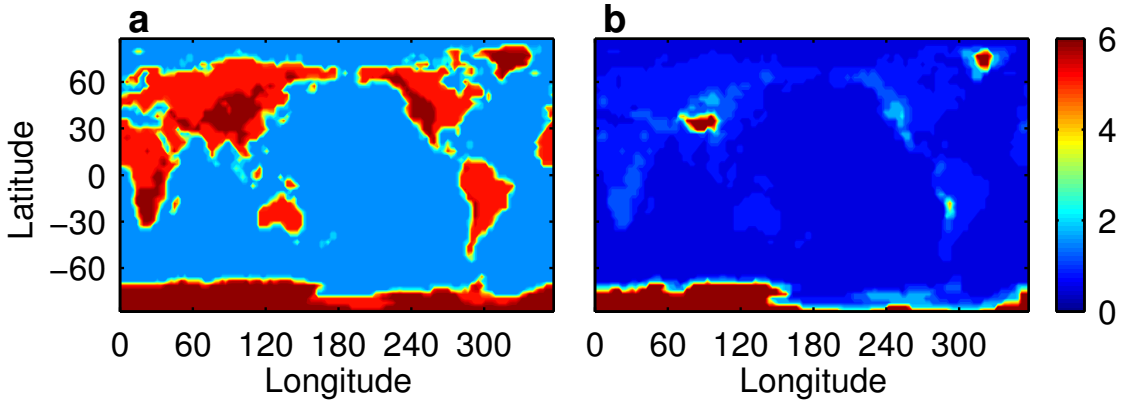

Figure 8.2: The linear friction relaxation frequency (day^{-1}) for the simulations we used zonally assymetric temperature distribtion for as a function latitude and longitude for two different levels (a) $\sigma = 0.98$ (b) $\sigma = 0.78$.

Since we use a zonally assymetric temperature distribution, EKE is examined based on temporal variance (both for the CMIP5 runs and our model runs). For variance statistics, daily or higher frequency data are needed. Thus we used 6-hourly data retrieved from the

[1] Near Antarctica, where there are large regions that are covered by high altitude land, we calculate the mean lapse rate at lower latitudes that are close to Antarctica and use this lapse rate value for the extrapolation.

CMIP5 archives for the GFDL-ESM2M model. CMIP5 provides 6-hourly pressure level data on selected levels only: 850, 500, and 250hPa, and the data is presented on these levels.

In sections 8.4 and 8.5, where we reproduce a zonally assymetric temperature distribution, it is necessary to integrate the model for a very long time in order to get a time non-dependent relaxation matrix that will produce the target temperatures accurately. To avoid these very long simulations, we use a time dependent relaxation matrix which is calculated as described in step 2 of section 2.3.1, but without zonal averaging the relaxation temperature. In order to avoid large fluctuations in the relaxation matrix we take $\alpha = 15000$, which guaranties that the relaxation temperature changes very slowly with time. Each of the simulations in sections 8.4 and 8.5 was integrated for 15000 days, where fields were calculated from the last 10000 days of each simulations. We note that the relaxation temperature has small changes after the first 5000 days, and only fluctuates around its mean value.

In the zonally symmetric simulations presented in section 8.2 the simulations are integrated for 2000 days and averaged over the last 1500 days, where simulations were also averaged over the two hemispheres such that the presented plots of the NH are actually an average over the two hemispheres.

8.2 The limitation of conventional diabatic heating methods

Idealized GCMs are useful since they can be used to deduct qualitative conclusions that are difficult to obtain from more complicated models. Therefore, different authors have studied the response of eddies to global warming-like trends in idealized GCMs with simplified diabatic heating methods (Polvani and Kushner, 2002; Kushner and Polvani, 2004; Lorenz and DeWeaver, 2007; Lim and Simmonds, 2009; Butler et al., 2010; Lu et al., 2014).

In this section the limitations of two idealized methods that can be used to investigate the effect of global warming-like temperature changes are demonstrated. We conclude that it is beneficial (and in some cases necessary) to consider a realistic 3-dimensional background state, and realistic temperature changes to investigate the response of eddies to global warming-like temperature trends. In section 8.2.1 we show that the standard method of modifying the relaxation temperature is not enough to understand the effect of global warming-like temperature changes on the circulation, since modifications in the relaxation temperature in a certain region, cause a response in other regions (this was also shown in chapter 2, but here it is shown in the context of global warming-like changes). These unwanted temperature changes affect eddies, and there is uncertainty if the eddy field changes are due to the wanted or unwanted temperature changes.

Furthermore, we show that the zonally symmetric approach that was used in previous chapters, where the temperature field is predetermined, is problematic from two main reasons: (a) eddies are sensitive to the exact shape of the temperature changes; (b) in different reference states eddies respond differently to similar changes in the temperature field. The sensitivity

of eddies to the background states implies that in order to study the effect of global warming-like temperature changes on the atmosphere, a realistic (3-dimensional) reference is needed. Furthermore, the sensitivity of simulations to the exact shape of temperature changes implies that it is necessary to consider a realistic global warming-like temperature changes.

8.2.1 Eddy response to different diabatic heating fields

One useful method to investigate the response of global warming-like temperature trends on the atmospheric circulation, which was used in many studies (e.g., Polvani and Kushner, 2002; Lorenz and DeWeaver, 2007; Butler et al., 2010; Lu et al., 2014), is to modify the diabatic heating in regions where the temperature is predicted to change, and study the circulation response. As was shown in chapter 2, this method is problematic since heating an atmospheric region leads to temperature changes in different regions, and it is difficult to obtain an accurate global warming-like temperature trends. To demonstrate this point, and to show that this method is sensitive to the heating profile which is used, HS-like simulations with increased relaxation temperature were conducted. The heating profile in the tropics that is used can be expressed as (after Butler et al., 2010)

$$\delta T^{\text{relax}}_{\text{tropics}} = A \exp\left[-\frac{(\sigma-\sigma_{\text{c}})^2}{\sigma_{\text{w}}} - \frac{\phi^2}{\phi_{\text{w}}}\right], \tag{8.1}$$

where A is the amplitude change, σ_c is the center of heating in the vertical, σ_w is the vertical width of the heating, ϕ is the latitude and ϕ_w is the meridional width of the heating.

The colors in Fig. 8.3 show the difference between simulations with upper tropospheric tropical heating to the HS reference simulation (the HS was used also used in other chapters, and see appendix B for its diabatic heating parametrizations) of the relaxation temperature, temperature, zonal wind, EKE and EHF. The upper tropospheric heating parameters used in these simulations are given in the caption of Fig. 8.3. In all of these simulations, the eddy fields increase, and for the three left most simulations, there is a clear poleward shift in the circulation, which is consistent with previous results of similar simulations (Butler et al., 2010; Sun et al., 2013).

Furtheremore, the three left columns show that when an upper tropospheric heating is applied, the temperature field and the meridional temperature gradient are modified in regions out of the upper tropics, such as the lower levels around latitude 40° (Fig. 8.3e,f,g). The poleward shift of the circulation is relatively robust, and when using the parameter combinations of $A = 10$ K, $\sigma_c = 0.3, 0.5$, $\sigma_w = 0.07, 0.11$ and $\phi_w = 0.21, 0.4$, there is also a poleward shift of the circulation (total of 8 simulations, not shown), though in all of these simulations the temperature changes are not constrained to the upper tropics. Although there is a poleward shift in the circulation, it is difficult to isolate the contribution of the upper tropospheric temperature changes to this shift since other regions change their temperature distribution as well. Furthermore, in these simulations the temperature gradient increases at midlatitudes in all atmospheric levels, which is similar to the predicted temperature gradient changes in the

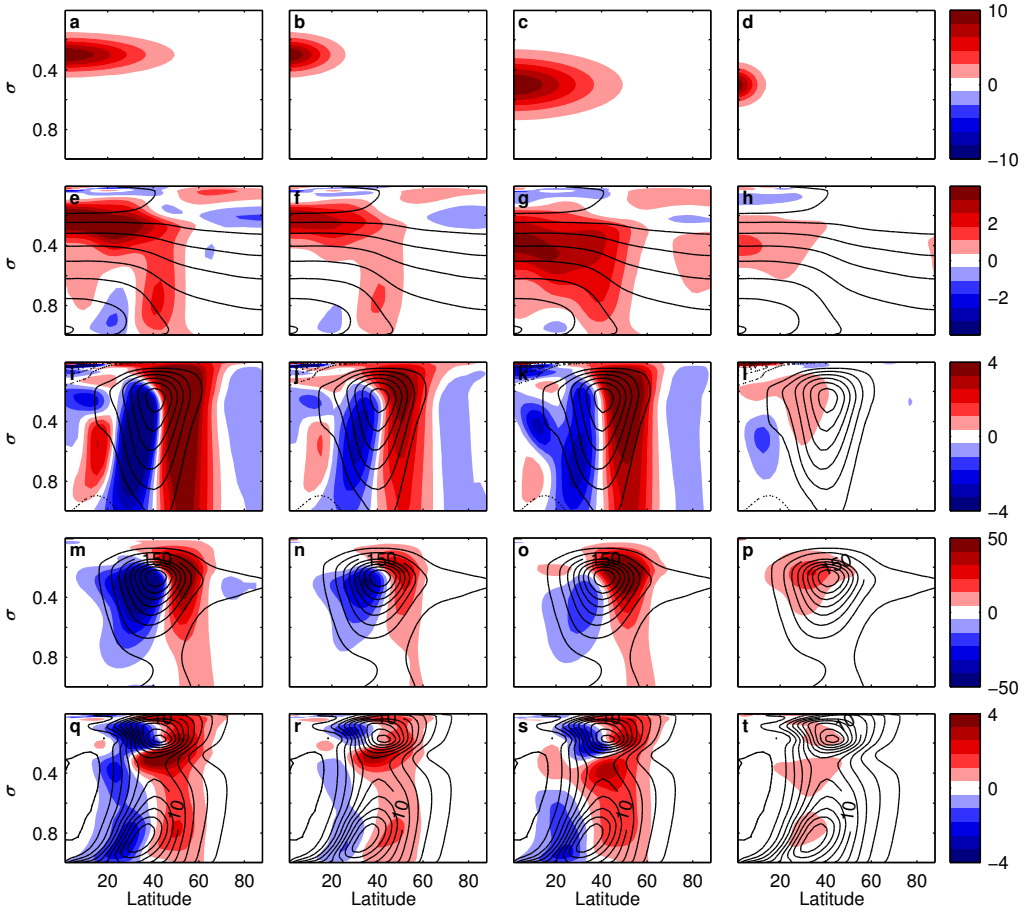

Figure 8.3: Relaxation temperature (a-d), temperature (e-h), zonal wind (i-l), EKE (m-p) and EHF (q-t) for simulations that the upper tropical troposphere was modified with different heating shapes. The parameters used in these simulations are $A = 10$ K, $\sigma_c = 0.3$, $\sigma_w = 0.07$ and $\phi_w = 0.4$ (first column), $A = 10$ K, $\sigma_c = 0.3$, $\sigma_w = 0.07$ and $\phi_w = 0.21$ (second column), $A = 10$ K, $\sigma_c = 0.5$, $\sigma_w = 0.11$ and $\phi_w = 0.4$ (third column), $A = 10$ K, $\sigma_c = 0.5$, $\sigma_w = 0.07$ and $\phi_w = 0.11$ (fourth column). Colors indicate deviation from a reference, and contour show the reference fields. The contour intervals are 15 K (temperature), 5 m s^{-1} (zonal wind), 50 m^2 s^{-2} (EKE) and 2 Km s^{-2} (EHF).

SH (Fig. 8.1), but not to the projections in the NH. It is possible that the similarity of the temperature changes between these simulations to the SH projections are the underlying reason that the circulation response of these simulations agree with the SH circulation response in the CMIP5 models in the sense that the jet and storm tracks shift poleward (Chang et al., 2012). We do note, that in most of the conducted simulations the temperature gradient also reduces in the subtropics at the lower levels (e.g., Fig. 8.3e,f), which is not predicted in a global warming scenario in the SH, but such a signal exists in the NH (see Fig. 8.1).

On the right panels of Fig. 8.3 there are the results of a simulation in which the upper troposphere heating was narrower, and the temperature changes occurring almost only in the upper tropical troposphere. In these simulation there is no poleward shift of the circulation. This implies that eddy response to upper tropical heating is shape dependent, and narrower heating can lead to a different circulation response (see similar results also in Sun et al., 2013).

Since the temperature response in these simulations is partly different from the projected

changes (especially in the NH), we conclude that it is difficult to rely on these results to derive conclusions regarding the effects of the temperature changes on the circulation. Furthermore, we note that even if the temperature changes would look similar to projected temperature changes, it would not necessarily imply that we could rely on the results to be robust in different background states, since the circulation response could be different in different background states (as demonstrated in the next section).

One solution to the unwanted changes in the temperature changes, and enables changing the temperature only in a selected region is to use the methods used in this thesis to control the temperature distribution (methods described in sections 2.3.1 and 2.3.2). As we show in the next section, using these methods raises other ambiguity in the results.

8.2.2 Eddy response to different temperature fields

In this section it is demonstrated that the zonally symmetric approach that was used in previous chapters, has ambiguities regrading the response of eddy fields to global warming-like temperature changes. We find that the response of eddy fields to global warming-like temperature changes is reference dependent and dependent of the exact parametrization of the temperature changes.

To demonstrate the sensitivity of eddies to the chosen reference simulation, the fast zonal mean relaxation method is used (see section 2.3.2 for method details) with two different target temperature references. The first target temperature reference is the HS simulation, which was presented also in other chapters. The second target temperature reference is taken from a model which is described in details in Schneider (2004). The main differences between the HS reference and the Schneider (2004) reference simulations are: (a) different relaxation temperature, though both aim to represent an Earth-like atmospheres and (b) the boundary layer in the Schneider (2004) is represented by quadratic term and not by a linear term as in the HS. [2] The contours in the left column of Fig 8.4 show the temperature, zonal wind, EKE, EMFC and EHF for the HS target temperature reference, and on the right column of the Fig 8.4 for the Schneider (2004) target temperature reference. We note that some differences between the references exist, such as stronger surface winds and larger EKE near the surface in the HS reference. Nevertheless, the two references have similar temperature structure and circulation regime, and both references can be used to represent an Earth-like atmosphere.

To consider a global warming-like temperature changes in the upper troposphere, the target temperature was modified as follows:

$$\delta T_{\text{tropical}} = -A * \left((\tanh \left[\frac{|\phi| - \phi_c}{\phi_w} \right] \exp \left[\frac{-(\sigma - \sigma_c)^2}{2\sigma_w^2} \right] - \exp \left[\frac{-(\sigma - \sigma_c)^2}{2\sigma_w^2} \right] \right), \tag{8.2}$$

where A determines the amplitude of the temperature change, ϕ is the latitudinal coordinate,

[2] The equator to pole temperature difference we use to obtain the reference temperature in the Schneider (2004) reference is 100 K (using 60 K results in a state with very weak eddies, but different response of eddies is obtained also for this state when comparing to the HS run

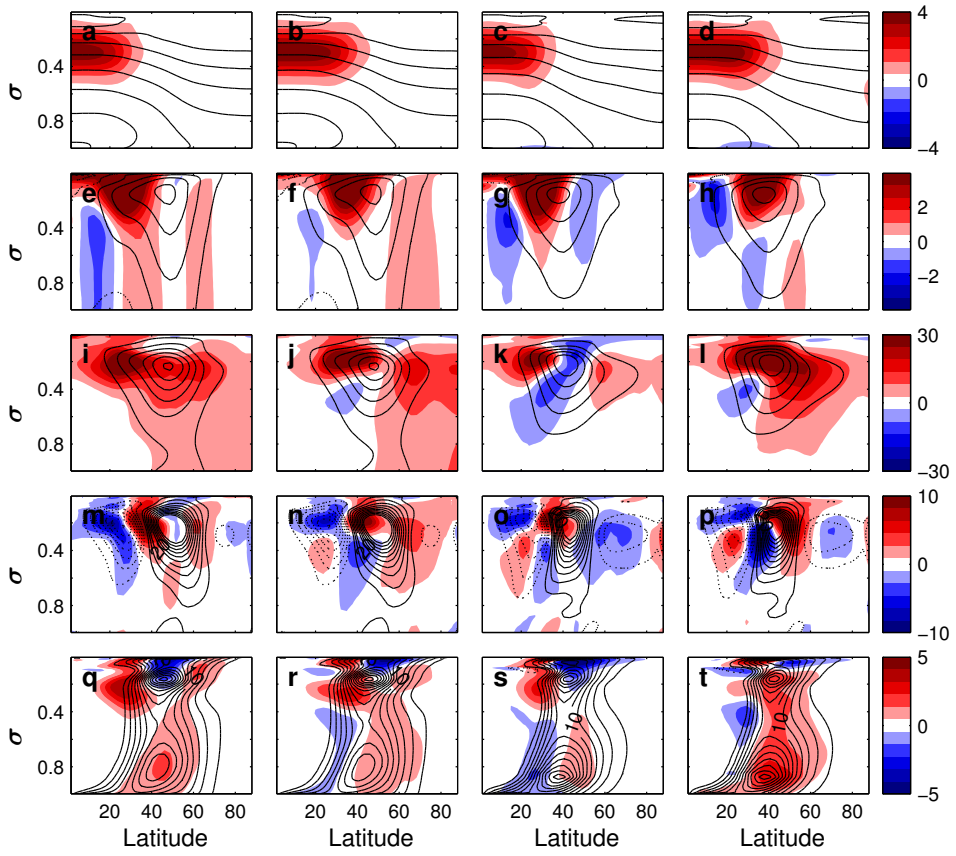

Figure 8.4: Temperature (a-d), zonal wind (e-h), EKE (i-l), EMFC$\times 10^6$ (m-p) and EHF (q-t) for simulations that the upper troposphere was modified with the parameters $A = 2$ K, $\phi_c = 25°, 35°$, $\phi_w = 10°$, $\sigma_c = 0.3$, $\sigma_w = 0.11$ for the HS reference (two left columns) and Schneider (2004) reference (two right columns). Colors represent deviation from reference and contours show the reference simulation fields. The contour intervals are 15 K (temperature), 5 m s^{-1} (zonal wind), 50 m^2 s^{-2} (EKE), 5 m s^{-2} (EMFC) and 2 K m s^{-2} (EHF).

ϕ_c determines the region where the gradient is modified, ϕ_w determines the latitudinal width of the region where the gradient is modified, σ is the vertical coordinate, σ_c is the center vertical level that the gradient is modified and σ_w determines the vertical width of of the region where the gradient is modified. The tanh function that parametrizes the latitudinal shape of heating is preferred over an exponential dependency because it produces a more similar shape to the predicted gradient changes in global warming simulations, where the gradient change is concentrated in midlatitudes and not inside the tropics (Fig. 8.1b).

The temperature, zonal wind, EKE, EMFC and EHF are shown in Fig. 8.4 for simulations with the parameters $A = 2$ K, $\phi_c = 25°, 35°$, $\phi_w = 10°$, $\sigma_c = 0.3$, $\sigma_w = 0.11$ with the HS reference (two left columns) and with the Schneider (2004) reference in the two right columns. The simulations presented in the first and third column of Fig. 8.4 have the same temperature modification relatively to their reference simulations, but have different reference state. The EKE response in these two simulations is very different. In Fig. 8.4i that uses the HS reference, there is an increase in the EKE in all latitudes, while in Fig. 8.4k that uses the Schneider (2004) reference there is a decrease in EKE near the jet core. Furthermore, also the EHF and EMFC have significant differences between the simulations. This implies that the reference state can

play a role in the response of eddies to temperature changes even when the two background states are relatively similar. The fact that different reference states respond differently to similar temperature changes is not too surprising because different reference states have their Hadley cell, jet stream and other general circulation features located at different latitudes (and pressure levels), and therefore similar temperature changes can result in a different circulation response. For example, if two simulations have their jet located at different latitudes, similar increase in temperature gradient can increase in one simulation the jet in its poleward flank, and in another reference in its equatorward flank, this in turn can lead to different eddy response. This dependency is noted here since it is usually overlooked, and in this set of simulation, the specific reference plays an important role in determining the results of the eddy fields changes. We conclude that the circulation response to temperature changes should be considered reference dependent.

Furthermore, the simulations in the third and fourth column of Fig. 8.4, which have the same reference simulation, have very different eddy response to increased temperature in the upper tropics. In general, eddies can have large sensitivity to the specific shape of the temperature change, and two relatively similar temperature changes can lead to a different circulation response. We note that the sensitivity of eddies to the meridional position of the upper tropospheric heating, was also seen in chapter 5 and is shown also in the next section. These results imply that in order to investigate the response of eddy fields to global warming-like temperature changes, an accurate temperature changes should be simulated.

The main conclusion from this section is that since the eddy response in simulations is sensitive to both the reference, and the shape of the heating, it implies that in order to use idealized simulations to get a more reliable response of eddies to global warming like simulations, one would have to use a reference simulation that resembles the Earth atmosphere, and temperature changes that resembles global warming projections (see section 8.5). Furthermore, even if the sign of the eddy response would not have been shape/reference dependent, in order to estimate the magnitude of eddy changes as a response to temperature changes, it would be more useful to use more realistic reference, and a more realistic projections of temperature changes.

8.3 Response of zonally symmetric simulations to global warming-like temperature changes

In section 8.2.2 it was shown that the use of the fast zonal relaxation method described in section 2.3.2 has limitations when investigating the circulation response to global warming-like temperature changes. Nevertheless, since the fast zonal relaxation method was never applied in the literature to global warming-like changes (to our knowledge), it is used here to demonstrate a few important points regarding the effects of global warming-like temperature changes on the circulation. Although conclusions regarding the circulation response to global warming-like temperature changes shown here can not be considered to be robust (see previous section), they assist to understand better the circulation response in the more realistic zonally asymmetric

simulations presented in section 8.5.

8.3.1 Tropical upper tropospheric warming - the role of lapse rate changes

Since the NH meridional temperature gradient has different signs in the upper and lower levels, the main focus of this thesis (and many studies) was concentrated on trying to understand if eddies are more sensitive to the upper or lower meridional temperature gradient. To emphasize the important role of the local lapse rate changes, which was also demonstrated in section 5.2.2, two sets of simulations with identical changes in the meridional temperature gradient, but different changes in the lapse rate are considered. The temperature gradient is modified as described in Eq. 8.2 with the HS reference temperature with the parameters $\phi_c = 25°, 35°, 45°, 55°$, $\phi_w = 10°$, $\sigma_c = 0.3$, $\sigma_w = 0.11$. The temperature, zonal wind, EKE, EMFC and EHF of these simulations are plotted in Fig. 8.5.[3]

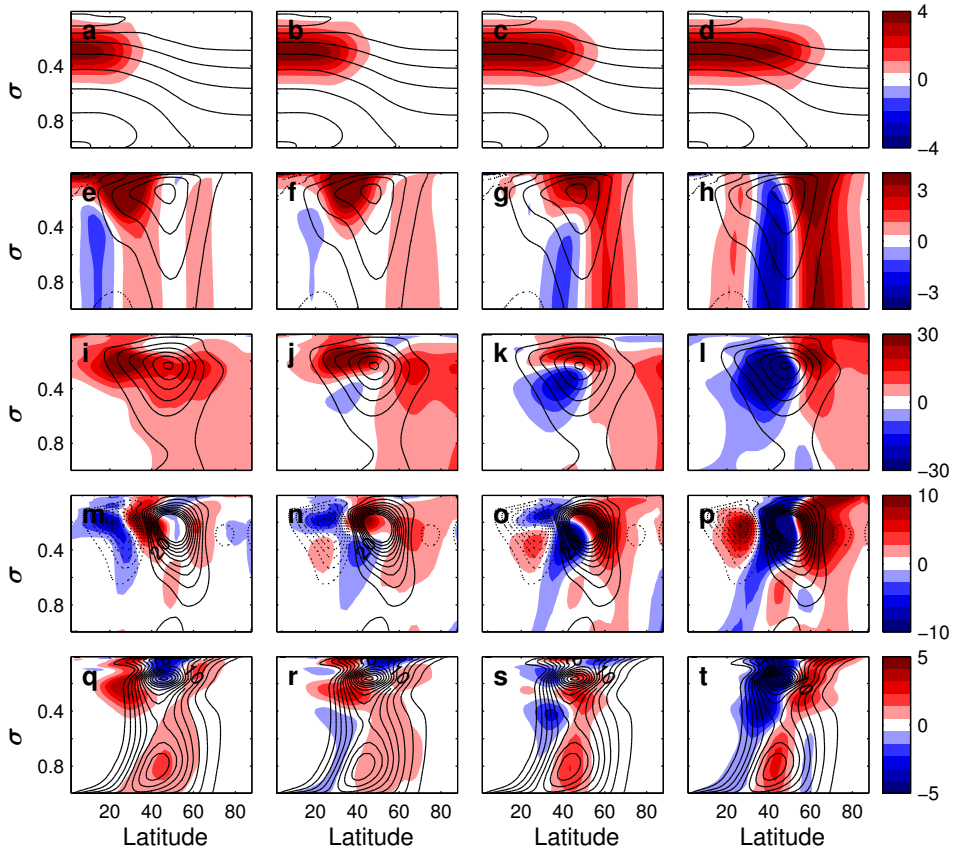

Figure 8.5: Temperature (a-d), zonal wind (e-h), EKE (i-l), EMFC$\times 10^6$ (m-p) and EHF (q-t) for simulations that the upper troposphere was modified with different upper tropospheric warming with the HS reference. Colors represent deviation from reference and contours show the reference simulation fields. The contour intervals are 15 K (temperature), 5 m s^{-1} (zonal wind), 50 m^2 s^{-2} (EKE), 5 m s^{-2} (EMFC) and 2 K m s^{-2} (EHF).

In order to demonstrate that lapse rate changes play a crucial role in these simulations, an-

[3]Similar sets of simulations with the parameter combinations $\sigma_w = 0.07, 0.11$, $\phi_w = 7, 10°$ showed qualitatively similar results (total of 4 sets of simulations).

other set of simulations with identical meridional temperature gradient changes was conducted, but instead of increasing the upper tropical temperature gradient, the temperature was reduced at higher latitudes.[4] In Fig. 8.6 the same quantities are plotted for this simulation set. Note that the meridional temperature gradient is identical in Figs. 8.5 and 8.6.

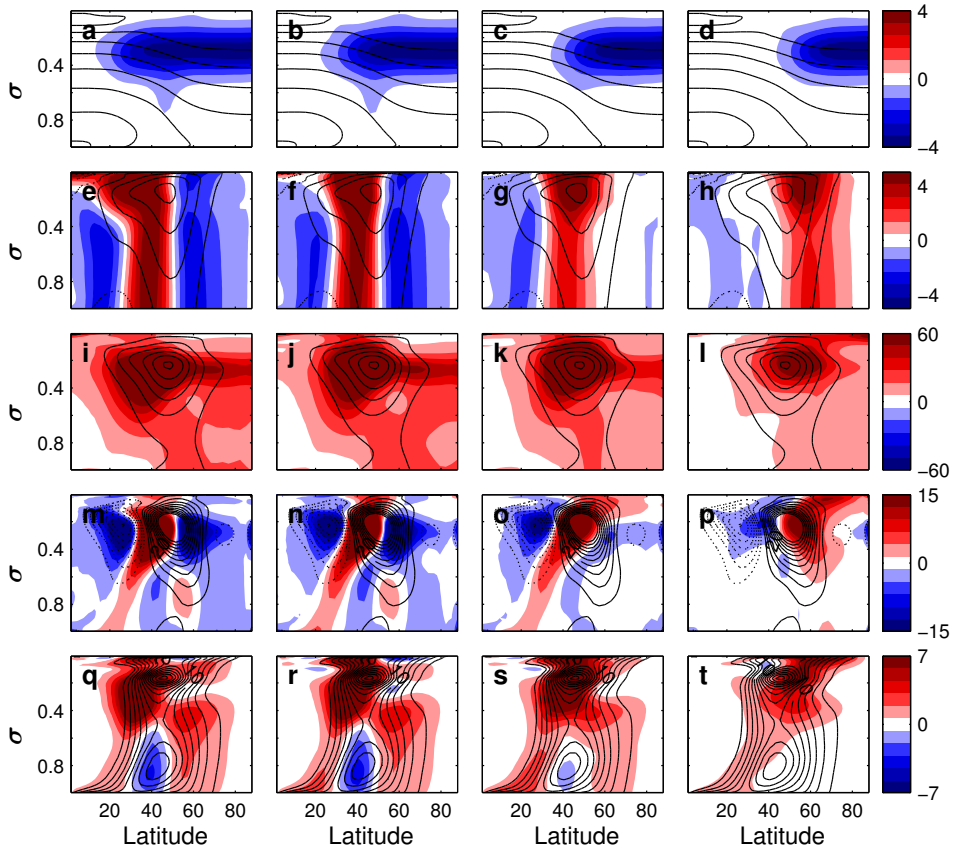

Figure 8.6: Temperature (a-d), zonal wind (e-h), EKE (i-l), EMFC$\times 10^6$ (m-p) and EHF (q-t) for simulations that the upper troposphere was modified with different upper polar cooling with the HS reference. Colors represent deviation from reference and contours show the reference simulation fields. The contour intervals are 15 K (temperature), 5 m s^{-1} (zonal wind), 50 m^2 s^{-2} (EKE), 5 m s^{-2} (EMFC) and 2 K m s^{-2} (EHF).

Fig. 8.5(i-l) shows a moderate response in EKE to these temperature changes, where there is even a different EKE trends in Fig. 8.5i,j (increased EKE) and in Fig. 8.5k,l (mostly decrease in EKE). The EHF tend to increase mostly in the lower levels near the maximal value of the EHF of the reference. Furthermore, the EMFC tends to shift polewards in most of the simulations (Fig. 8.5n,o,p), and consequently also the surface wind tends to shift poleward (Fig. 8.5f,g,h). This poleward shift is qualitatively similar to the shift seen in CMIP5 models, and also in the idealized simulations shown in Fig. 8.3.

On the other hand, the circulation response to similar meridional temperature gradient changes that results from cooling at upper high latitudes is different. The EKE tends to increase dramatically in these simulations Fig. 8.6(i-l). Furthermore, in most of these simulations there is no shift in EMFC (Fig. 8.6m,n,o), and consequently no poleward shift of the wind (Fig. 8.6e,f,g). The response of the EHF occurs mostly at high levels, and the response in the lower level is

[4]This temperature modification was done by reducing from Eq. 8.2 its temperature change at the equator.

weak (Fig. 8.6q-t).

The large eddy response differences, as well as the different zonal wind response emphasize that changing the meridional temperature gradient in the upper troposphere as a result of high latitude upper level temperature reduction as in Fig. 8.6 or as a result of upper level tropical warming as in Fig. 8.5 leads to very different circulation response. These large differences in the response are due to the different changes in lapse rate. When the temperature gradient is increased by warming the upper tropics, the static stability increases at mid-upper levels of the troposphere. The simultaneous increase in meridional temperature gradient and the increased static stability has opposite effects on eddies, and therefore eddy fields have a relatively weak response. Furthermore, in some simulations EKE increases (Fig. 8.5i,j) and in other it decreases (Fig. 8.5k,l), which implies that the sign change is determined by an interplay between these quantities. As the meridional temperature gradient is modified in higher latitudes, the static stability in the upper troposphere increases in larger region, and this is possibly the reason why the simulations on the two right panels of Fig. 8.5 have a reduced EKE, and the two left panels (which have a smaller average increase in static stability) show an increase in EKE. A similar EKE reduction as a response to increased temperature gradient in the tropical upper levels is seen in the zonally asymmetric simulations in section. 8.5.2.

When the temperature gradient is increased in the upper levels by reducing the temperatures at high latitude, the static stability decreases at mid-upper levels of the troposphere. Since the meridional temperature gradient increases at the same time, these two changes act to reduce the atmospheric stability and eddy fields respond strongly (Fig. 8.6).

8.3.2 Surface polar temperature changes

Since in a global warming scenario, the temperatures are predicted to significantly increase in the NH polar surface, we also show here results of simulations that the temperatures are modified in the lower troposphere at the polar region. The target temperature was modified as follows:

$$T_{\text{polar}} = -A * \exp\left[\frac{-(\sigma-1)^2}{2\sigma_{\text{w}}^2} - \frac{(|\phi|-90)^2}{2\phi_{\text{w}}^2}\right], \tag{8.3}$$

where the parameters used in the simulations were $A = 4$ K, $\sigma_w = 0.1, 0.2, 0.3$ and $\phi_w = 45°$. In Fig 8.7, the temperature, zonal wind, EKE, EMFC and EHF are plotted for four of these simulations (see parameters in the figure caption). We find that in these simulations the zonal wind tend to weaken in poleward flank of the jet (this result is expected from thermal wind balance). Furthermore, the EMFC tend to shift equatorward, and EHF tend to weaken in close to the surface in the poleward flank of the jet. In most of these simulations there is a decrease in EKE at the poleward flank of the jet, but this result is not robust in all simulations. For example, the simulation in presented in the second column of Fig. 8.7 increases its EKE in a response to the polar heating. It is possible that the increase in EKE is a result of an increased static stability in this simulation that destabilizes the atmosphere (this is similar explanation as in section section 8.3.1). This response is also similar to the response shown in chapter 3 of

simulations to increased temperature gradient in the lower level.

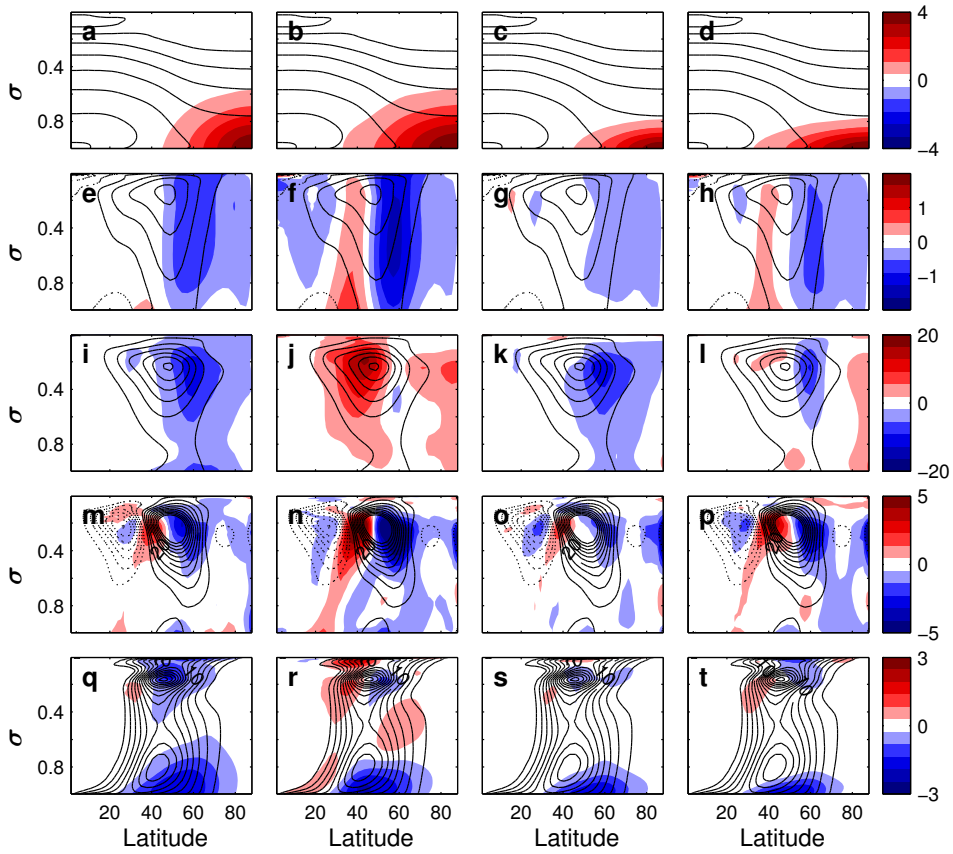

Figure 8.7: Temperature (a-d), zonal wind (e-h), EKE (i-l), EMFC$\times 10^6$ (m-p) and EHF (q-t) for simulations where the polar surface temperatures were modified with the parameters $\phi_w = 35°$, $\sigma_w = 0.2$ (first columns), $\phi_w = 45°$, $\sigma_w = 0.2$ (second column), $\phi_w = 35°$, $\sigma_w = 0.1$ (third column) and $\phi_w = 45°$, $\sigma_w = 0.1$ (fouth columns). Colors represent deviation from reference and contours show the reference simulation fields. The contour intervals are 15 K (temperature), 5 m s^{-1} (zonal wind), 50 m^2 s^{-2} (EKE), 5 m s^{-2} (EMFC) and 2 K m s^{-2} (EHF).

The poleward shift of the circulation, and the weakening of eddies in response to surface polar heating in idealized models is not a new result (Butler et al., 2010), but here it is demonstrated that this result has some sensitivity to the shape of the temperature change, and the EKE can have a different response when the shape of the temperature is different (Fig. 8.7j).

Comparing the magnitude of changes of eddy fields in the simulations where the upper troposphere temperature was modified (Fig. 8.4) and the simulations that the polar surface temperature was modified (Fig. 8.7), we find that for similar change in temperature magnitude, there are larger changes in eddy fields as a result of upper tropospheric temperature changes (although it is difficult to determine this accurately since each simulation in each of the simulations sets have a different change in eddy fields, so it can be dependent on the exact simulations we compare). These differences are of the order of factor 2-3, and since the temperature changes in most of IPCC models show larger changes in the NH polar surface, it is difficult to determine which of these effects would be dominant in a future global warming scenario. In order to study the importance of realistic global warming-like temperature changes (both in shape and in amplitude) on eddy fields, a realistic 3-dimensional temperature changes

are necessary.

8.4 Comparison between idealized model to the GFDL-ESM2G model

The temperature field from the historical and RCP8.5 scenarios of the GFDL-ESM2G model are used to produce an idealized historical and idealized RCP8.5 scenario as described section 8.1. The zonal wind and the EKE of the historical run of the GFDL-ESM2G model (left column) and of the idealized historical run (right column) are plotted in Fig. 8.8 and Fig. 8.9, respectively, for different pressure levels (850, 500 and 250 hPa). In general there is good agreement between the historical run of the GFDL-ESM2G model and the idealized run, though the wind amplitudes in the idealized model are generally weaker, especially close to the surface and in the SH. Furthermore, in the SH the EKE is weaker in the idealized run, while the EKE in the NH is stronger in the idealized run in mid and lower levels.

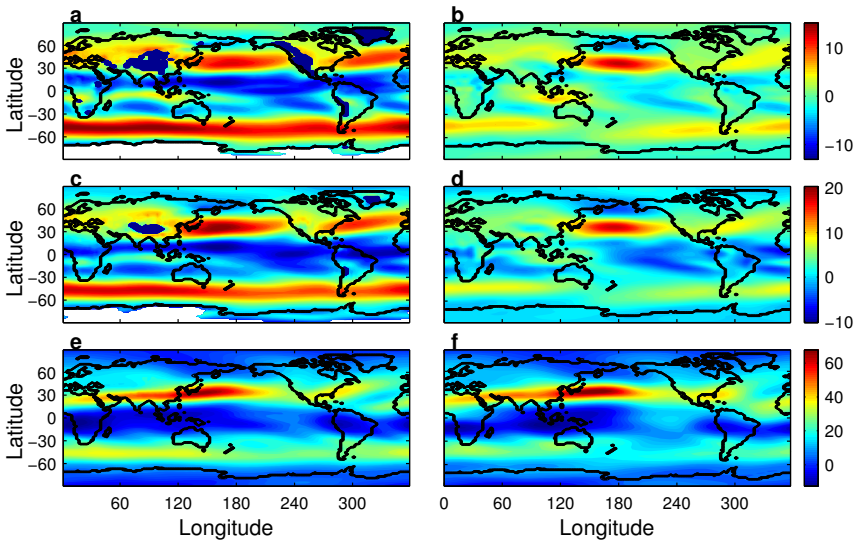

Figure 8.8: The zonal wind for the historical run of the GFDL-ESM2G model (left panels) and the idealized historical simulation (right panels) as a function of longitude and latitude at different pressure levels. Panels a,b are at 850 hPa, c,d are at 500 hPa, e,f are at 250 hPa.

There are many possible reasons why the idealized model does not reproduce well the wind and eddy fields, such as different land representation, the lack of moisture, clouds, radiation and other important physical processes that are not included in the idealized model (for a further discussion see 7.2). Nevertheless, the idealized simulation captures the majority of the general features, such as the jet location and the northern Pacific and Atlantic storm tracks. Note that despite the fact that our model is very idealized, the temperature field we use to reconstruct the climate is influenced with many of the complexities which are not included in the model such as clouds, air-sea fluxes, topography etc.

The zonal wind and the EKE differences between the RCP8.5 and the historical runs of the GFDL-ESM2G model (left column) and of the idealized simulations (right column) are shown

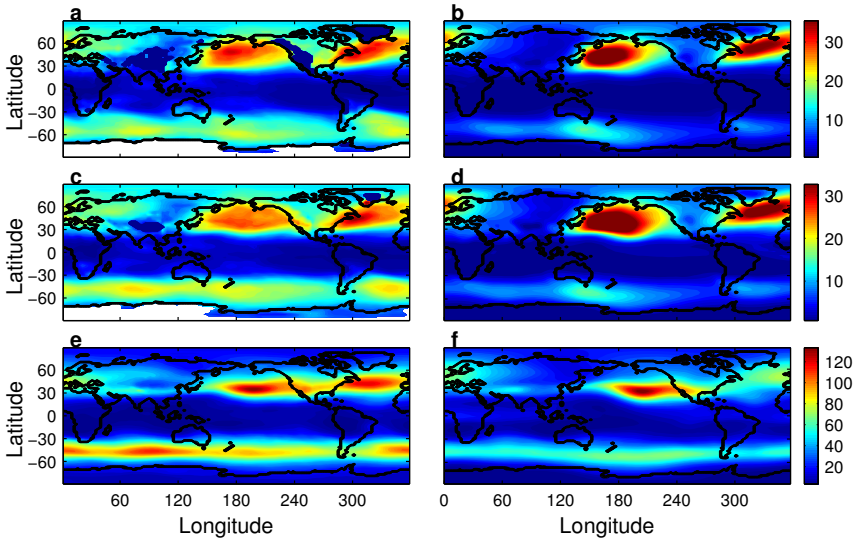

Figure 8.9: The EKE for the historical run of the GFDL-ESM2G model (left panels) and the idealized historical simulation (right panels) as a function of longitude and latitude at different pressure levels. Panels a,b are at 850 hPa, c,d are at 500 hPa, e,f are at 250 hPa.

in Fig. 8.10 and Fig. 8.11, respectively, for different levels (850, 500 and 250 hPa). Figs. 8.10 and 8.11 show that the idealized model succeeds to capture the wind and EKE changes mostly in the SH, and in the upper levels, while the wind differences in the mid-lower levels in the NH are different between the GFDL-ESM2G and the idealized model. In general, it is reasonable that the NH differences shown in Figs. 8.10 and 8.11 between the GFDL-ESM2G and the idealized model are larger in the NH than the SH because of the large land masses that exist in the NH and are not represented realistically in the idealized model. Furthermore, the circulation response in the NH varies significantly between CMIP5 models, and we do not expect that the idealized model could reproduce accurately eddy changes only by simulating its temperature distribution. Nevertheless, different studies showed that the temperature distribution, or more specifically the MAPE, is correlated with eddy fields in different CMIP5 models (O'Gorman, 2010a; Chang, 2013), which implies that the mean temperature distribution is the primary driver of eddy fields.

We conclude that the idealized historical run we use can reproduce the general features of the 3-dimensional circulation (Figs. 8.8 and 8.9), and can serve as a more realistic reference state than idealized zonally symmetric models such as the HS. In the next section we study the response of the idealized model with the historical background to global warming-like changes in the temperature gradient that results from polar surface warming and upper tropospheric tropical warming.

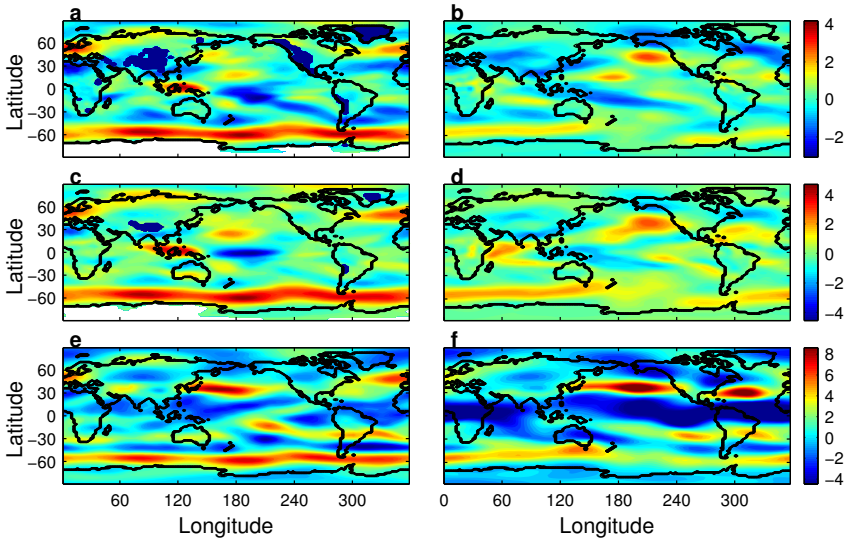

Figure 8.10: The zonal wind differences between the RCP8.5 scenario and the historical simulations of the GFDL-ESM2G model (left panels) and of the idealized simulations (right panels) as a function of longitude and latitude at different pressure levels. Panels a,b are at 850 hPa, c,d are at 500 hPa, e,f are at 250 hPa.

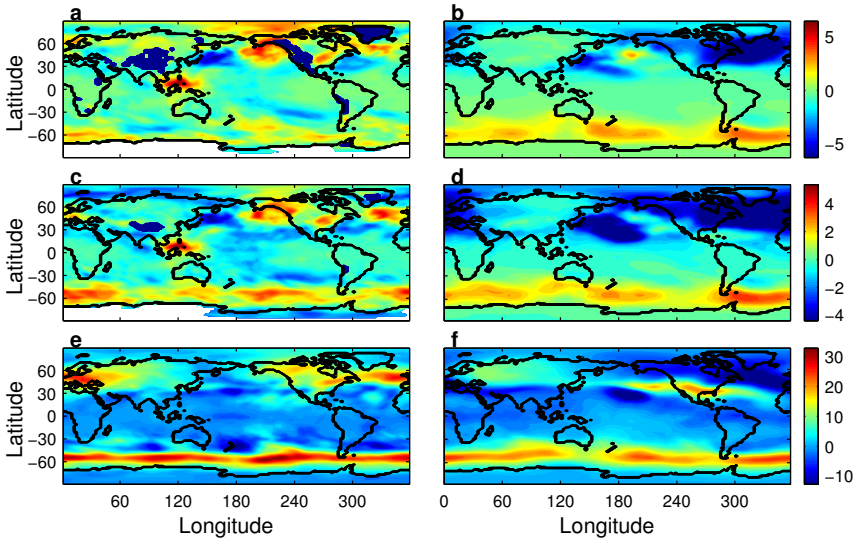

Figure 8.11: The EKE differences between the RCP8.5 scenario and the historical simulations of the GFDL-ESM2G model (left panels) and of the idealized simulations (right panels) as a function of longitude and latitude at different pressure levels. Panels a,b are at 850 hPa, c,d are at 500 hPa, e,f are at 250 hPa.

8.5 Eddy response to global warming-like 3D temperature changes in idealized GCM

8.5.1 Eddy response to polar surface warming

The polar amplification in the temperature trends has large differences between different models (Fig. 1.2). These differences in the temperature trends might lead to different circulation response in different models. In order to isolate the effect of increased surface polar temperatures on the circulation, the historical target temperature was modified at the NH polar surface region

such that its gradient resembles a global warming-like temperature gradient. The temperature modification can be expressed as

$$\delta T_{\text{target}} = Ae^{-\frac{(\sigma-1)^2}{\sigma_w}} \int_{\phi_1}^{\phi} \partial_y (T_{\text{RCP8.5}}(\phi_i) - T_{\text{hist}}(\phi_i)) d\phi_i, \tag{8.4}$$

where ∂_y is the meridional gradient, T_{hist} is the historical temperature distribution, $T_{\text{RCP8.5}}$ is the temperature distribution of the RCP8.5 scenario, ϕ_1 is the latitude that poleward of it the temperature gradient is modified, A is the amplitude of change relative to the RCP8.5 polar amplification scenario in the GFDL-ESM2G model and σ_w determines the vertical width of the gradient change. This formulation is chosen because the temperature changes expressed in Eq. 8.4 give the same surface meridional temperature gradient as the difference between the RCP8.5 and the historical gradients. In order to investigate the sensitivity of the circulation to the temperature gradient, 18 different temperature changes were simulated. The parameter combinations in these simulations were $A = 0.5, 1, 1.5$, $\sigma_w = 0.4, 0.6$ and $\phi_1 = 27°, 35°, 43°$. The choice of the parameter ϕ_1 was such that it includes regions where the lower gradient changes significantly (see Fig. 8.1b for the gradient change in the GFDL-ESM2M model). The different warming amplitudes were used to study the sensitivity of eddy fields to the circulation.

The surface temprature differences and zonal wind and EKE differences at 500 hPa between simulations with increased polar temperatures and the idealized historical run are plotted in Fig. 8.12 for simulations with the parameters $A = 1$, $\sigma_w = 0.4$ and $\phi_1 = 27°, 35°, 43°$. The main results from these simulations are that the polar amplification leads to: (a) an equatorward shift in the zonal wind (Fig. 8.12 d-f); (b) a decrease in the Atlantic storm tracks (Fig. 8.12 g-i) and ; (c) an increase in the Pacific storm tracks (Fig. 8.12 g-i). All the 18 simulations show qualitatively similar results.

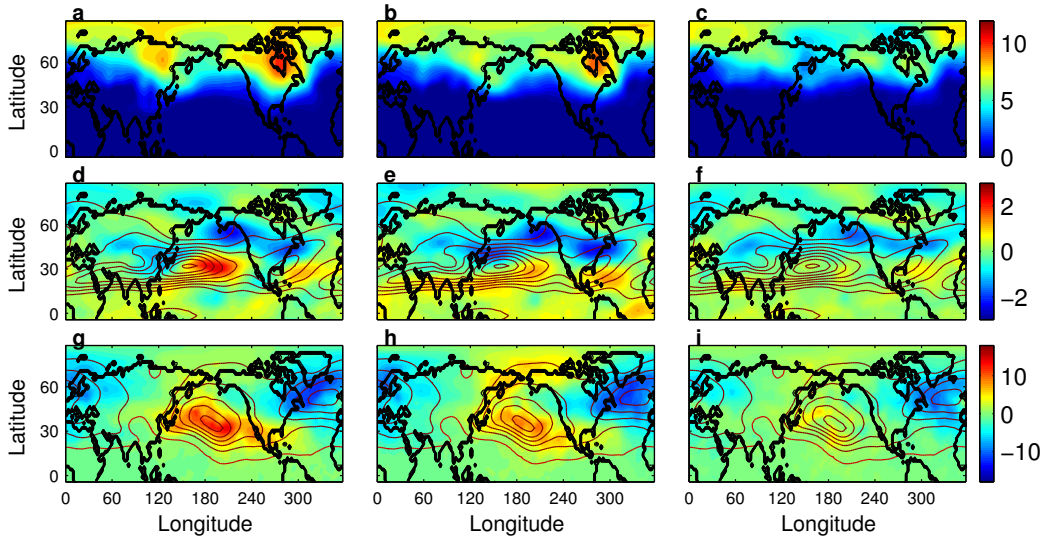

Figure 8.12: The difference between simulations of the polar amplified runs and the historical run simulation for the surface temperature (a-c) zonal wind at 500 hPa (d-f) and EKE at $\sigma = 0.5$ (g-i) as a function of longitude and latitude. The contours show the historical simulation zonal wind (d-f, 5 m s^{-1} contour interval) and the historical simulation EKE (h-i, 15 m^2 s^{-2} contour interval).

The equatorward shift in the jet stream as a response to the polar surface warming is consistent with other studies that used more complicated models (e.g., Deser et al., 2010; Screen et al., 2013), and also the idealized zonally symmetric model used in previous sections (Fig. 8.7) show an equatorward shift in the circulation as a response to polar warming (see also Butler et al., 2010). Moreover, the decrease in the Atlantic storm tracks intensity in our simulations is consistent with other studies that found that there is a significant decrease in storm tracks especially in the North Atlantic late winter (Magnusdottir et al., 2004; Seierstad and Bader, 2009). Surprisingly, it is shown here that the effect of the temperature trend has different effects on the Atlantic and Pacific storm tracks. The increase in EKE in the Pacific is not expected because the meridional temperature gradient, that is usually used as a baroclinicity measure, decreases. We note that as was discussed in section 8.5.2, a possible cause for the increase in EKE is the strong decrease in the static stability in regions where the gradient is modified. One possible reason for the different response in the Atlantic and the Pacific, are the significant zonal asymmetries, both in the reference simulation and in the temperature trends, which might also play an important role in the different response in the Pacific and Atlantic sectors. We note that an increase in EKE as a response to polar warming was also shown in idealized zonally symmetric simulations in chapter 3 and in Fig. 8.7.

To understand if the different EKE changes in the Pacific and Atlantic are a result of the different background state, or due to the different change in the projected temperatures, the zonal mean temperature changes described in Eq. 8.4 are used. Fig. 8.13 shows the surface temperature changes and the zonal wind and EKE at $\sigma = 0.5$ changes as a result of two such simulations with the parameters $A = 1.5$, $\sigma_w = 0.4$ and $\phi_1 = 27°, 35°$.[5]

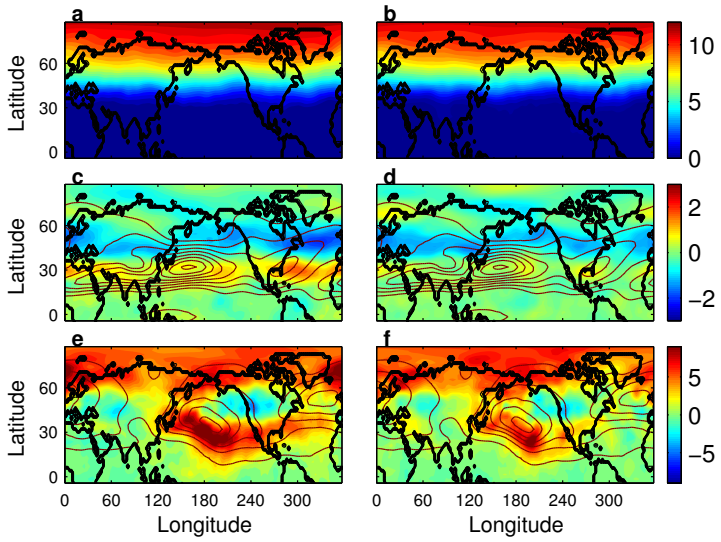

Figure 8.13: The difference between simulations with zonally symmetric polar surface increase and the historical run simulation for the surface temperature (a-b) zonal wind at 500 hPa (c-d) and EKE at $\sigma = 0.5$ (e-f) as a function of longitude and latitude. The contours show the historical simulation zonal wind (c-d, 5 m s^{-1} contour interval) and the historical simulation EKE (e-f, 15 m^2 s^{-2} contour interval).

[5]Similar results were obtained in additional four simulations with the parameter combinations $A = 0.5$ and $\sigma_w = 0.4, 0.7$ and $\phi_1 = 27°, 35°$.

The simulations show that EKE increases in both Atlantic and Pacific sectors when considering the zonally mean temperature changes (Fig. 8.13e,f). This implies that the differences in the EKE response between the Atlantic and Pacific regions when the increased polar temperatures with the zonal asymmetries were simulated (Fig. 8.12) are a result of the zonal asymmetric temperature tendencies in a global warming-like scenario. The zonal wind response to the symmetric temperature changes is an equatorward shift in the wind, which is similar to the asymmetric case.

To study the EKE sensitivity to different polar warming amplitudes, the temperature, wind and EKE changes at $\sigma = 0.5$ are plotted for simulations with different amplitude warming of the tropical surface in Fig. 8.14. The parameters used in these simulations are $A = 0.5, 1, 1.5$, $\sigma_w = 0.6$ and $\phi_1 = 27°$.

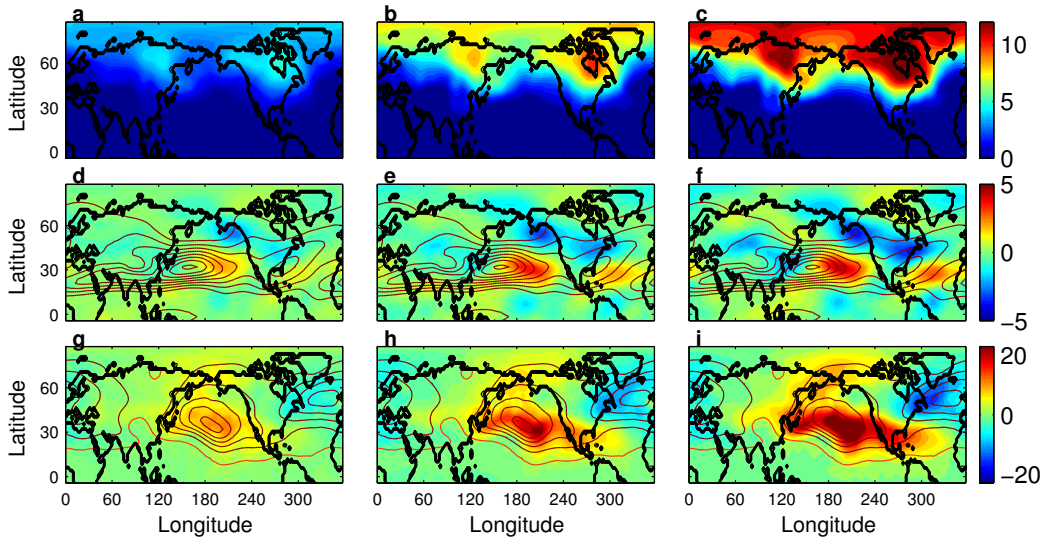

Figure 8.14: The difference between simulations of the polar amplified runs with different amplitude (left column $A = 0.5$, middle column $A = 1$, right column $A = 1.5$) and the historical run simulation for the surface temperature (a-c) zonal wind at 500 hPa (d-f) and EKE at $\sigma = 0.5$ (g-i) as a function of longitude and latitude. The contours show the historical simulation zonal wind (d-f, 5 m s^{-1} contour interval) and the historical simulation EKE (g-i, 15 m^2 s^{-2} contour interval).

The spatial shape of the wind and EKE changes are similar in all three simulations. This implies that even for the larger simulated temperature change the circulation response is similar to the linear response to these temperature changes. When the polar amplification is modified by factor of 0.5 (left column in Fig. 8.14) or factor 1.5 (right column in Fig. 8.14), which are differences that do occur between models (see Fig. 1.2), the EKE modifications are as large, or even larger, than the changes that occur in RCP8.5 scenario compared to the historical run (at $\sigma = 0, 5$, Fig. 8.11c,d). This implies that polar amplification differences between CMIP5 models could cause EKE differences that are as big as the response to a RCP8.5 forcing in mid-lower levels.

8.5.2 Eddy response to upper tropospheric tropical temperature gradient

In order to investigate the effect of the upper tropospheric temperature gradient on the circulation in the NH, the meridional temperature gradient is modified in the NH as follows:

$$\delta T_{\text{target}}(\phi > 0) = -Ae^{-\frac{(\sigma-\sigma_c)^2}{\sigma_w}} \int_{\phi}^{\phi_1^\circ} \partial_y (T_{\text{RCP8.5}}(\phi_i) - T_{\text{hist}}(\phi_i)) d\phi_i, \tag{8.5}$$

and in the SH as follows

$$\delta T_{\text{target}}(\phi < 0) = -A\exp\left[-\frac{(\sigma-\sigma_{\text{c}})^2}{\sigma_{\text{w}}} - \frac{(\phi)^2}{30}\right](\text{T}_{\text{RCP8.5}}(\phi < 0) - \text{T}_{\text{hist}}(\phi < 0)), \tag{8.6}$$

where the parameters represents the same quantities as in Eq. 8.4, with the exception that the gradient is modified from the equator to latitude ϕ_1. In this section the gradient modifications is modified in the tropical upper troposphere. Although the temperatures are modified in both hemispheres, these temperatures are used to investigate the circulation changes in the NH alone since these modifications produce the same NH meridional temperature gradient changes in the upper troposphere as in the RCP8.5 projections. In order to keep the temperature field smooth in the SH, we use a decay of the temperature change in latitude.

To investigate the effect of upper tropospheric warming on the circulation, the following parameters are used for the simulations in the NH: $A = 1$, $\sigma_w = 0.3$, $\sigma_c = 0.3$ and $\phi_1 = 32°, 40°, 49°, 57°$. Fig. 8.15 shows the zonally averaged temperature, zonal wind and EKE differences between these simulations and the idealized historical run.

In all simulations a poleward shift of the upper level jet is present. This shift is more pronounced when the gradient is modified at higher latitudes (Figs. 8.15f-h). This result implies that upper tropical warming contributes to a poleward jet shift. The poleward jet shift was also present in the zonally symmetric simulations when the tropical upper tropospheric temperatures were increased (Fig. 8.5f-h), but in the zonally symmetric simulations also surface winds were increased. When the gradient changes are confined to lower latitudes, EKE increases (left column in Fig. 8.15i,j), but when gradient changes in higher latitudes are also included included, EKE tends to decrease (Fig. 8.15k,l). This result is similar to the result shown in Fig. 8.5 which was obtained with the zonally symmetric model. As explained in section 8.3.1 the decrease in EKE as the gradient is modified in more poleward regions, is possibly due to the increase in static stability in the upper troposphere (see also Lim and Simmonds, 2009). These result implies that changes in the static stability could potentially have as large effect on eddy fields as changes in the meridional temperature gradient.

We note that these are dry simulations and only the dry static stability is discussed. In a more realistic scenario, such as CMIP5 simulations, the moisture content in the atmosphere increases as a response to global warming. This means that even if the dry static stability increases, it does not necessarily imply that also the moist static stability increases.

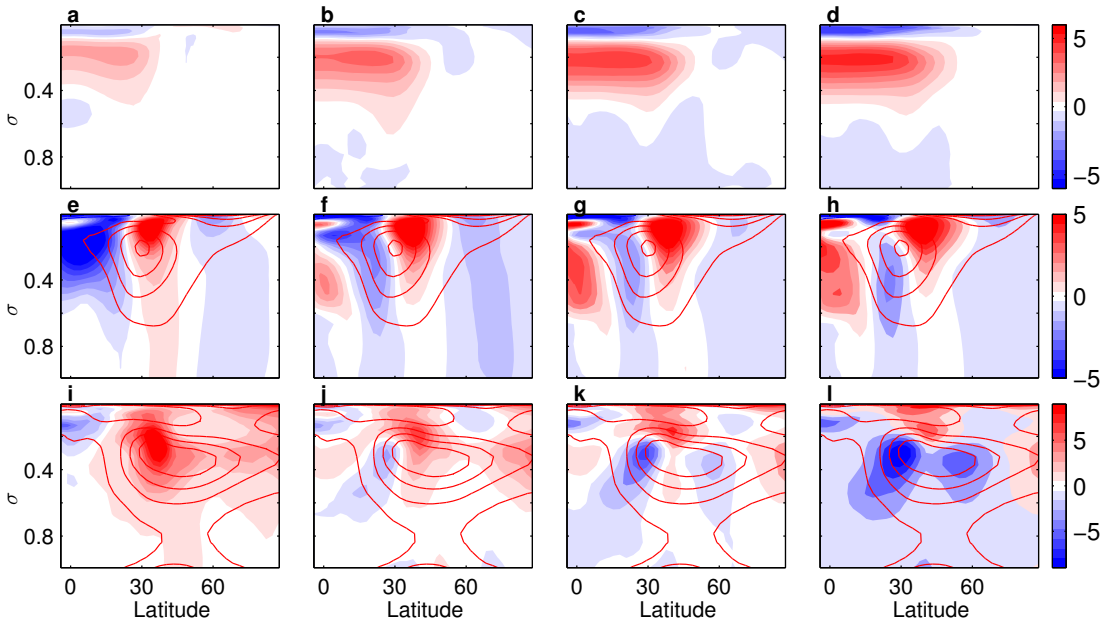

Figure 8.15: The difference between simulations of upper tropical tropospheric heating with different latitudinal extent of meridional gradient temperature change (first column $\phi_1 = 32°$, second column $\phi_1 = 40°$, third column $\phi_1 = 49°$, fourth column $\phi_1 = 57°$) and the idealized historical run simulation for the zonally averaged temperature (a-d) zonal wind (e-h) and EKE (i-l) as a function of latitude and σ level. The contours show the historical idealized simulation zonal wind (e-h, 5 m s^{-1} contour interval) and the historical simulation EKE (i-l, 15 m^2 s^{-2} contour interval).

8.6 Summary and discussion

In this chapter we aimed to understand the effect of global warming-like temperature changes on the atmospheric circulation using an idealized GCM. As a first step, two different zonally symmetric idealized methods were used. These methods were useful to investigate simplified global warming-like temperature trends, and were used to better understand the results from realistic zonally asymmetric simulations. It was difficult to obtain a robust result regarding the eddy response to global warming-like temperature changes from these zonally symmetric idealized methods. The main problem with using the traditional approach, where the relaxation temperature is modified in regions that are predicted to change their temperature, is that it is difficult to confine the temperature changes to the "correct" regions (see Fig. 8.3). The two main problems in using the fast zonal relaxation method (section 2.3.2) are that the circulation changes are reference dependent (Fig: 8.4), and are sensitive to the exact shape of temperature changes (Fig: 8.4). These difficulties encouraged us to use a realistic 3-dimensional reference simulation and a realistic 3-dimensional temperature change field in order to investigate the circulation response to global warming-like temperature changes.

The temperature field from the historical run of the GFDL-ESM2M model from the CMIP5 was used in order to produce a realistic target temperature. It was demonstrated that the main features of the historical run can be reproduced in an idealized GCM (Figs. 8.8,8.9). To investigate whether the idealized model can reproduce the circulation changes in a RCP8.5 scenario, an idealized simulation with the target temperature of this scenario was used. It

was found that the circulation changes are similar to the GFDL-ESM2M only in the SH and in the upper troposphere (Figs. 8.10,8.11). The fact that the circulation changes are not reproduced accurately implies that other factors besides the temperature changes contribute to the circulation changes.

To investigate the effect of the polar temperature amplification and of the tropical upper tropospheric warming on the circulation, a realistic temperature gradient changes were imposed on the historical reference. It was shown that the polar amplification leads to an equatorward shift in the jet (Fig. 8.12d-f). This result is also consistent with some of the zonally symmetric simulations with increased temperature near the polar surface (Fig. 8.5f,h). Furthermore, it was found that the EKE response to a zonally asymmetric polar amplification is different above the Atlantic and above the Pacific. Above the Atlantic there is a decrease in EKE, while above the Pacific there is an increase in EKE (Fig. 8.12g-i).

The different EKE response is possibly due to different temperature changes above the two oceans. Above the Atlantic ocean, the temperature gradient changes occur mostly at very high latitudes (Fig. 8.12a-c). The decreased meridional temperature gradient tends to decrease baroclinicity, while the lapse rate increases in very high latitudes and tends to increase baroclinicity, but only in a very small region. The decrease in the EKE in the Atlantic region implies that the decreased meridional temperature gradient plays a more important role than the increased lapse rate, which occurs only over a small region, in affecting eddies over the Atlantic. On the other hand, above the Pacific ocean, the surface meridional temperature gradient changes occur at lower latitudes (Fig. 8.12a-c). The decreased meridional temperature gradient tends to decrease baroclinicity, while the lapse rate increases and tends to increase baroclinicity in a large region (poleward of latitude 50°). The increase in EKE above the Pacific implies that the increased lapse rate, which takes place over many latitudes plays a more important role than the meridional gradient changes. Similar sensitivity to the latitudinal extent of the surface temperature changes was also found in zonally symmetric simulations. Namely, simulations with increased polar surface temperature that were confined to very high latitudes (which resembles the Atlantic changes) show a decrease in EKE (Fig. 8.7 - first and third columns), but simulations that the temperature gradient was increased in lower latitudes (which resembles the Pacific changes) had an increased or neutral EKE response (Fig. 8.7 - second and fourth columns).

It was shown that the jet tends to shift poleward as a response to upper troposphric tropical temperature changes (Fig. 8.15e-h). The response of the EKE to these temperature changes was found to be dependent on the details of the warming. When the upper troposphric tropical temperature gradient change is confined to lower latitudes, EKE increases (Fig. 8.15i-j). On the other hand, when the temperature is also modified at higher latitudes it decreases (Fig. 8.15k-l). It is possible to explain this dependency with similar argument that was used to explain the EKE dependency in cases the polar surface was warmed. Namely, when there is an increased upper level temperatures, there is an increase in the static stability which stabilizes the atmosphere. The changes in the temperature gradient and in the static stability have an opposite effect on

atmospheric stability, and therefore the EKE response is dependent on the exact details of the temperature changes. This dependency was also shown in zonally symmetric simulations in Fig. 8.5. Our results imply that the changes in the static stability can also play an important role in the circulation changes, and the opposite changes in the meridional temperature gradient in climate change projections are accompanied with opposite changes in the static stability. We note that we use dry simulations, and since moisture affects are absent, the role of the static stability in the simulation might be exaggerated. For example, in a dry simulations, the static stability increases when the temperature is increased in the tropical upper troposphere (lapse rate decreases). On the other hand, in a model that contains moisture, this is not the case since the moist adiabatic lapse rate decreases, and therefore the moist static stability remains approximately constant.

The sensitivity of EKE to changes in the polar amplification amplitude was also investigated. This sensitivity is interesting since different CMIP5 models predict significantly different polar temperature changes (Fig. 1.2). It is found that reducing or increasing the polar amplification amplitude by 50% lead to EKE changes that are as large as the EKE differences between the RCP8.5 and the historical run (Fig. 8.14g-i). Therefore, the polar amplification differences between CMIP5 models could potentially lead to large differences in the circulation predictions of different models.

Chapter 9

Summary

During my Ph.D I have been studying the sensitivity of eddies to changes in the vertical and meridional structure of the mean temperature field. The main tool used to study this topic was an idealized GCM with a modified Newtonian relaxation schemes. The schemes used in this thesis, allowed simulating any chosen predetermined mean temperature profile, and to study the circulation response to changes in the vertical and meridional structure of baroclinicity systematically.

The main reason that we used diabatic heating schemes, which allows controlling the mean temperature distribution of simulations, was that they enabled us to study the eddy field response to a prescribed temperature modification. This philosophy resembles the classic eddy-mean flow problem, where for a given mean field, the goal is to deduce the meaningful eddy characteristics. This approach could be very useful when knowledge about the temperature field exists, but knowledge about the diabatic heating is missing. For example, on Earth and other planets, we often have observations of the temperature field but there is no direct measurement of the diabatic forcing. Furthermore, GCMs used in climate projections have a reasonable agreement regarding the trends in temperatures, and these relatively robust temperature trends can be used to study their effect on eddies.

The main topic we addressed in this work was the sensitivity of eddies to the vertical structure of baroclinicity. The relation between the mean meridional temperature gradient and eddy fluxes has been addressed by several eddy flux closure theories. However, these theories give little information on the dependence of eddy fluxes on the vertical structure of the temperature gradient. The response of eddies to changes in the vertical structure of the temperature gradient is especially interesting since global circulation models suggest that as a result of greenhouse warming, the lower tropospheric temperature gradient will decrease where as the upper tropospheric temperature gradient will increase. We find that eddies are sensitive to the vertical structure of the meridional gradient. Our results indicate that eddy activity is more sensitive to temperature gradient changes in the upper troposphere. We suggested that the larger eddy sensitivity to the upper tropospheric temperature gradient is a consequence of large baroclinicity concentrated in upper levels. To support this hypothesis, we showed in a separate simulations set that the EKE is more sensitive to changes in the lapse rate in the mid-

upper troposphere where baroclinicity is predominantly large. Furthermore, we showed in a 1D Eady-like model that the linear growth rate of eddies is more sensitive to shear concentration rather than to the vertical mean shear, which is consistent with these results. To further support this hypothesis, we showed that it is consistent with a linear scaling between MAPE and EKE. Because MAPE is a nonlinear function of the meridional temperature gradient and of the lapse rate (MAPE $\propto \frac{\partial_y \mathrm{T}^2}{\partial_z \mathrm{T}}$), in regions where the meridional temperature gradient or lapse rate are large, a change in them will cause larger change in MAPE than similar change in regions where the MAPE is small. Namely, in cases that EKE and MAPE have a linear relationship, EKE would be more sensitive to changes in baroclinicity where it is large. We find that although a linear relationship between MAPE and EKE was found by Schneider and Walker (2008) to exist over wide range of parameter, there is no universal linear relationship between MAPE and EKE when the vertical baroclinicity structure is modified. Therefore, it is not quantitatively reliable to estimate EKE changes based on MAPE changes alone. The agreement between the linear growth rate calculation, the change in MAPE and our simulations that eddy fields are more sensitive to changes in baroclinicity where it is larger gives us a conceptual understanding and increases the confidence that this result is robust.

In a different set of simulations the sensitivity of eddies to changes in the meridional structure of the temperature gradient and jet types was studied. We find that the eddy fields are most sensitive to changes in the temperature gradient in the vicinity the EDJ, less sensitive to gradient changes in the equatorward flank of the STJ (latitudes inside the Hadley cell), even less sensitive to gradient changes significantly poleward of the EDJ, and least sensitive in cases where the gradient was modified between the jets (at the poleward flank of the STJ). This implies that a poleward shift of the jet, which makes the jet more EDJ like, leads to an increase in eddy fields. We used the conclusions from this study and applied them to real atmospheric phenomena - the Pacific MWM. We showed that a poleward shift in the jet during transition seasons (compared to midwinter), contributes to the presence of a MWM in the EKE, and succeeded to reproduce such a minimum in idealized simulations.

The final part of the thesis, which is ongoing work, is aimed to understand the sensitivity of eddies to realistic global warming-like simulations. An important result that we found, which is usually overlooked in the literature, is that the response of eddy field to a prescribed temperature change, can be reference dependent. Furthermore, we find that the response of eddies to a prescribed temperature change, can have large sensitivity to the specific temperature change and two relatively similar temperature changes can lead to a different circulation response. These conclusions imply that in order to obtain meaningful results regarding the effects of global warming-like temperature trends from an idealized model, a realistic 3-dimensional reference simulation and a realistic 3-dimensional temperature change field are needed to be simulated. To do that we reproduced a realistic 3-dimensional zonally asymmetric temperature field which is taken from a CMIP5 model, both for a historical reference run and a RCP8.5 run. We showed that the idealized model we use can reproduce the main features of a realistic circulation, and used this "realistic" run as a reference for simulations that the temperature field was

modified to be a global warming-like, namely, temperature increase near the polar surface and in the upper tropical troposphere. We consistently find that the increased temperatures in the NH polar surface, which decrease the meridional temperature gradient, lead to a poleward shift of the circulation, the EKE tends to decrease in above the Atlantic as a result of these temperature changes. On the other hand, we find that the EKE tends to increase as a result of these temperature changes. This results imply that the Pacific and Atlantic sectors might not be affected by polar amplification in the same manner, though other feedbacks that are not included in the simulations (latent heat, radiation, clouds and etc.) might change this response. Nevertheless, we succeeded to isolate the effect of temperature changes near the polar surface on the circulation, and found that the effect of the predicted temperature changes near the polar surface on the EKE is different in the Pacific and Atlantic. We relate the counter intuitive EKE increase in the Pacific to the decrease in static stability in these runs. Furthermore, we show that the increase in the upper tropospheric temperature causes a poleward jet shift.

The approach of reproducing a realistic 3-dimensional circulation in idealized model can be used in many other studies in order to create a more realistic circulation, and study how different changes in the parameters regime (temperature changes, frictional changes and etc.) affect the circulation.

9.1 List of publications

- J. Yuval, R. Chemke and Y. Kaspi, "The effect of small wavenumbers on the general circulation of the atmosphere", (in prep).
- J. Yuval and Y. Kaspi, "Circulation response to global warming-like temperature changes in idealized GCM", (in prep).
- J. Yuval and Y. Kaspi, "Eddy response to changes in jet characteristics", Journal of the Atmospheric Science (submitted).
- J. Yuval and Y. Kaspi, "The effect of vertical baroclinicity concentration on atmospheric macroturbulence scaling relations", Journal of the Atmospheric Science, Vol. 74, 1651-1667 (2017).
- J. Yuval and Y. Kaspi, "The effect of vertical baroclinicity concentration on the scaling of eddy kinetic energy with mean available potential energy", Journal of the Atmospheric Science, Vol. 73, 1709-1726 (2016).

Bibliography

Ait-Chaalal, F. and Schneider, T. (2015). Why eddy momentum fluxes are concentrated in the upper troposphere. *J. Atmos. Sci.*, 72:1585–1604.

Alexeev, V. A. (2003). Sensitivity to CO2 doubling of an atmospheric GCM coupled to an oceanic mixed layer: a linear analysis. *Clim. Dyn.*, 20:775–787.

Andrews, D. G., D., M. J., and W., S. R. (1983). Eliassen-Palm diagnostics of wave-mean flow interaction in the GFDL SKYHI general circulation model. *J. Atmos. Sci.*, 40:2768–2784.

Barnes, E. A. and Screen, J, A. (2015). The impact of arctic warming on the midlatitude jet-stream: Can it? has it? will it? *Wiley Interdisciplinary Reviews: Climate Change*, 6:277–286.

Bengtsson, L. and Hodges, K. I. (2006). Storm tracks and climate change. *J. Climate*, 19:3518–3543.

Blumen, W. (1979). On short-wave baroclinic instability. *J. Atmos. Sci.*, 36:1925–1933.

Bourke, W. (1974). A multi-level spectral model. I. formulation and hemispheric integrations. *Mon. Weath. Rev.*, 102(10):687–701.

Brayshaw, D. J., Hoskins, B., and Blackburn, M. (2008). The storm-track response to idealized SST perturbations in an aquaplanet GCM. *J. Atmos. Sci.*, 65:2842–2860.

Britanja, R., Graversen, R. G., and W., H. (2011). Arctic winter warming amplified by the thermal inversion and consequent low infrared cooling to space. *Nature Geoscience*, 4:758–761.

Butler, A. H., J., T. D. W., and R., R. (2010). The steady-state atmospheric circulation response to climate change-like thermal forcings in a simple general circulation model. *J. Climate*, 23:3474–3496.

Cai, M. (2005). Dynamical amplification of polar warming. *Geophys. Res. Lett.*, 32:L22710.

Cai, M. (2006). Dynamical greenhouse plus feedback and polar warming amplification. Part I: a dry radiative-transportive climate model. *Clim. Dyn.*, 26:661–675.

Chang, E. K. M. (2001). GCM and observational diagnoses of the seasonal and interannual variations of the Pacific storm track during the cool season. *J. Atmos. Sci.*, 58:1784–1800.

Chang, E. K. M. (2005). The impact of wave packets propagating across Asia on Pacific cyclone development. *Mon. Weath. Rev.*, 133:1998–2015.

Chang, E. K. M. (2006). An indealized nonlinear model of the northern hemisphere winter storm tracks. *J. Atmos. Sci.*, 63:1818–1839.

Chang, E. K. M. (2013). CMIP5 projection of significant reduction in extratropical cyclone activity over north america. *J. Climate*, 26.

Chang, E. K. M., Gou, Y., and Xia, X. (2012). CMIP5 multimodel ensemble projection of storm track change under global warming. *J. Geophys. Res.*, 117.

Charney, J. G. (1947). The dynamics of long waves in a baroclinic westerly current. *J. of Meteorology*, 4:136–162.

Charney, J. G. and Stern, M. E. (1962). On the stability of internal baroclinic jets in a rotating atmosphere. *J. Atmos. Sci.*, 19:159–172.

Chen, G., Held, I. M., and Robinson, W. A. (2007). Sensitivity of the latitude of the surface westerlies to surface friction. *J. Atmos. Sci.*, 64:2899–2915.

Deng, Y. and Mak, M. (2005). An idealized model study relevant to the dynamics of the dynamics of the midwinter minimum of the Pacific storm track. *J. Atmos. Sci.*, 62:1209 – 1225.

Deser, C., Tomas, R., M., A., and D., L. (2010). The seasonal atmospheric response to projected arctic sea ice loss in the late 21st century. *J. Climate*, 23:333–351.

Eady, E. T. (1949). Long waves and cyclonic waves. *Tellus*, 1:33–52.

Eichelberger, S. J. and Hartmann, D. L. (2007). Zonal jet structure and the leading mode of variability. *J. Climate*, 20:5149–5163.

Ferrari, R. and Nikurashin, M. (2010). Suppression of eddy diffusivity across jets in the southern pacific. *J. Phys. Oceanogr.*, 40:1501–1519.

Green, J. G. A. (1970). Transfer properties of the large scale eddies and the general circulation of the atmosphere. *Q. J. R. Meteorol. Soc.*, 96:157–185.

Hall, N. M. J., Hoskins, B. J., and Valdes, P. J. (1994). Storm tracks in a high-resolution GCM with doubled carbon dioxide. *Q. J. R. Meteorol. Soc.*, 120:1209–1230.

Hall, N. M. J. and Sardeshmukh, P. D. (1998). Is the time-mean northern hemisphere flow baroclinically unstable?. *J. Atmos. Sci.*, 55:41–56.

Hansen, J. E., Lacis, A., Russel, G., Stone, P., Fung, I., R., R., and J., L. (1984). Climate sensitivity: analysis of feedback mechanisms. In Hansen, J. E. and Takahashi, T., editors, *Climate processes and climate sensitivity, AGU Geophysical Monograph 29, Maurice Ewing vol 5.*, pages 130–163. American Geophysical Union.

Harnik, N. and Chang, E. K. M. (2004). The effects of variations in jet width on the growth of baroclinic waves: Implications for midwinter Pacific storm track variability. *J. Atmos. Sci.*, 61:23–40.

Hartmann, D. L. and Zuercher, P. (1998). Response of baroclinic life cycles to barotropic shear. *J. Atmos. Sci.*, 55:297–313.

Hayashi, Y. and Golder, D. (1981). The effects of condensational heating on midlatitude transient waves in theur mature stage: Control experiments with a GFDL GCM. *J. Atmos. Sci.*, 38:2532 – 2539.

Held, I. (2000). The general circulation of the atmosphere, paper presented at 2000 woods hole oceanographic institute geophysical fluid dynamics program.

Held, I. M. (1975). Momentum transport by quasi-geostrophic eddies. *J. Atmos. Sci.*, 32:1494–1497.

Held, I. M. (1978). The vertical scale of an unstable baroclinic wave and its importance for eddy heat flux parameterizations. *J. Atmos. Sci.*, 35:572–576.

Held, I. M. (1993). Large-scale dynamics and global warming. *Bull. Am. Meteor. Soc.*, 74:228–242.

Held, I. M. and Hou, A. Y. (1980). Nonlinear axially symmetric circulations in a nearly inviscid atmosphere. *J. Atmos. Sci.*, 37:515–533.

Held, I. M. and Larichev, V. (1996). A scaling theory for horizontally homogeneous, baroclinically unstable flow on a beta plane. *J. Atmos. Sci.*, 53:946–952.

Held, I. M. and O'Brien, E. (1992). Quasigeostrophic turbulence in a three-layer model: effects of vertical structure in the mean shear. *J. Atmos. Sci.*, 49:1861–1870.

Held, I. M. and Suarez, M. J. (1994). A proposal for the intercomparison of the dynamical cores of atmospheric general circulation models. *Bull. Am. Meteor. Soc.*, 75:1825–1830.

Hoskins, B. J. and Valdes, P. J. (1990). On the existence of storm-tracks. *J. Atmos. Sci.*, 47:1854–1864.

Ioannou, P. and Lindzen, R. S. (1986). Baroclinic instability in the presence of barotropic jets. *J. Atmos. Sci.*, 43(2):2999–3014.

Iwasaki, T. and Kodama, C. (2011). How Does the Vertical Profile of Baroclinicity Affect the Wave Instability? *J. Atmos. Sci.*, 68:863–876.

James, I. N. (1987). Suppression of baroclinic instability in horizontally sheared flows. *J. Atmos. Sci.*, 44:3710–3720.

James, I. N. and Gray, L. J. (1986). Concerning the effect of surface drag on the circulation of a baroclinic planetary atmosphere. *Q. J. R. Meteorol. Soc.*, 112:1231–1250.

Kodama, C. and Iwasaki, T. (2009). Influence of the SST rise on baroclinic instability wave activity under an aquaplanet condition. *J. Atmos. Sci.*, 66:2272–2287.

Kushner, P. J. and Polvani, L. M. (2004). Stratosphere–troposphere coupling in a relatively simple agcm: The role of eddies. *J. Climate*, 17(3):629–639.

Lachmy, O. and Harnik, N. (2014). The transition to a subtropical jet regime and its maintenance. *J. Atmos. Sci.*, 71:1389–1409.

Lee, S. and Kim, H. (2003). The dynamical relationship between subtropical and eddy-driven jets. *J. Atmos. Sci.*, 60:1490–1503.

Lee, S. S., Lee, J. Y., Ha, K. J., Wang, B., Kitoh, A., and Kajikawa, Y. (2013). Role of the Tibetan plateau on the annual variation of the mean atmospheric circulation and storm-track activity. *J. Climate*, 26:5270 – 5286.

Li, C. and Battisti, D. S. (2008). Reduced Atlantic storminess during last glacial maximum: Evidence from a coupled climate model. *J. Climate*, 21:3561–3579.

Lim, E.-P. and Simmonds, I. (2009). Effect of tropospheric temperature change on the zonal mean circulation and sh winter extratropical cyclones. *Clim. Dyn.*, 33(1):19–32.

Lindzen, R. S. and Farrel, B. (1980). A simple approximate result for the maximum growth rate of baroclinic instabilities. *J. Atmos. Sci.*, 37:1648–1654.

Lorenz, D. J. and DeWeaver, E. T. (2007). Tropopause height and zonal wind response to global warming in the IPCC scenario integrations. *J. Geophys. Res.*, 112:D10119.

Lorenz, D. J. and Hartmann, D. L. (2001). Eddy-zonal flow feedback in the southern hemisphere. *J. Atmos. Sci.*, 58:3312–3327.

Lorenz, E. N. (1955). Available potential energy and the maintenance of the general circulation. *Tellus*, 7:157–167.

Lu, J. and Cai, M. (2010). Quantifying contributions to polar warming amplification in an idealized coupled general circulation model. *Clim. Dyn.*, 34:669–687.

Lu, J., Sun, L., Wu, Y., and Chen, G. (2014). The role of subtropical irreversible PV mixing in the zonal mean circulation response to global warming-like thermal forcing. *J. Climate*, 27:2297–2316.

Lunkeit, F., Fraedrich, L., and Bauer, S. E. (1998). Storm tracks in warmer climate: sensitivity studies with a simplified global circulation model. *Clim. Dyn.*, 14:813–826.

Magnusdottir, G., Deser, C., and Saravanan, R. (2004). The effects of north atlantic sst and sea ice anomalies on the winter circulation in ccm3. part i: Main features and storm track characteristics of the response. *J. Climate*, 17(5):857–876.

Manabe, S. and Wetherald, R. T. (1975). The Effects of Doubling the CO2 Concentration on the climate of a General Circulation Model. *J. Atmos. Sci.*, 32:3–15.

Manabe, S. and Wetherald, R. T. (1980). On the distribution of climate change resulting from an increase in CO2 content of the atmosphere. *J. Atmos. Sci.*, 37:99–118.

Meehl, G. A., Stocker, T. F., Collins, W. D., Friedlingstein, P., Gaye, A. T., Gregory, J. M., Kitoh, A., Knutti, R., Murphy, J. M., Noda, A., Raper, S. C. B., Watterson, I. G., Weaver, A. J., and Zhao, Z.-C. (2007). Global climate projections. In Solomon, S., Qin, D., Manning, M., Chen, Z., Marquis, M., Averyt, K., Tignor, M., and Miller, H., editors, *Climate Change 2007: The Physical Science Basis. Contribution of Working Group I to the Fourth Assessment Report of the Intergovernmental Panel on Climate Change*, pages 747–845. Cambridge Univ. Press, Cambridge, UK, and New York, NY, USA.

Merlis, T. M. and Schneider, T. (2009). Scales of linear baroclinic instability and macroturbulence in dry atmospheres. *J. Atmos. Sci.*, 66:1821–1833.

Muller, J. (1991). Baroclinic instability in a two-layer, vertically semi-infinite domain. *Tellus*, 43:275–284.

Nakamura, H. (1992). Midwinter suppression of baroclinic wave activity in the Pacific. *J. Atmos. Sci.*, 49:1629–1642.

Nakamura, H. and Sampe, T. (2002). Trapping of synoptic-scale disturbances into the North-Pacific subtropical jet core in midwinter. *Geophys. Res. Lett.*, 29.

Nakamura, H. and Shimpo, A. (2003). Seasonal variations in the Southern Hemisphere strom tracks and jet streams as revealed in a reanalysis dataset. *J. Climate*, 17:1828–1844.

O'Gorman, P. A. (2010a). Understanding the varied response of the extratropical storm tracks to climate change. *Proc. Natl. Acad. Sci. U.S.A.*, 107:19176–19180.

O'Gorman, P. A. (2010b). Understanding the varied response of the extratropical storm tracks to climate change. *Proc. Natl. Acad. Sci. U.S.A.*, 107:19176–19180.

O'Gorman, P. A. (2015). Precipitation extremes under climate change. *Curr. Clim. Change Rep.*, 1:49–59.

O'Gorman, P. A. and Schneider, T. (2008). Energy in midlatitude transient eddies in idealized simulations of changed climates. *J. Climate*, 21:5797–5806.

Panetta, R. L. (1993). Zonal jets in wide baroclinically unstable regions: Persistence and scale selection. *J. Atmos. Sci.*, 50(14):2073–2106.

Park, H., Chiang, J. C. H., and Son, S. (2010). The role of the central Asian mountains on the midwinter suppression of North Pacific storminess. *J. Atmos. Sci.*, 67:3706–3720.

Pavan, V. (1996). Sensitivity of a multi-layer quasi-geostrophic beta-channel to the vertical structure of the equilibrium meridional temperature gradient. *Q. J. R. Meteorol. Soc.*, 122:55–72.

Pedlosky, J. (1987). *Geophysical Fluid Dynamics*. Spinger.

Penny, S., Battisti, D. S., and Roe, G. H. (2013). Examining mechanisms of variability within the pacific storm track: Upstream seeding and jet-core strength. *J. Climate*, 26:5242–5259.

Penny, S., Roe, G. H., and Battisti, D. S. (2010). The source of the midwinter suppression in storminess over the North Pacific. *J. Climate*, 23:634–648.

Penny, S., Roe, G. H., and Battisti, D. S. (2011). Reply to comments on "the source of the midwinter suppression in storminess over the North Pacific". *J. Climate*, 24:5192–5194.

Polvani, L. M. and Kushner, P. J. (2002). Tropospheric response to stratospheric perturbations in a relatively simple general circulation model. *Geophys. Res. Lett.*, 29:L014284.

Rhines, P. B. (1975). Waves and turbulence on a beta plane. *J. Fluid Mech.*, 69:417–443.

Sampe, T., Nakamura, H., Goto, A., and Ohfuchi W. (2010). Significance of a midlatitude sst frontal zone in the formation of a storm track and an eddy driven westerly jet. *J. Climate*, 23:1793–1814.

Schneider, E. K., Lindzen, R. L., and Kirtman, B. P. (1997). A tropical influence on global climate. *J. Atmos. Sci.*, 54:1349–1358.

Schneider, T. (2004). The tropopause and the thermal stratification in the extratropics of a dry atmosphere. *J. Atmos. Sci.*, 61:1317–1340.

Schneider, T. and Walker, C. C. (2008). Scaling laws and regime transitions of macroturbulence in dry atmospheres. *J. Atmos. Sci.*, 65:2153–2173.

Screen, J. A., Simmonds, I. Deser, C., and Tomas, R. (2013). The atmospheric response to three decades of observed arctic sea ice loss. *J. Climate*, 26:1230–1248.

Seierstad, I. A. and Bader, J. (2009). Impact of a projected future arctic sea ice reduction on extratropical storminess and the nao. *Clim. Dyn.*, 33(7-8):937–943.

Smith, K. S. (2007). The geography of linear baroclinic instability in Earth's oceans. *J. Mar. Res.*, 65:655–683.

Sobel, A. H., Nilsson, J., and Polvani, L. M. (2001). The weak temperature gradient approximation and balanced tropical moisture waves. *J. Atmos. Sci.*, 58:3650–3665.

Son, S.-W. and Lee, S. (2005). The response of westerly jets to thermal driving in a primitive equation model. *J. Atmos. Sci.*, 62:3741–3757.

Stephenson, D. B. and Held, I. M. (1993). GCM response of northern winter stationary waves and storm tracks to increasing amounts of carbon dioxide. *J. Climate*, 6:1859–1870.

Stone, P. H. (1972). A simplified radiative-dynamical model for the static stability of rotating atmospheres. *J. Atmos. Sci.*, 29:405–418.

Stone, P. H. (1978). Baroclinic adjustment. *J. Atmos. Sci.*, 35:561–571.

Sun, L., Chen, G., and Lu, S. (2013). Sensetivities and mechanisms of the zonal mean atmospheric circulation response to tropical warming. *J. Atmos. Sci.*, 70:277–286.

Thompson, D. E. J. and Barnes, E. A. (2014). Periodic variability in the large-scale southern hemisphere atmospheric circulation. *Science*, 343:641–645.

Vallis, G. K. (2006). *Atmospheric and Oceanic Fluid Dynamics*. pp. 770. Cambridge University Press.

Vallis, G. K., Kidston, J., and Zurita-Gotor, P. (2014). Response of the large-scale structure of the atmosphere to global warming. *Q. J. R. Meteorol. Soc.*

Walker, C. C. and Schneider, T. (2006). Eddy influences on Hadley circulations: Simulations with an idealized GCM. *J. Atmos. Sci.*, 63:3333–3350.

Wittman, M. A. H., Charlton, A. J., and Polvani, L. M. (2007). The Effect of Lower Stratospheric Shear on Baroclinicity. *J. Atmos. Sci.*, 64:479–496.

Wu, Y., Ting, M., Seager, R., Huang, H., and Cane, M. A. (2010). Changes in storm tracks and energy transports in a warmer climate simulated by the GFDL CM2.1 model. *Clim. Dyn.*, pages 53–72.

Yin, J. H. (2005). A consistent poleward shift of the storm tracks in simulations of 21st century climate. *Geophys. Res. Lett.*, 32:L18701.

Yuval, J. and Kaspi, Y. (2016). Eddy activity sensitivity to changes in the vertical structure of baroclinicity. *J. Atmos. Sci.*, 73:1709–1726.

Yuval, J. and Kaspi, Y. (2017). The effect of vertical baroclinicity concentration on atmospheric macroturbulence scaling relations. *J. Atmos. Sci.*, 74(5):1651–1667.

Zhang, Y. and Held, I. M. (1999). A linear stochastic model of a GCM's midlatitude storm tracks. *J. Atmos. Sci.*, 56:3416–3435.

Zurita-Gotor, P. (2007). The relation between baroclinic adjustment and turbulent diffusion in the two layer model. *J. Atmos. Sci.*, 64:1284–1300.

Appendices

Appendix A

Consistency of two methods for controlling the mean temperature

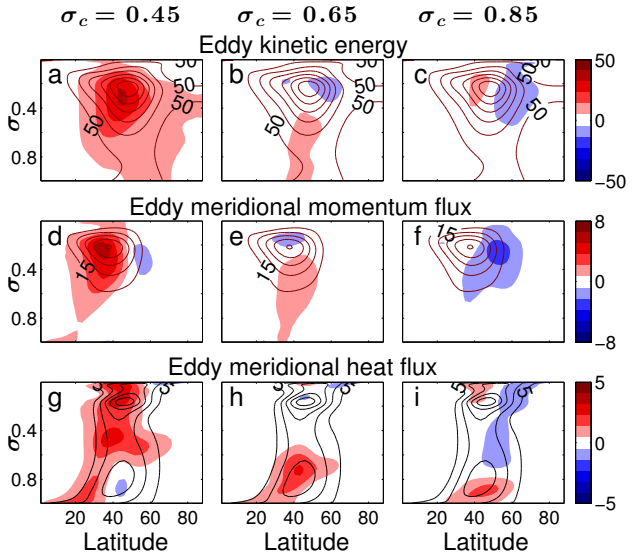

Figure A.1: The EKE (a-c), EMF - $\overline{u'v'}$ (d-f) and EHF - $\overline{v'T'}$ (g-i) for simulations where the meridional temperaure gradient was modified at different levels with a gradient percent change $x = 0.05$ using the iterative method described in section 2.3.1. Colors show the deviation from the reference and contours represent reference simulation values. Contours intervals are 50 m^2 s^{-2} for the EKE, 15 m^2 s^{-2} for the EMF 5 K m s^{-1} for the EHF.

In chapter 5 a method that was suggested by Zurita-Gotor (2007) where the zonally mean temperature and the deviations from the zonally mean temperature (eddies) are relaxed with different relaxation times to a chosen profile was used. A very fast relaxation of the mean state was chosen, such that the mean temperature of the simulation is almost identical to the relaxation temperature). In chapter 3 we used a different method to control the mean state of the simulation, by an iterative calculation of the relaxation temperature that will produce a chosen target temperature (see also Lunkeit et al., 1998 and Yuval and Kaspi, 2016). In this method the relaxation time of the mean state and eddies is the same. Although the methods are different, it is shown here that for the case that the temperature gradient is modified at certain levels of the atmosphere, eddies respond similarly in both methods. This provides additional confidence that such methods enable prediction of a reliable response of eddy fields in response to changes in the mean temperature profile. In Fig. A.1 the EKE, EMF and the eddy temperature flux are plotted for the case the temperature gradient was increased by 5 percent at different levels of the atmosphere as described in Eq. 3.1 using the iterative method

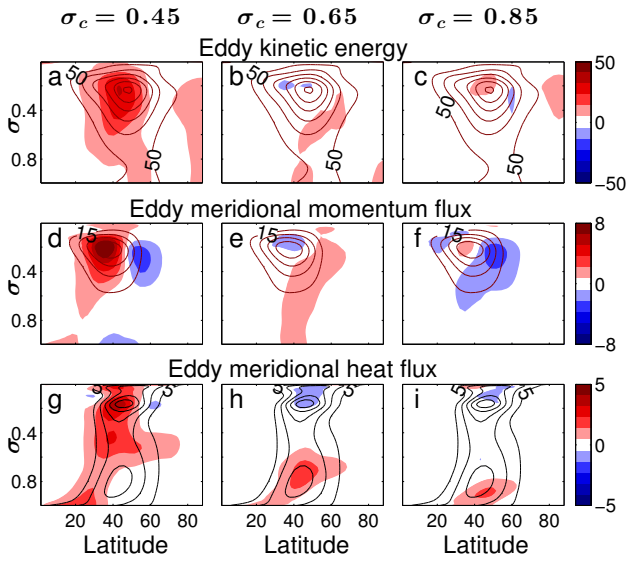

Figure A.2: The EKE (a-c), EMF - $\overline{u'v'}$ (d-f) and EHF - $\overline{v'T'}$ (g-i) for simulations where the meridional temperaure gradient was modified at different levels with a gradient percent change $x = 0.05$ using the fast zonal relaxation method described in section 2.3.2. Colors show the deviation from the reference and contours represent reference simulation values. Contours intervals are 50 m^2 s^{-2} for the EKE, 15 m^2 s^{-2} for the EMF 5 K m s^{-1} for the EHF.

described in 2.3.1, and in Fig. A.2 the same quantities are plotted for similar simulations using the fast zonal relaxation method described in section 2.3.2. The resemblance of Fig. A.1 to Fig. A.2 indicates that the response of the eddies to mean temperature changes are similar in the two methods.

It should be noted that the iterative method allows obtaining also zonal asymmetric mean temperature distribution (see also similar methods with asymmetric mean state in Lunkeit et al., 1998 and Chang, 2005), while the method described in section 2.3.2 was designed to obtain a zonal symmetric temperature distribution. The advantage in using this method is that it requires less computation time since the computation of the relaxation matrix is trivial (it is just the target temperature), while the iterative method demands a separate simulation to obtain a relaxation matrix that produces the target temperature.

Appendix B

Held-Suarez diabatic heating parametrization

This appendix describes the Held and Suarez (1994) parametrization for the relaxation temperature, relaxation time and the linear drag coefficient, which is commonly used in the literature. The thermodynamic equation in the GCM we can be written as:

$$\frac{DT}{Dt} = \frac{1}{\rho}\frac{Dp}{Dt} + k_T(\phi, \sigma)(T_{\text{relax}} - T),$$

where $\frac{D}{Dt}$ is the material derivative that includes the nonlinear advection terms, T is the temperature, ρ is the density, p is the pressure, σ is the vertical coordinate, ϕ is the latitude, T_{relax} is the relaxation temperature and k_T is the relaxation frequency.

The Held and Suarez (1994) parameters for these quantities are:

$$T_{\text{relax}} = \max\left(200\text{K}, \left(315\text{K} - \delta\text{T}_\text{y}\sin^2\phi - \delta\theta_\text{z}\log\frac{\text{p}}{\text{p}_0}\cos^2\phi\right)(\frac{\text{p}}{\text{p}_0})^\kappa\right), \tag{B.1}$$

where $\delta T_y = 60$ K is the equator to pole temperature difference, $\delta\theta_z = 10$ K, $\kappa = R/c_p = 2/7$ (R is the gas constant, and c_p is the heat capacity) and $p_0 = 1000$ mb is the mean pressure surface. The relaxation frequency can be expressed as

$$k_T = k_a + (k_s - k_a)\max(0, \frac{\sigma - \sigma_\text{b}}{1 - \sigma_\text{b}})\cos^4\phi, \tag{B.2}$$

where $k_a = 1/40$ day^{-1} is the relaxation frequency at the upper atmosphere, $k_2 = 1/4$ day^{-1} is the relaxation frequency at the surface in the tropics and $\sigma_b = 0.7$ is the upper extent of the boundary layer.

The linear drag in the GCM, which appears in the momentum equations can be written as:

$$\frac{\partial\vec{v}}{\partial t} = ... - k_v(\sigma)\vec{v},$$

where $k_v = k_f\max(0, \frac{\sigma-\sigma_\text{b}}{1-\sigma_\text{b}})$ is the linear drag coefficient and $k_f = 1$ day^{-1}.

Appendix C

Heating applied in z coordinats vs. σ coordinates

In the schemes described in sections 2.3.1 and 2.3.3, the vertical interval of the modifications applied to the temperature/heating field were taken in σ coordinates. Namely, the modifications at different levels where taken in the same interval in σ coordinates ($\delta\sigma$ was the same for different choices of σ_c). This choice changes the temperature for the same amount of mass at different levels. Another possibility is to change the temperature/heating profile in such a way that the vertical interval of change will be similar in z coordinates.

One possible argument to prefer z coordinates rather than σ coordinates is that changes in the meridional temperature gradients in same σ intervals will lead to different changes in the zonal wind. This is because thermal wind balance in pressure coordinates is expressed as $p\partial_p u_g = \frac{R_d}{f}\partial_y T$, where u_g is the geostrophic zonal wind, p is the pressure, R_d is the gas constant, f is the Coriolis parameter, y is the meridional coordinate and T is the temperature. As long as the simulation obeys thermal wind balance, it is expected that the change in the zonal wind will be larger in cases where the upper troposphere was modified, because of the pressure term (p) that appears in the LHS. One might expect that the changes in eddy activity will be related to the changes in the mean geostrophic wind, which might explain why gradient temperature changes in the upper troposphere causes a larger changes in eddy activity than gradient temperature changes in the lower troposphere. To test this hypothesis, simulations were performed such that the vertical interval of temperature modifications in z coordinates was similar (For $\sigma_c = 0.65, 0.85$ we used $\delta\sigma = 0.15, 0.2$ respectively). The results of these simulations (not shown) show that the response of the EKE change is larger when the upper temperature gradient is modified, which is consistent with the results presented in section 3.2.

Appendix D

The relation between EAPE and MAPE

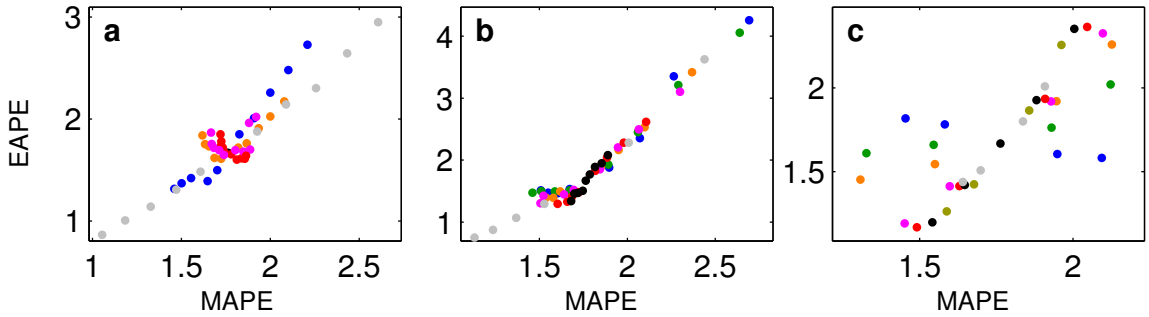

Figure D.1: The EAPE as a function of MAPE for simulations that (a) the vertical structure of the meridional temperature gradient was modified (as in section 5.25.2.1, colors as in Fig. 5.4) (b) the lapse rate was modified in different levels (as in section 5.25.2.2, colors as in Fig. 5.5) and (c) when the meridional structure of the temperature gradient was modified (as in section 5.25.2.3, colors as in Fig. 5.6).

To highlight that the deviations from linear scaling between eddy fields and the MAPE not only occur in the relation between EKE and MAPE, but also for the relation between the EAPE and MAPE, the EAPE and MAPE are plotted for different relaxation temperature profiles in Fig. D.1. The figure shows that when the meridional/vertical structure of the meridional temperature gradient is modified, there are deviations from a linear relationship between EAPE and MAPE (Fig. D.1a,c). When the lapse rate is modified, the relationship is close to linear (Fig. D.1b), as is the relation between EKE to MAPE in these simulations (Fig. 5.5d). The relation between EAPE and MAPE in all the simulations in this paper, qualitatively resemble the relation between the EKE and MAPE, such that the linear relation between EKE and EAPE still holds (Figs. 5.4g, 5.5g and 5.6g).

Appendix E

Changing the subtropical jet and eddy-driven jet simultaneously

A complimentary experiment for the purpose of studying the eddy response to simultaneous changes in the jets' magnitude the parameters $(\phi_1, \phi_2, \phi_3, \phi_4)$ were chosen such that the jets would change their magnitude in an opposite manner, and are described in row c of Table 6.1. We note that the chosen latitudes for the merged jet reference were different from the separated jet reference since the jet location is more poleward than in the separated jet reference case.

Fig. E.1 shows the temperature (a,b), zonal wind (c,d) and the response of the EKE (e,f), EHF (g,h) and EMFC (i,j) to simultaneous wind changes in the EDJ and STJ for the separated jet reference. When the jets are modified simultaneously, but with opposite tendencies, eddies are more affected by the change in the EDJ (if the EDJ is strengthened, so do the eddies, and vice versa). This result is consistent with the results shown in Fig. 6.3, where it is shown that eddies are more sensitive to meridional gradient changes in the vicinity of the EDJ than near the STJ. The results are shown for gradient modifications at latitudes $(\phi_1, \phi_2, \phi_3, \phi_4) \approx [(18°, 26°, 35°, 43°)]$, but the results are qualitatively similar for other parameters shown in Table 6.1 (row c). Also for the merged jet reference, simulations that both jets are modified simultaneously were conducted, and we find that eddy fields are more sensitive to changes in the EDJ (not shown).

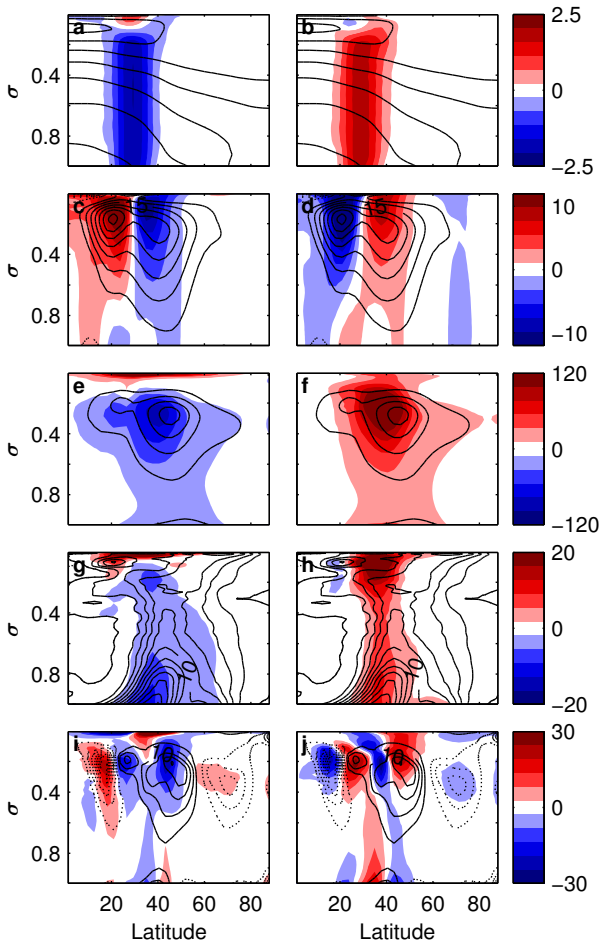

Figure E.1: Temperature (a-b), zonal wind (c-d), EKE (e-f), EHF (g-h) and EMFC$\times 10^6$ (i-j) for simulations where the gradient was modified simultenously and with opposite magnitudes at these latitudes - increased gradient near the STJ and decreased near the EDJ is in the left column and the opossite change in the right column. Contours show the separated jet reference (dashed contours for negative values) and the colors represent deviation from this reference. The contour intervals are 15 K (temperature), 5 m s^{-1} (zonal wind), 50 m^2 s^{-2} (EKE), 5 Km s^{-2} (EHF) and 5 m s^{-2} (EMFC).